AD-A275 762

‖‖‖‖‖‖‖‖‖‖‖‖‖‖‖‖

PHOTOREFRACTIVE ADAPTIVE ANTENNA ARRAY PROCESSOR

Harris Corporation

Robert Montgomery, William Beaudet, David Graves,
Michael Lange, and Michael Luntz

DTIC
ELECTE
FEB 16 1994
B

DTIC QUALITY INSPECTED 2

94-05094

‖‖‖‖‖‖‖‖‖‖‖‖‖‖‖‖

Rome Laboratory
Air Force Materiel Command
Griffiss Air Force Base, New York

4   2   15   080

This report has been reviewed by the Rome Laboratory Public Affairs Office (PA) and is releasable to the National Technical Information Service (NTIS). At NTIS it will be releasable to the general public, including foreign nations.
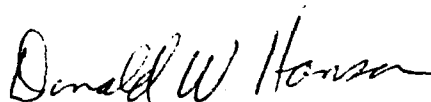
RL-TR-93-245 has been reviewed and is approved for publication.

APPROVED:

JAMES L. DAVIS
Project Engineer

FOR THE COMMANDER

DONALD W. HANSON, Director
Surveillance & Photonics

REPORT DOCUMENTATION PAGE

Form Approved
OMB No. 0704-0188

1. AGENCY USE ONLY (Leave Blank)	2. REPORT DATE	3. REPORT TYPE AND DATES COVERED
	December 1993	Final Dec 90 – Jun 93

4. TITLE AND SUBTITLE

PHOTOREFRACTIVE ADAPTIVE ANTENNA ARRAY PROCESSOR

6. AUTHOR(S)

Robert Montgomery, William Beaudet, David Graves,
Michael Lange, and Michael Luntz

5. FUNDING NUMBERS

C - F30602-91-C-0005
PE - 62702F
PR - 4519
TA - 21
WU - 93

7. PERFORMING ORGANIZATION NAME(S) AND ADDRESS(ES)

Harris Corporation
Government Communication Systems Division
P.O. Box 91000
Melbourne FL 32902

8. PERFORMING ORGANIZATION REPORT NUMBER

N/A

9. SPONSORING/MONITORING AGENCY NAME(S) AND ADDRESS(ES)

Rome Laboratory (OCPC)
25 Electronic Pky
Griffiss AFB NY 13441-4515

10. SPONSORING/MONITORING AGENCY REPORT NUMBER

RL-TR-93-245

11. SUPPLEMENTARY NOTES

Rome Laboratory Project Engineer: James L. Davis/OCPC/(315) 330-3145

12a. DISTRIBUTION/AVAILABILITY STATEMENT

Approved for public release; distribution unlimited.

12b. DISTRIBUTION CODE

13. ABSTRACT (Maximum 200 words)

The objective of this contract was to build a laboratory model of a six channel
adaptive antenna array processor using acousto-optic delay lines with a photorefractive
structure which both computes and applies the adaptive tap weights. The major perform-
ance goal of greater than 40 dB suppression for a single narrowband interferer at a
fixed frequency in the band was exceeded by 10 dB suppression for narrow band
interference. This substantially exceeds that attained by previous optical processors.
A goal of greater than 37 dB suppression for a narrow band signal at any frequency in
a 20 MHz band was also exceeded. The goal of 20 dB rejection for a signal with 10 MHz
instantaneous bandwidth was met with difficulty. To meet this goal, an extensive
analysis of the limitations of LMS algorithm processors was required. This analysis
indicates that the system was actually performing close to theoretical limits for
this design. The analytic and experimental results are reported here.

14. SUBJECT TERMS

Photorefractive, Acousto-Optic Processing, LMS Algorithm,
Interference rejection, Adaptive Processor, Indium Phosphide,
Bragg Cell

15. NUMBER OF PAGES

96

16. PRICE CODE

17. SECURITY CLASSIFICATION OF REPORT	18. SECURITY CLASSIFICATION OF THIS PAGE	19. SECURITY CLASSIFICATION OF ABSTRACT	20. LIMITATION OF ABSTRACT
UNCLASSIFIED	UNCLASSIFIED	UNCLASSIFIED	UL

TABLE OF CONTENTS

LIST OF ILLUSTRATIONS

LIST OF ILLUSTRATIONS (Continued)

LIST OF TABLES

1.0 INTRODUCTION

This program is part of an ongoing effort to utilize the power of acousto-optic analog processors to solve the computationally intensive problems associated with adaptive antenna arrays. The processor developed and tested here is directed at antenna beamforming and null steering. The experiment used as a guiding baseline for the present contract is an adaptive, wideband, sidelobe cancelling system employing the Howells-Appelbaum algorithm. In this algorithm a central antenna lobe, the "main beam," is provided either by a large, main-dish antenna or by a fixed set of tap weights on the array.

The underlying scenario, valid in many practical situations, is that the main-beam signal contains the desired signal plus a large interference component. The interference is coming from a high-power interferer which is collected by the sidelobes of the main beam. Auxiliary, omnidirectional, antenna elements collect interferer components which are comparable to those collected by the main beam. The main beam is pointed at the emitter of the desired signal. Therefore, the desired signal collected by the main beam is large compared to the desired signal content of auxiliary elements. With this scenario, the sidelobe cancelling processor may be designed to use a linear combination of the auxiliary outputs to cancel the main-beam signal. Since the desired signal content of the auxiliary elements is negligible, the desired signal is not cancelled but the interfering signals collected by the main-beam sidelobes are cancelled. Hence, this system is referred to as a "sidelobe canceller."

It is well known in antenna array theory that phase weighting of antenna elements produces a frequency dependent antenna pattern if the phase weights are constant in frequency. This phenomenon, referred to as "beam squint," will cause the sidelobe cancelling pattern to be frequency dependent and the cancellation will be degraded for broadband interferers.

This problem can be resolved by adding more auxiliary antenna elements or by adding phase compensating filters to the existing elements[1]. The processor under discussion here utilizes a tapped delay line on each auxiliary element. This variable tapped delay line may be thought of as a general Finite Impulse Response (FIR) filter where the impulse response of the filter may be adapted arbitrarily within the bandwidth and time delay constraints imposed by the tapped delay device. This versatile architecture was first described by Widrow[2]. An acousto-optic implementation of this architecture has been reported in a number of papers by Penn[3] and, more recently, by Friedman[4].

The length of the delay lines need only be equal to the delay time across the antenna array to achieve phase compensation for the delays induced by the array itself. However, another important regime of processing can be achieved if the processor can be implemented with delay elements which are much longer than the transit time across the antenna. Long delay elements make it possible to exploit the longer-term temporal properties of interfering signals in cancelling them. The primary case of interest here is that of interferers which exhibit multipath characteristics. That is, the same signal appears a multiplicity of times due to scattering from various obstacles which create multiple paths from interferer to antenna. In general, these multiple delayed components will also arrive from different directions. For this type of application the length of the delay lines must be longer (in general, they should be much longer) than the multipath delay. Acoustic

delay lines are well suited to this longer delay requirement since delays in the tens of microseconds are readily achieved.

On this contract a concept of loop gain was developed whereby the closed loop gain for CW signals is used as a reference value for system loop gain. One of the important contributions of this work is the development of a model which takes into account the effects of finite loop gain and relates the broadband cancellation performance to total delay time and loop gain. This model is used to compute the expected cancellation of broadband interference based on the CW loop gain, the interferer bandwidth, and the total delay time.

The processor described here is a unique implementation of the LMS algorithm using a patented[5] combination of photorefractive and acousto-optic techniques. The goal of the program is to build an operating processor which implements the basic LMS algorithm in the multichannel configuration described by Widrow. This basic structure can then be used to experimentally evaluate several specific antenna processing configurations. The Howells-Appelbaum processor is chosen as the basic configuration for laboratory demonstrations on this contract.

1.1 Executive Summary

The objective of this contract is to build a laboratory model of a six-channel adaptive antenna array processor using acousto-optic delay lines with a photorefractive structure which both computes and applies the adaptive tap weights.

The six-channel acousto-optic Bragg cell operates at a center frequency of 70 MHz and has a bandwidth of 30 MHz and a delay length of 1 μs.

The performance goals for the system are:
1. Suppression of greater than 40 dB for a single narrow-band interferer at a fixed frequency in the band.
2. Greater than 37 dB suppression for a single CW interferer at any frequency within a 20 MHz band.
3. Greater than 20 dB rejection for a broadband interferer with an instantaneous bandwidth of 10 MHz.

In addition to these goals, the proposed design had a predicted adaptation response time constant of 30 μs for CW interference.

A diagram of the system is shown in Figure 1.1. This system occupies approximately 12 inches of length on a small optical rail. The proximity arrangement of Bragg cell and photorefractive crystal allows for a simple, compact, and robust optical system containing only three, 1 cm diameter, lenses.

This laboratory system met the narrow-band interference suppression goal of 40 dB suppression over a 20 MHz band. The goal of 20 dB suppression with a 10 MHz instantaneous was also met by using a low-noise diode pumped YAG ring laser for readout in conjunction with the reference filtering arrangement developed on the program. The initial design achieved only 8–10 dB of suppression for a 10 MHz bandwidth.
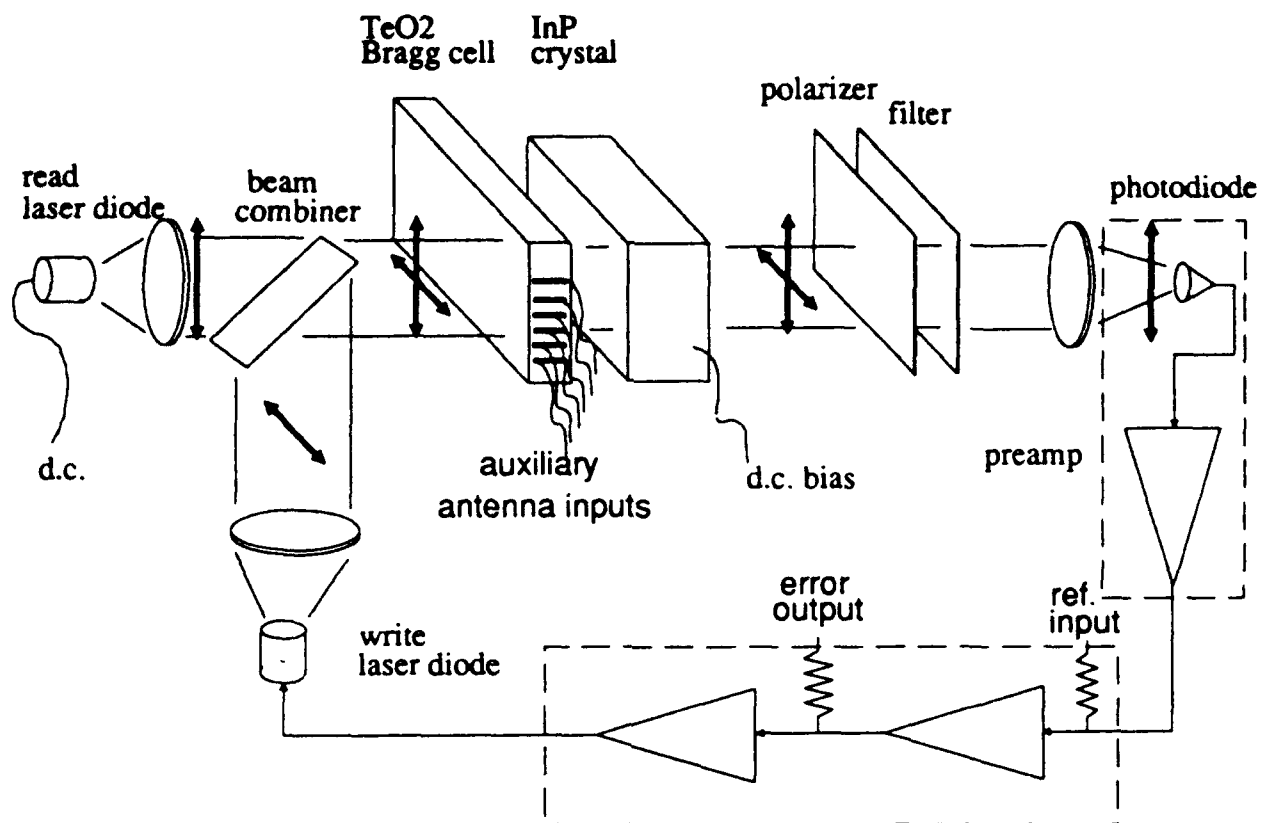
Figure 1.1. System Schematic Diagram

An extensive analysis indicated that the system was actually performing close to theoretical limits for this design. In order to reach the level of performance achieved by the experimental system we were forced to develop a detailed understanding of the performance limits for this type of system.

We conceived a potentially patentable concept of placing the bandwidth limiting filter in the reference input path while leaving the auxiliary channel paths as broadband as possible. This technique produced a 23 dB suppression with a 7 MHz bandwidth filter in the reference channel.

During the final months of the contract a Harris capital equipment diode pumped YAG laser was substituted in place of the 1.3 μm diode read laser. This substitution resulted in a dramatic improvement in the suppression of narrow-band interference. We obtained a suppression of 50 dB over a bandwidth of 15 MHz. This result is 20 dB better than any other reported optical system. The wideband suppression was also improved, and a suppression of 25 dB was obtained for a 3.5 MHz instantaneous bandwidth.

The processor implemented meets the suppression goals of this program and it performs close to the theoretical limits for the design parameters used. Also, this processor far exceeds the performance of other known optical processors in size, stability, ease of operation, and suppression performance.

2.0 SYSTEM MODELS APPLICABLE TO THE PHOTOREFRACTIVE PROCESSOR

In this section we provide a brief summary of the theory of the LMS adaptive structure used in the photorefractive processor. This is not a rigorous derivation of the mathematical principles but an intuitive guide to provide a basis for analysis of this specific system. This system is a estimator subtractor type cancellation system. That is, it uses a set of basic signals $\{s_i(t)\}$ to estimate a desired signal D. The signal set will be represented as a vector s which has components $s_i(t)$. The signal estimate is a scalar function E. The error in the estimate is a scalar function, ε, defined by

$$\varepsilon = D - E. \qquad \text{(Eq. 2.1)}$$

The estimate consists of a linear combination of the signal components

$$E = w \bullet s \qquad \text{(Eq. 2.2)}$$

where the vector w is the array of weights applied to the signal vector components. When the estimator produces an accurate estimate, D is eliminated or greatly reduced in the error output. If D is a jamming or interference signal then that interference is reduced or "cancelled." Throughout this report the desired function will also be referred to as the "reference" in the sense of a tracking loop which tracks a reference function.

The photorefractive material used in the processor will be approximated to have a first order exponential response with a time constant, τ, which varies inversely with the light intensity. For the intensity values of approximately 100 mW/cm^2 the time constant is approximately 3 ms. The signals being processed will be assumed to be time stationary (constant power and constant correlation between various signal vector components) on a time scale comparable to the photorefractive time constant. The photorefractive material properties and device design are covered in detail in Paragraph 6.1.3 of this report.

When the error signal is applied as an intensity modulation to the write laser the photorefractive material forms a diffraction grating with strength proportional the correlation between the error and the delayed signal in the Bragg cell. This diffraction grating diffracts the read laser light in such a way that it interferes with the light diffracted by the delayed signal in the Bragg cell. This process performs the adaptive weight generation for the adaptive filter. We will use a discrete representation of this process although the actual Bragg cell and diffraction gratings are a continuous delay and weighting process. This discrete representation may be thought of as an approximation to the continuous situation and the sums used here could be replaced by appropriate integrals in the limit of infinitesmal space increments. The Bragg cells are therefore represented as discrete tapped delay lines with a constant power (when averaged over the photorefractive time constant) signal of unit power at each tap. The array of tap weights defines the tap weight vector w.

A noise N is added to the desired signal to represent the effect of photodetector preamplifier noise in the system. This detector noise is the dominant noise in our experiments. The noise term will be ignored in the initial analysis to simplify the algebra. The effect of the additive noise at the photodetector can be treated independently as a desired function which is randomly varying and which is uncorrelated with the signal components. Since the noise is uncorrelated the mean value of the

noise contribution to the weight function will be zero. However, there will be a mean squared fluctuation in the weights caused by the noise.

In the LMS algorithm and in the photorefractive processor the rate of change of the tap weight is proportional to the product of the error times the signal at the given tap. This statement is expressed mathematically to obtain a differential equation for the tap weights.

$$\frac{dw}{dt} = \frac{G}{\tau} E s - \frac{w}{\tau} \qquad \text{(Eq. 2.3)}$$

The term $\frac{w}{\tau}$ is included to model the photorefractive as a first order time constant low pass filter instead of a true integrator. We use Eqns. 2.1 and 2.2 to write the equation for the tap weight vector as

$$\frac{dw}{dt} = \frac{G}{\tau} (D + N - w \bullet s) \, s - \frac{w}{\tau} . \qquad \text{(Eq. 2.4)}$$

G is a gain parameter determined by the net system gain. This equation may be rewritten in a more conventional form by expressing the product of s times the dot product as a matrix C operating on the weight vector w. C is the matrix formed by the outer product of the s vector with itself.

$$\frac{dw}{dt} - \frac{G}{\tau} (\bar{C} \bullet w) + \frac{w}{\tau} = \frac{G}{\tau} (D + N) s \qquad \text{(Eq. 2.5)}$$

Eq. 2.5 has the form of a simple array of linear equations with constant coefficients except for the fact that $\bar{C}$ and τ are, in general, not constant in time. We make the usual assumption here that both τ and C are constant when averaged over the filtering time of the photorefractive material (milliseconds). In that case, we treat τ and C as constants. Also it is convenient to think of the time averaged constant elements of C as the ensemble average C then may be thought of as the covariance matrix of the signal vector s. This matrix is square and symmetric. This procedure of assuming the matrix terms constant does not model the actual device adequately under all conditions. In some conditions there are observable fluctuations in the tap weights which are caused by variations in the signal correlations and/or the fluctuation in correlation between the signal and detector noise. These conditions and assumptions will be revisited later when specific situations are discussed. They can be examined and tested in specific cases as we describe, analyze, and test the experimental system.

In our tapped delay line system with six identical auxiliary antenna elements it is evident that there is equal power in every signal component. We will define the signal vector components such that they are normalized; that is, the diagonal components of $\bar{C}$ are all unity. The total power is normalized. Therefore, when the signal is comprised of a multiplicity of uncorrelated subsignals, i.e., different frequencies, each subsignal has only a fraction of the normalized total power.

The representation of the continuous delay line as an array of discrete delays raises the issue of the maximum spacing of the discrete elements which provides an accurate representation of the

system. As previously mentioned, the vector **s** could be thought of as a continuous function of distance along the direction of propagation. In that case, the dot product becomes a sum of integrals and the outer product matrix becomes an integral operator. We choose to represent the system in the discrete format and choose a sampling rate which is very high compared to the reciprocal bandwidth. This is done as an approximation to the continuous representation. In computations performed with this matrix model several runs are made with increasing sample rate. The rate is taken to be adequately high when the result becomes essentially independent of sample rate. This introduces some computational complexity because the high sample rate ensures a high correlation between samples and the covariance matrix is ill conditioned. Fortunately, powerful computers and computing methods are available to solve this problem at reasonable cost.

2.1 Solution by Eigenfunction Expansion

When the (nominally constant) covariance matrix is assumed in Eq. 2.5 this equation represents an array of linear differential equations with constant coefficients. For such systems of equations it is well known from the theory of linear systems that a set of independent eigenvectors, $\{e_i\}$, exists which satisfy the equations $Ce_i = \lambda_i e_i$.

$\{e_i\}$ are the eigenvectors of the correlation matrix $\bar{C}$ and λ_i are the corresponding eigenvalues. For real symmetric matricies such as C the eigenvalues are real and positive. The eigenvectors are orthogonal, ($e_i \bullet e_j = 0$ when $i \neq j$), and they form a complete set over the signal space. Because of this completeness, the weight vector, **w**, and the product of signal vector times desired function, (D+N) **s**, may be expressed as a weighted sum of these eigenvectors in the form.

$$w = \sum a_k e_k \tag{Eq. 2.6}$$

$$(D + N)\, s = \sum b_k e_k \tag{Eq. 2.7}$$

We substitute these expressions for **w** and **s** into Eq. 2.5 to obtain a set of uncoupled differential equations for the coefficients a_k,

$$\frac{da_k}{dt} + \frac{(G\lambda + 1)}{\tau} a_k = \frac{G}{\tau} b_k. \tag{Eq. 2.8}$$

Since the equations represented by Eq. 2.8 are uncoupled, each of them can be solved directly and independently. For those components with eigenvalues such that $G\lambda \gg 1$, the time constant for adaptation is $\tau/(G\lambda)$. For those components with eigenvalues such that $G\tau \ll 1$, the time constant for adaptation is equal to the photorefractive time constant τ. Also, the ideal noise-free signal suppression for each eigenvector is $1/(G\lambda+1)$.

Throughout this report we have normalized the variables such that the mean squared value is unity for all the components of **s**. This is possible because all of our signal vector components are simply delayed replicas of one another. With this normalization the sum of all the eigenvalues λ_k is equal to one. Since they are all positive, the largest eigenvalue must be less than one. The largest possible suppression for any signal component associated with a single eigenvector is $1/(G+1)$ and the shortest possible convergence time constant is $\tau/(G+1)$.

These relationships show that each eigenstate the system behaves similarly to a simple, one-dimensional, feedback amplifier system with a gain value equal to $G\lambda$. For the special, but common, case where all the signal vector components are delayed versions of the same signal, the harmonic functions (sine, cosine) are eigenfunctions for the problem. The eigenfunction expansion becomes a Fourier expansion and the eigenvalues are the power levels for the various Fourier components. This concept forms a basis for the analysis in the following section of the system performance in the case of a CW sine wave input.

2.2 CW Interference As a Special Case

The special case of CW interference provides insight into the performance with broadband interference, provides a basis for defining loop gain, and provides a model for this important system test mode. CW performance is easily measured and it provides information for characterizing a system. For these reasons this is the test mode for most systems which have been reported in the technical literature. Performance in this mode provides a good measure for comparing systems.

For this CW case we will change temporarily to the integral format instead of the discrete sums and we will choose Eq. 2.4 as a starting point. In the integral format the dot product in Eq. 2.4 becomes an integral over the length of the delay line taken along the x axis.

$$\frac{dw}{dt} = 2\frac{G}{L\tau}\left(D(t)\,s(x,t) - s(x,t)\int w(x)\,s(x,t)\,dx\right) - \frac{w}{\tau} \qquad \text{(Eq. 2.9)}$$

G/L is the open loop gain per unit length of delay. The total gain G plays a key role in many aspects of the analysis of the adaptive filter. If the term containing the integral in Eq. 2.9 is set to zero this effectively opens the loop. In the actual system, for example, this would be accomplished by simply disconnecting the output of the photodetector preamplifier. In this open loop situation the weights approach a steady state distribution of

$$w_{ol} = \frac{2G}{L} < D(t)\,s\left(x, t - \frac{x}{v}\right) > \qquad \text{(Eq. 2.10)}$$

where the brackets indicate a low pass filtering operation with a filter time constant equal to τ, the time constant of the photorefractive material. This bracket will also be recognized as the correlation between the desired, or reference, function and the signal arriving at the auxiliary antenna element. This open loop configuration is an acousto-optic time integrating correlator.

The form of the interfering signal in the delay line is

$$s\left(x, t - \frac{x}{v}\right) = \sqrt{2}\cos\left(\omega t - \omega\frac{x}{v}\right). \qquad \text{(Eq. 2.11)}$$

The reference is a delayed version of the signal with an unknown amplitude, B, and an unknown delay,

$$D(t) = B\cos(\omega t + \phi). \qquad \text{(Eq. 2.12)}$$

The performance under open loop conditions will be examined first. The steady state weight distribution under open loop conditions and CW input is found by direct substitution into Eq. 2.10,

$$w_{ol} = \sqrt{2} \frac{B}{L} \cos \left(\omega \frac{x}{v} + \phi \right).$$
(Eq. 2.13)

We obtain the value of the feedback term or desired estimate, E, under these open loop conditions by substituting this weight distribution into the integral

$$E_{ol}(t) = GB \cos (\omega t + \phi).$$
(Eq. 2.14)

The open loop value of the estimate is the gain times the desired signal being estimated. It approaches this value exponentially with a time constant equal to the photorefractive time constant. When the desired signal function is removed from the system the tap weights and the estimate decay to zero with the same time constant. This open loop response was used throughout the program to evaluate the system performance, measure gain and to evaluate the photorefractive material time constant.

We now will examine the closed loop operation as described in Eq. 2.9. The integral in Eq. 2.9 is a finite length cosine transform when the signal is as given in Eq. 2.11. Therefore, the only weight distribution which produces a significant output is a cosine distribution with the same frequency. We therefore use a trial solution for the tap weight distribution of the form

$$w(x) = A \cos (\omega t + \alpha).$$
(Eq. 2.15)

When this form is substituted into Eq. 2.9, the solution requires that $\alpha = \phi$ and a differential equation for A results,

$$\frac{dA}{dt} + A \frac{(G+1)}{\tau} = \frac{\sqrt{2}}{L\tau} B + \frac{\sqrt{2}}{L\tau} N(t) \cos \omega t.$$
(Eq. 2.16)

The noise is reinserted here as a reminder that the noise term comes along as though it were part of the reference function. As previously mentioned, the average of this noise term is zero, but the rms fluctuation is not zero. The multiplication of the noise by coswt (the signal) translates the frequency spectrum of the noise in such a way that the noise at the signal frequency is translated to dc. This noise around dc is within the passband of the low pass filter represented by Eq. 2.9. The result is that the ratio of the average weight value to the rms fluctuation in the weight value is equal to the ratio of the desired function input to the rms noise level in a bandwidth equal to the closed loop bandwidth of the adaptive system.

This simple equation for the amplitude of a sinusoidal (in x) distribution of tap weights shows that the CW case may be represented as a one-dimensional problem since all the tap weights move as a single sine curve. Furthermore, the closed loop time constant is equal to the photorefractive time constant divided by the open loop gain plus 1. Eq. 2.16 indicates that the closed loop response will be a simple exponential response with a time constant of $(G+1)/\tau$ and a steady state weight amplitude of

$$w_{ss} = \frac{\sqrt{2}BG}{(G+1)L} \cos\left(\omega \frac{x}{v} + \phi\right).$$
(Eq. 2.17)

This result may be used in Eq. 2.2 to find the estimate, E.

$$E = \int s(x, t)\, w(x)\, dx = \frac{BG}{G+1} \cos(\omega t + \phi)$$
(Eq. 2.18)

The error in this estimate, (D-E), is

$$E = \frac{B}{G+1} \cos(\omega t + \phi)$$
(Eq. 2.19)

A simple block diagram representing Eq. 2.9 under these specialized CW conditions is shown in Figure 2.1.

The presence of the two signal multipliers shows that the effective loop gain is proportional to the signal squared. Since the signal power is normalized to 1 in our equations this does not show explicitly in the equations. However, when two separate frequencies are present in the system the total power is unity and the signals must share this power. The result is that two equal strength signals with different frequencies will each have a loop gain equal to 1/4 that of a single frequency alone. This well-known shortcoming of the LMS algorithm has important implications for broad-band signals since they may be represented as sums of many narrow-band signals.
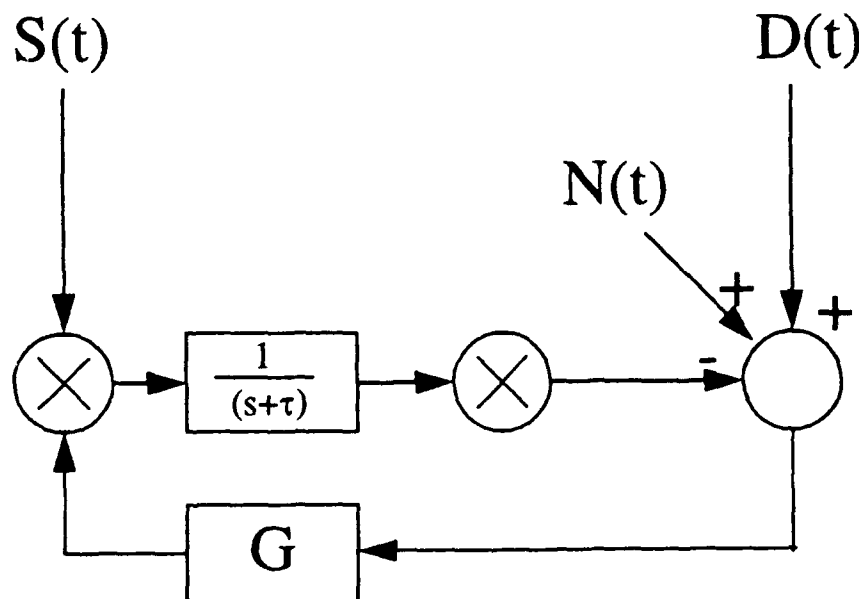
Figure 2.1. Block Diagram of CW Model

When multiple frequencies of unequal amplitudes are present the large amplitude signals are suppressed more than the small amplitude signals. Thus, the situation where the small signals at the system input become the dominant contributors at the system output. This problem becomes a major limitation on broadband suppression performance when the power spectrum of the interfering signal is not uniform over the frequency band. A $1/f^2$ type power spectrum such as that generated by a random square wave is particularly damaging.

The formulation presented above and the simplified diagram of Figure 2.1 are applicable to a multichannel antenna array processor. The dimensionality of the signal vector is multiplied by the number of antenna elements or channels and the correlation matrix for the signal vector is much more complex. However, it still has the same symbolic representation used above.

3.0 BROADBAND CANCELLATION PERFORMANCE ANALYSIS

The array processor previously described has many limits on its ability to suppress interference. There are, of course, limitations imposed by imperfections of implementation. Additionally, after the processor has converged, the processor will jitter about the best solution due to randomness of the input signal. This jitter can be controlled by reducing the loop bandwidth of the processor which also slows its convergence time. Another limit on the suppression performance is fundamental to the processing algorithm. In this processing algorithm there must be an error signal to maintain the solution in steady state. This is due to the fact that the integrators in the feedback path are "leaky." Some error input is required to maintain the charge on the integrators.

3.1 Analysis Model

The following development analysis is for a system consisting of a primary radar antenna plus a single auxiliary antenna element but the results can easily be extended to a system consisting of multiple auxiliary elements. The adaptive processor, shown in Figure 5.4 of Paragraph 5.3, consists of read and write lasers, the crystal that forms the weight, and electrical amplifiers. The read processing computes a weighted average of the input signal with the weighting function determined by the write processing. The equation for the output of the read process is

$$y(t) = \frac{1}{T} \cdot \int_{-\frac{T}{2}}^{\frac{T}{2}} w(x, t) \, s(t - x) \, dx \qquad \text{(Eq. 3.1)}$$

where

$s(t)$ is the input signal from an auxiliary antenna element,
$y(t)$ is the processor output,
t is time,

and

x is the time equivalent of the spacial distance along the processor.

This electrical output is subtracted from a reference signal $r(t)$, which is the output of the radar main-dish antenna, to form an error signal, $e(t)=r(t)-y(t)$, which is used in the write process to set the weight function $w(x, t)$. In the write processing the input signal interacts with the amplified error signal to generate the weight distribution. The model for this interaction is given by the equation

$$g \cdot e(t) \cdot s(t - z) = \tau \cdot \frac{\partial}{\partial t} w(z, t) + w(z, t) \qquad \text{(Eq. 3.2)}$$

which is the equation for a first order filter with time constant τ. The variable g in Eq. 3.2 is the system open loop gain. When the filter bandwidth is small so that there is little random jitter in the weight function, it is reasonable to replace Eq. 3.2 by its average value. Furthermore, the interest in this section is the steady-state performance limits of the processor so that the time derivative of

the average value of the weight function is zero. Thus, the approximate equation describing the steady-state processor becomes, upon substituting Eq. 3.1 and Eq. 3.2 and computing ensemble, the average

$$R_{rs}(z) - \frac{1}{T} \int_{-\frac{T}{2}}^{\frac{T}{2}} w(x) R_s(z-x) \, dx = \frac{w(z)}{g} \qquad \text{(Eq. 3.3)}$$

where
    $R_{rs}(z)$ is the cross-correlation function between the signal and reference

and
    $R_s(z)$ is the signal autocorrelation function.

If time is scaled such that the signal has unity bandwidth, then Eq. 3.3 can be written as

$$R_{rs}(z) - \int_{-\frac{BT}{2}}^{\frac{BT}{2}} w(x) R_s(z-x) \, dx = \frac{w(z) \cdot BT}{g} \qquad \text{(Eq. 3.4)}$$

and Eq. 3.1 becomes

$$y(t) = \int_{-\frac{BT}{2}}^{\frac{BT}{2}} w(x, t) s(t-x) \, dx \qquad \text{(Eq. 3.5)}$$

where B is the bandwidth of the signal and where $R_{rs}(z)$ and $R_s(z)$ are the correlation functions of the equivalent unity bandwidth signals. The total power in the error $e(t)$ with a weighting function $w(x)$ can be found by averaging $e^2(t)$ to be

$$\overline{e^2} = \int_{-\frac{BT}{2}}^{\frac{BT}{2}} \int w(x) R_s(z-x) w(z) \, dx dz - 2 \int_{-\frac{BT}{2}}^{\frac{BT}{2}} w(x) R_{rs}(x) \, dx + R_r(0) \qquad \text{(Eq. 3.6)}$$

where $R_r(0)$ is the total power in the reference signal.

Eq. 3.4 shows that the time-bandwidth product of the processor has the effect of changing the effective loop gain of the signal processing. As will be shown later, the cancellation performance of the processor is proportional to the loop gain. Thus, it is seen from this equation that as the time-bandwidth product increases, the effective gain of the processor and, therefore, the cancellation performance of the processor is degraded.

This section is intended to provide numerical results showing theoretical performance limits of the optical processor. To provide these numerical results, it will be necessary to make some approximations to Eq. 3.4 to find a solution. Two approaches to a solution have been used, each requiring a different approximation. In the first approach the integral in Eq. 3.4 is approximated by a discrete sum. This results in a set of linear equations which are solved numerically. In the second approach the finite limits of the integration are ignored. This results in an integral equation that can be analytically solved. Ignoring the finite limits will generally produce results which are not as accurate as digitizing the integral, but the equations resulting from this analysis provide significant insight into the processor algorithm that is not provided by the brute force numerical approach.

3.2 Numerical Integration Approximation

If, in Eq. 3.4, we compute $w(z)$ only for discrete values of $z = n\Delta z$ and approximate the integral by a discrete sum, the equation is approximated by

$$R_{rs}(n\Delta z) - \sum_{m=-\frac{BT}{2\Delta x}}^{\frac{BT}{2\Delta x}} w(m\Delta x)\, R_s(n\Delta z - m\Delta x)\, \Delta x = \frac{w(n\Delta z) \cdot BT}{g} \qquad \text{(Eq. 3.7)}$$

which reduces to

$$R_{rs}(n) - \frac{BT}{N} \sum_{m=-\frac{N}{2}}^{\frac{N}{2}} w(m)\, R_s(n-m) = \frac{w(n) \cdot BT}{g} \qquad \text{(Eq. 3.8)}$$

whenever $\Delta z = \Delta x = \Delta$. In Eq. 3.8, the notation has been slightly changed so that the index of the correlation and weight functions is the discrete index. The value of N, the number of samples in the sum, is equal to BT/Δ. The set of equations given by Eq. 3.8 for each of the $N+1$ values of n forms a set of $N+1$ linear equations in $N+1$ unknowns, the solution of which is given by the matrix equation

$$W = \frac{N}{BT}\left(R_s + \frac{N}{g}I\right)^{-1} R_{rs} \qquad \text{(Eq. 3.9)}$$

where variables in bold type indicate vector or matrix quantities. Eq. 3.6 can be similarly digitized to yield

$$\overline{e^2} = \left(\frac{BT}{N}\right)^2 \sum_{m,n=-\frac{N}{2}}^{\frac{N}{2}} w(m)\,R_s(n-m)\,w(n) - 2\frac{BT}{N}\sum_{m=-\frac{N}{2}}^{\frac{N}{2}} w(m)\,R_{rs}(m) + R_r(0)$$

(Eq. 3.10)

which in matrix notation becomes

$$\overline{e^2} = W_1^T R_s W_1 - 2R_{rs}^T W_1 + R_r$$

(Eq. 3.11)

where

$$W_1 = \frac{BT}{N}W = \left(R_s + \frac{N}{g}I\right)^{-1} R_{rs}.$$

(Eq. 3.12)

Eqs. 3.11 and 3.12 will be used later to provide performance results for some typical interference suppression scenarios.

3.2.1 Infinite Integration Approximation

If the finite limits on the integral of Eq. 3.4 are ignored, the integral equation

$$R_{rs}(z) - \int_{-\infty}^{\infty} w(x)\,R_s(z-x)\,dx = \frac{w(z)\cdot BT}{g}$$

can be solved analytically by taking the Fourier transform of the equation to yield

$$S_{rs}(u) - W(u)\,S_s(u) = \frac{BT}{g}W(u$$

or

$$W(u) = \frac{\dfrac{g}{BT}S_{rs}(u)}{1 + \dfrac{g}{BT}S_s(u)}$$

(Eq. 3.13)

where

$W(u)$ is the Fourier transform of the weight distribution,
$S_{rs}(u)$ is the cross spectrum between the input signal and the reference,

- 14 -

and

$S_s(u)$ is the signal spectrum.

Ignoring the finite limits of the integral in Eq. 3.5, the correlation function of the error $e(t) = r(t) - y(t)$ can be computed and from that correlation the spectrum of the error is found to be

$$S_e(u) = \frac{S_r(u) + \left[S_r(u)\,S_s(u) - |S_{rs}(u)|^2\right]\left[2\dfrac{g}{BT} + \left(\dfrac{g}{BT}\right)^2 S_s(u)\right]}{\left[1 + \dfrac{g}{BT}S_s(u)\right]^2} \qquad \text{(Eq. 3.14)}$$

In the analysis of the adaptive processor, it is assumed that the reference waveform is a filtered version of the input signal and that the effects of additive noise on both the input signal and the reference are negligible. Under these assumed conditions,

$$S_r(u)\,S_s(u) = |S_{rs}(u)|^2$$

so that when this restriction is substituted into Eq. 3.14 the error spectrum is given by

$$S_e(u) = \frac{S_r(u)}{\left[1 + \dfrac{g}{BT}S_s(u)\right]^2} \qquad \text{(Eq. 3.15)}$$

and the total power in the error, which is a direct measure of the suppression performance of the adaptive processor, becomes

$$\overline{e^2} = \int_{-\infty}^{\infty} \frac{S_r(u)}{\left[1 + \dfrac{g}{BT}S_s(u)\right]^2}\,du. \qquad \text{(Eq. 3.16)}$$

These equations will be valid for larger time-bandwidth products for which the effects of time truncation are negligible.

The next section uses these equations to compute some limits on the performance of the adaptive processor under some simplified but representative scenarios of operation.

3.3 Single Element Processor Performance

In Paragraph 3.2 a simplified model was developed for analyzing the performance of a single element adaptive array processor. That paragraph developed equations which can be evaluated to compute the performance of the adaptive processor. In this paragraph these equations are used to provide some numerical results. Paragraph 3.3.1 provides results using the infinite integration

approximation. This approximation provides considerable insight into the performance limits of the processor. In Paragraph 3.3.2 the effect of the finite integration is evaluated using the numerical integration approximation.

3.3.1 Performance Results Using Infinite Integration Approximations

Eqs. 3.15 and 3.16 provide considerable insight into the performance of the adaptive processor. One of the first facts that is evident from these equations is that the power in the error signal is inversely proportional to the effective gain, where the effective gain is equal to the actual loop gain normalized by the time-bandwidth product. This is demonstrated by letting the signal have the aperture spectral shape,

$$S_s(u) = \begin{array}{ll} 1 & |u| \le 0.5 \\ 0 & \text{otherwise.} \end{array}$$

For this spectrum, the suppression, which is equal to the power in the error signal, is from Eq. 3.16, equal to

$$\overline{e^2} = \frac{1}{\left[1 + \dfrac{g}{BT}\right]^2}.$$

For large, effective loop gain the suppression will be the inverse of the effective power loop gain. But for spectra that have a more practical rolloff with frequency there is not nearly so large a suppression. This is demonstrated in Figure 3.1 which shows the error power for the case of the input signal equal to a delayed version of the reference waveform so that $S_r(u) = S_s(u)$. The input and reference have a Gaussian spectral shape. In this case, the suppression in dB for any effective loop gain is only about half the value one would expect if the spectrum had an aperture shape. The reason for this performance reduction can be seen in Figure 3.2, which shows the signal and error spectra with an effective loop gain of 40 dB. This loop gain only provides 20 dB suppression with the Gaussian spectrum rather than the anticipated 40 dB. The suppression, which is the difference between the signal and error spectral levels, is reduced as the spectral density falls off with increasing frequency. Because the signal spectrum falls off slowly, there is still significant energy in the signal at frequencies where the suppression is small. This causes the energy in the error to actually be higher on the skirts of the input spectrum than in the center of the band. The error spectral density peaks at a frequency for which the spectral density of the input is equal to the inverse of the voltage effective loop gain. This is another manifestation of the well-known adaptive array phenomenon that high-power jammers are suppressed more than lower-power ones. In this case, the spectrally spread input can be considered to be multiple jammers at different frequencies. The stronger jammers, that is the portions of the spectrum with high power spectral density, have less residual output power than the weaker jammers.

The curve of Figure 3.2 shows that the bandwidth is significantly higher for the error than it is for the signal. This suggests, that if the error signal were filtered, there could be a significant suppression performance improvement. The equivalent to filtering the error can be performed by filtering the reference signal as can be seen by reference to Eq. 3.16.
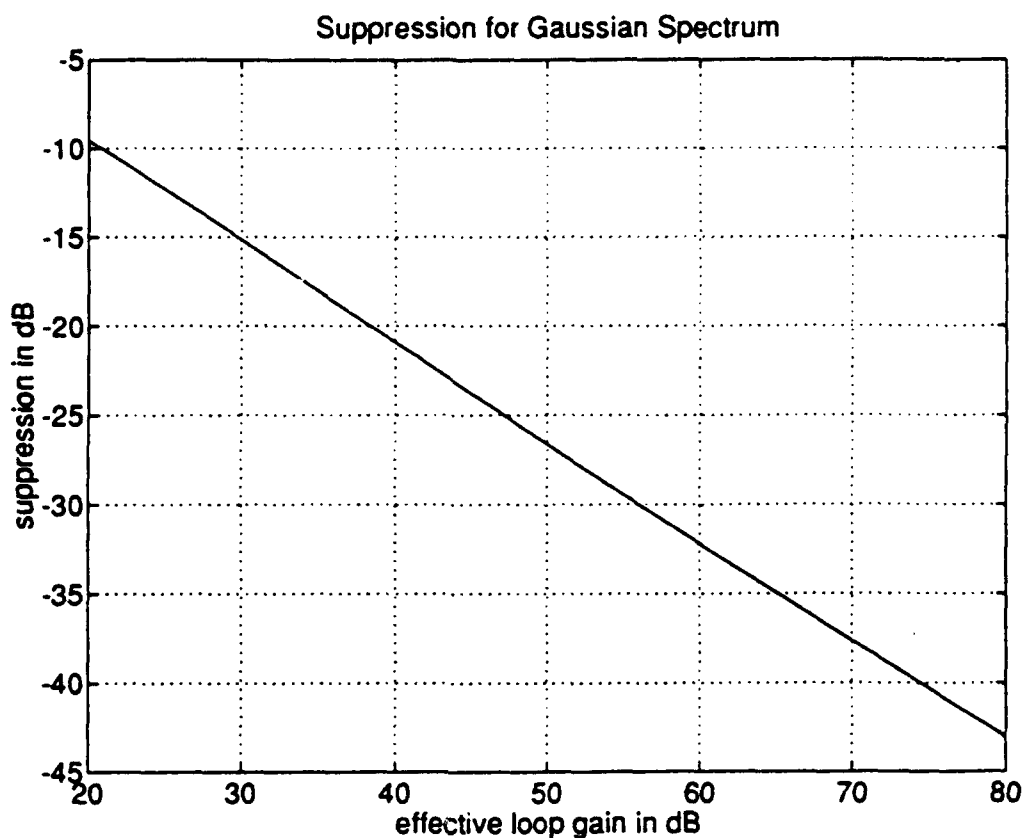
Figure 3.1. Suppression Performance With Gaussian Spectra

Figure 3.3 shows what effect filtering the reference has on the suppression performance of the processor. In this figure, the reference signal has been filtered with a Gaussian filter having the same bandwidth as the original signal. The filtered reference is scaled so that the total power in the reference remains at unity. This figure indicates that there can be significant performance improvement if the reference signal is filtered. Unfortunately, in a practical system in which the input is a jammer over which one has no control, it may not be practical to filter the reference signal.

The phenomenon of reduced signal suppression at frequencies for which the signal spectrum is low also manifests itself when there is multipath. In the presence of a single specular multipath component, the signal spectrum will fluctuate sinusoidally. At frequencies having a low signal spectral density, the suppression performance will be reduced. Figure 3.4 shows the effect that a single specular multipath component will have on the performance of the adaptive processor. In 3.4(a) the signal input has multipath with the indicated amplitude but there is no multipath on the reference. In 3.4(b) both the signal and the reference have identical multipath amplitude and delay. The two curves in this figure indicate the limits of performance depending on the phase of the multipath relative to the main signal. The lower curve is for the case that the multipath has the same phase for both the signal and the reference. In the upper curve the phase of the multipath on the reference is shifted 180 degrees with respect to that on the signal. It can be seen from this
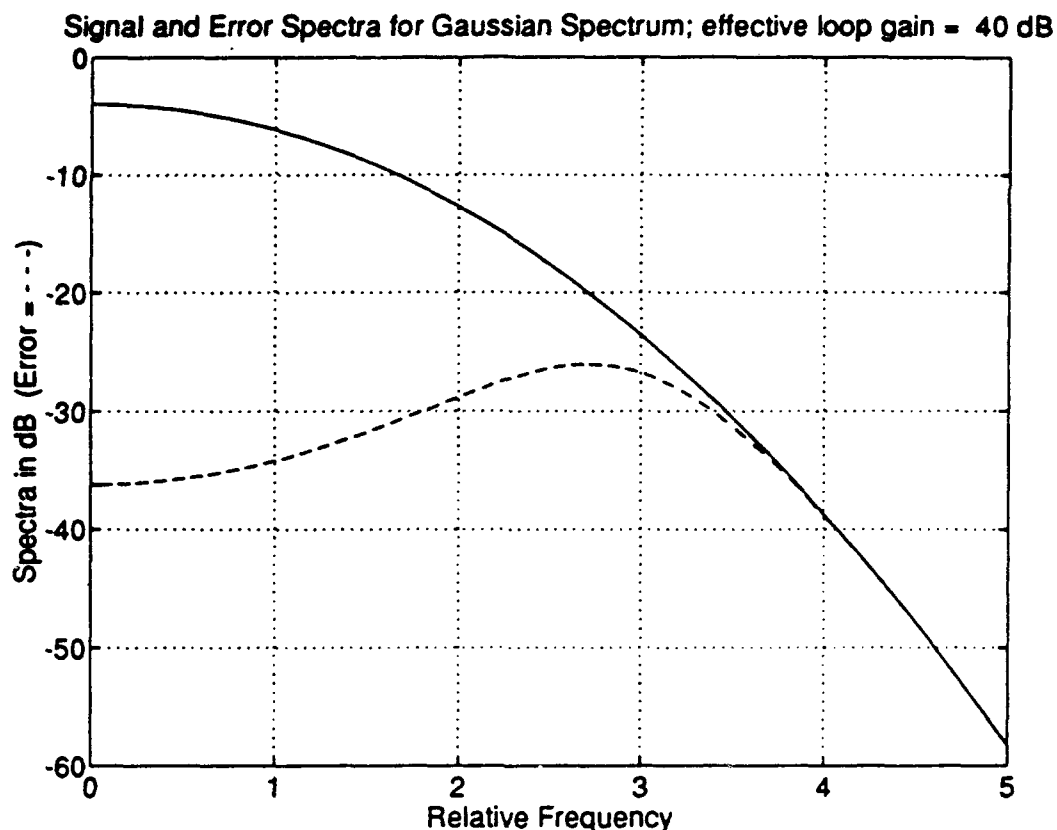
Figure 3.2. *Signal and Error Spectral Density*

figure that with significant multipath there is no guarantee that even an ideal adaptive processor will have particularly high performance.

3.3.2 Performance Results With Finite Integration

The effects of time truncation in the adaptive processor can be accommodated by using Eqs. 3.11 and 3.12. Although these equations do not provide the insight that the previous equations did, they have the advantage of accurately describing the effects of the truncation. For the most benign scenario in which there is no multipath, Figure 3.5 shows that the effects of truncation are not very significant in predicting performance of the processor. The figure shows an approximately 2 dB difference in predicted suppression for the two approximations which can be attributed to the truncation.

The effects of truncation on the processor are most apparent with multipath. Figure 3.6 shows the suppression of interference when the input signal has a single specular multipath component with an amplitude of half the main signal and a delay of 20 percent of the processor time delay. The loop gain in this figure is the actual loop gain rather than the effective loop gain and the time-bandwidth product is 4 so that the effective loop gain is 12 dB below the loop gain shown in the figure. From this figure, it is seen that with 40 dB of effective loop gain, which is equivalent to 52 dB of actual loop gain, the anticipated suppression should be between 17 and 18 dB. Reference

Effect of Filtered Reference with Gaussian Spectrum
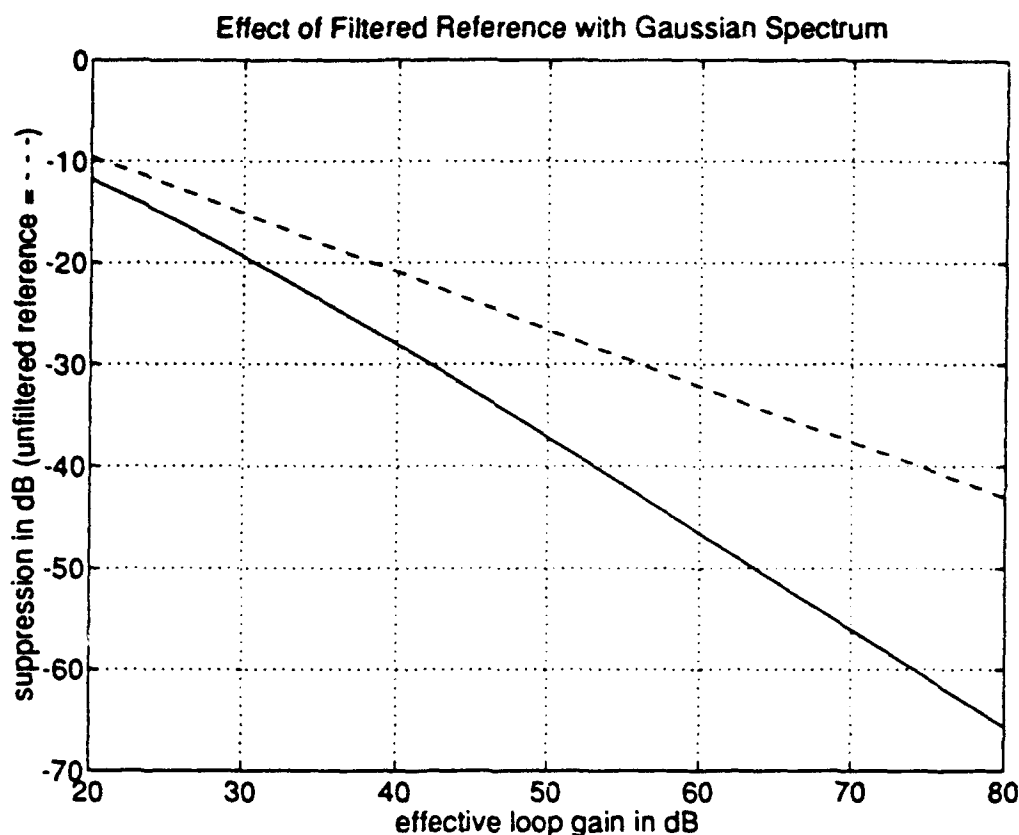
Figure 3.3.   Effect of Reference Signal Filtering on Suppression Performance

to Figure 3.4(a) shows that for multipath 6 dB below the main signal the suppression should be 18 dB. We conclude from this that there is little, if any loss in this case due to the finite length of the processor delay line.

Some insight to the reason for the low loss can be gained by looking at the weight function, $w(x)$. This function is shown in Figure 3.7 for several different values of loop gain. For this computation, the reference signal is a delayed version of the input without multipath; the delay value in this case is 10 percent of the overall processor delay. It can be seen from the figure that the processor has inserted time delay in the signal path to equalize the delay in the reference path. In addition to an overall delay, the processor has attempted to invert the multipath with a set of weights with alternating sign separated from one another by the multipath delay. If the processor were to exactly invert the multipath the weight function would be an infinite series of pulses with alternating sign and with amplitudes in the ratio of the multipath amplitude. From the figure, this amplitude ratio appears to be nearly 0.5 justifying the interpretation that the processor is inverting the multipath. The effect of finite time delay in the processor is to truncate the series.

With this interpretation it would appear that if the multipath delay were to increase the series would be truncated to fewer terms. This would result in a poorer approximation to the inverse and less suppression. Figure 3.8 shows that this is exactly what happens. This figure shows the suppression in a processor with 60 dB actual loop gain when the input signal has a single specular multipath component as a function of the delay on the multipath. The reference delay is 0.1 so that

- 19 -

Worst Case Multipath Effect for 40 dB Effective Loop Gain
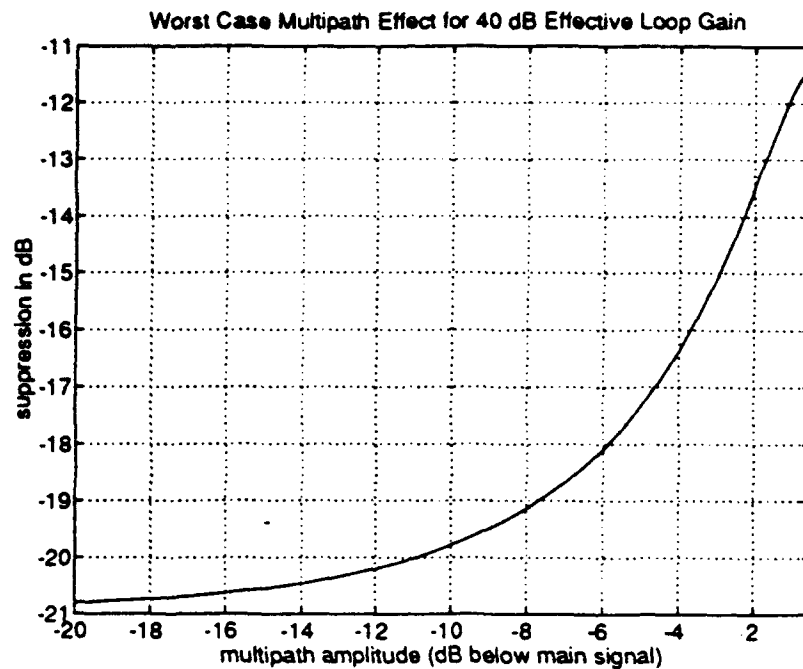
(a) Multipath-free Reference

Worst Case Multipath Effect for 40 dB Effective Loop Gain
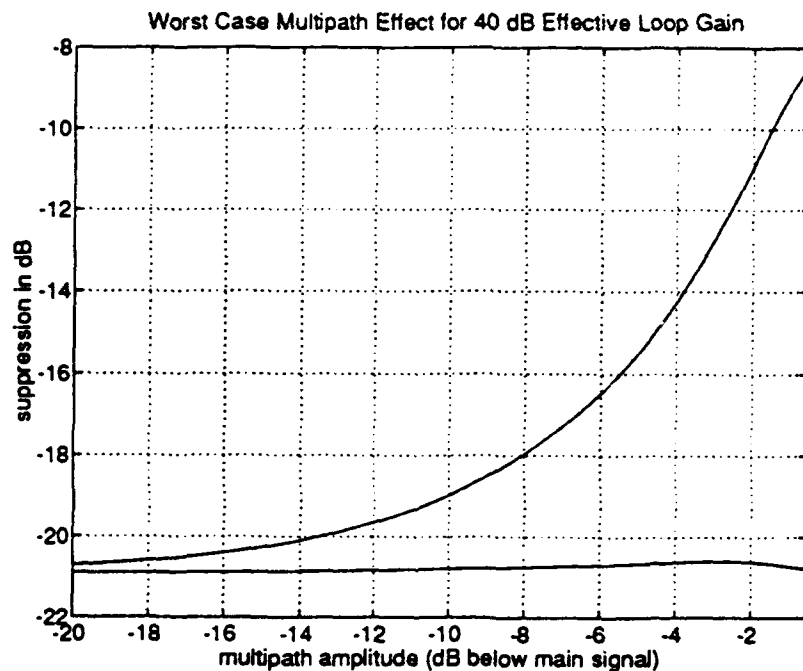
(b) Multipath on Reference

Figure 3.4. Effect of Multipath on Interference Suppression

Suppression for Gaussian Spectrum
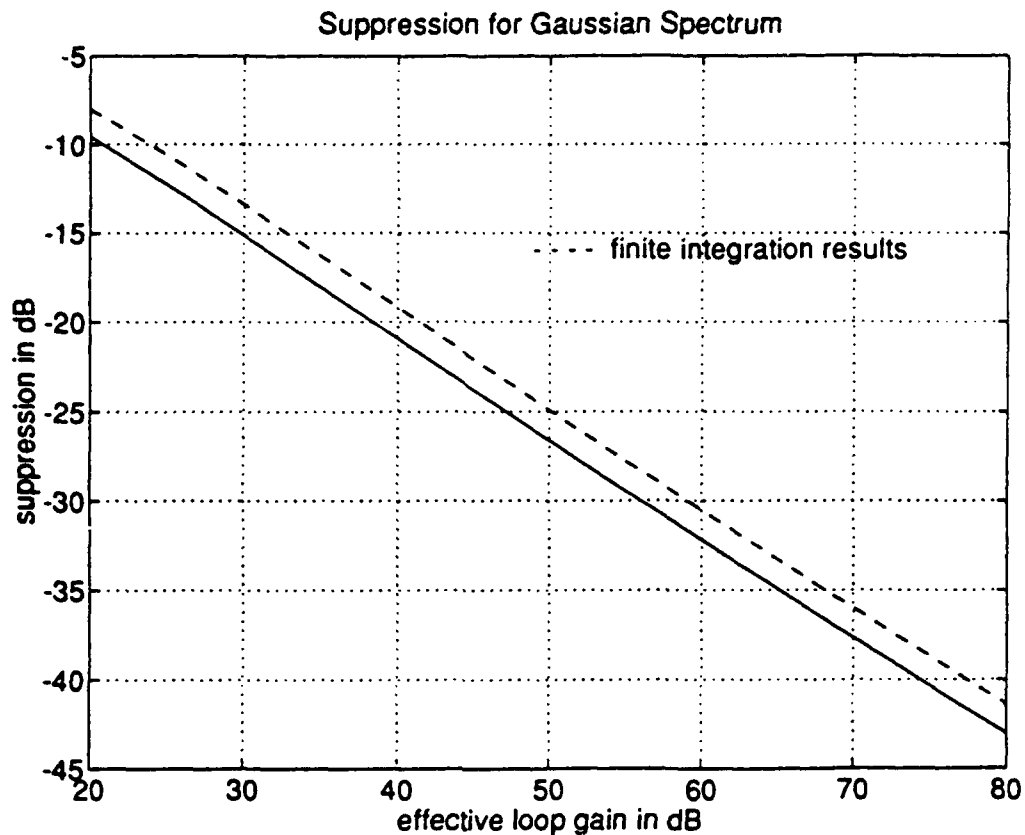
Figure 3.5.   Effect of Finite Integration Interval on Processor Performance

with a multipath delay of 0.1 there will be 9 terms to develop the inverse. There is very little difference in suppression performance until the delay exceeds 0.225. At that delay, the number of terms to develop the inverse drops from 4 to 3. Similar steps in performance loss occur at multipath delay values of 0.3 and 0.45. One concludes from this example that if the multipath is 6 dB below the main signal, a processor time delay of at least 4 times the multipath delay will be required. Unfortunately, increasing the processor delay to accommodate multipath will reduce the effective loop gain which will also reduce suppression performance. The selection of processor memory will be a tradeoff of these conflicting requirements.
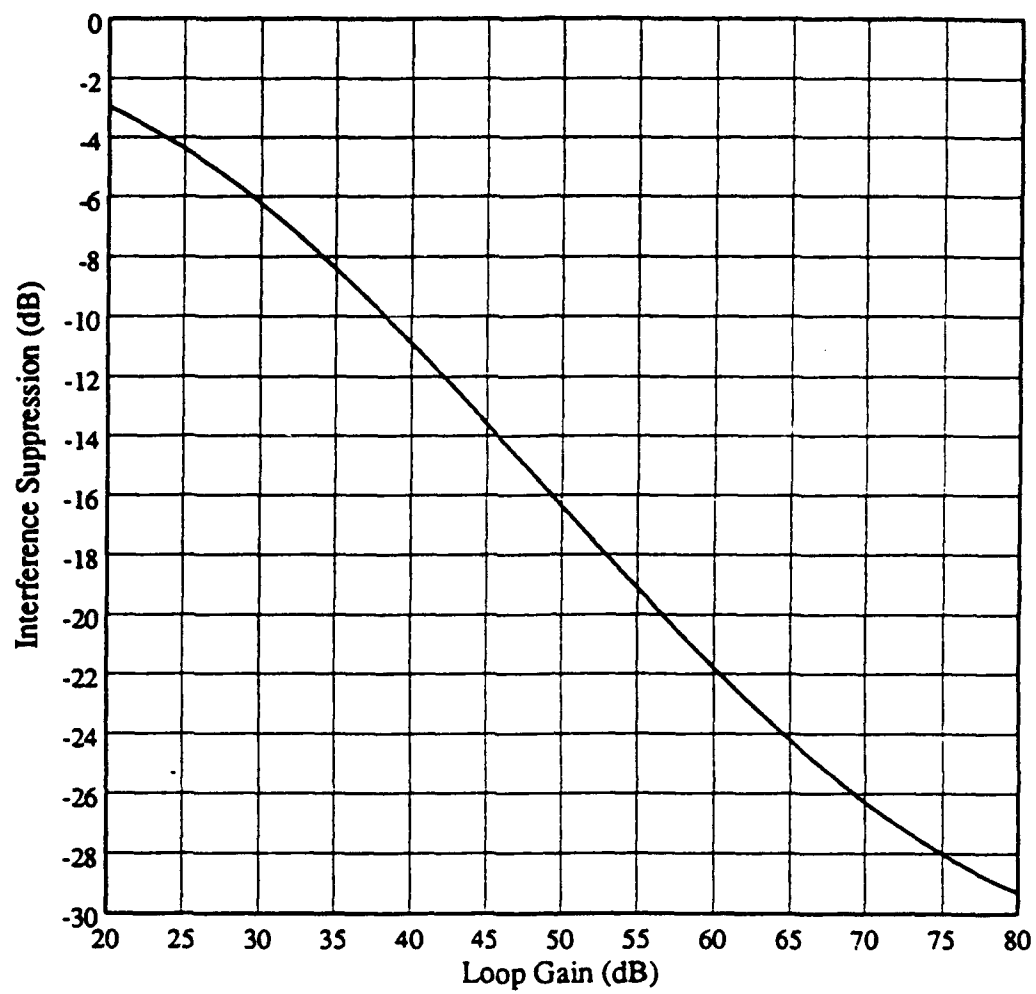
Figure 3.6.   Suppression With Short Delay Multipath
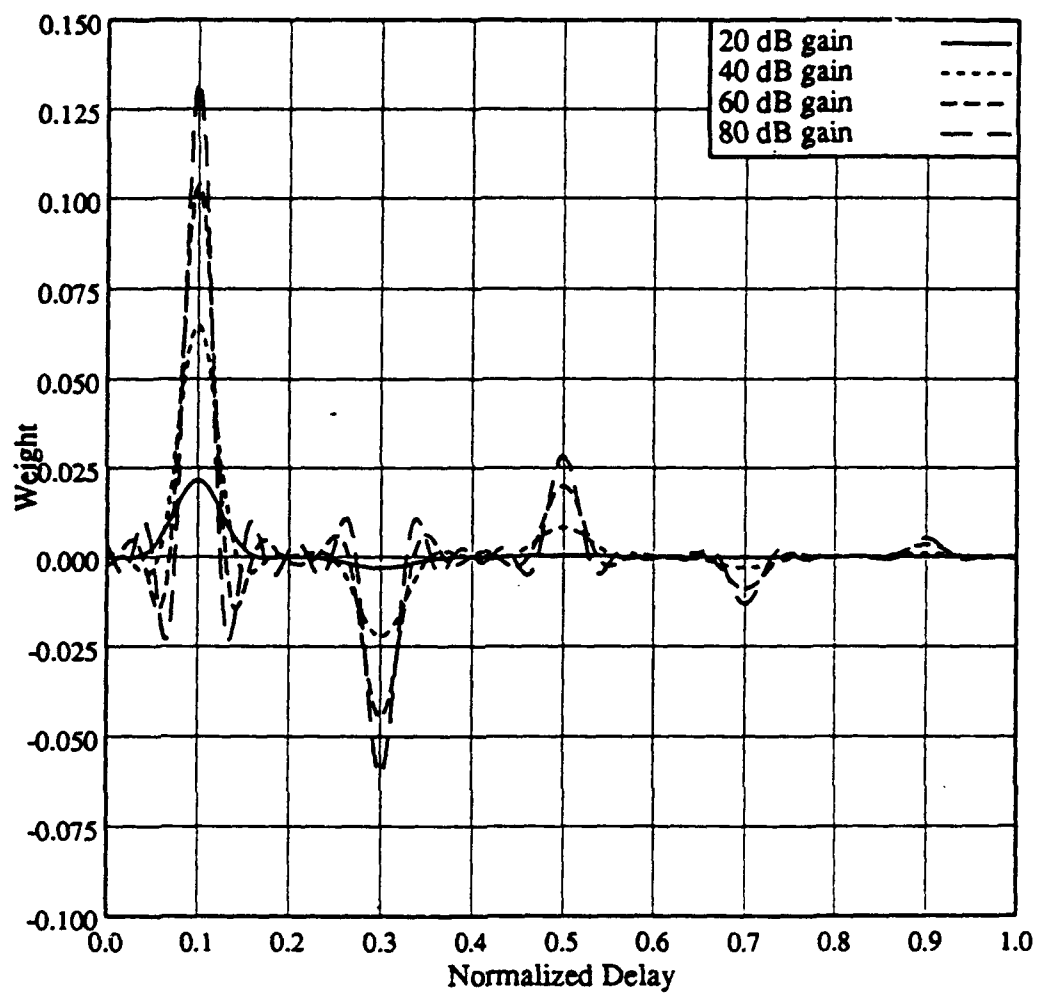
Figure 3.7. Weight Function With Multipath

Loop Gain = 60 dB
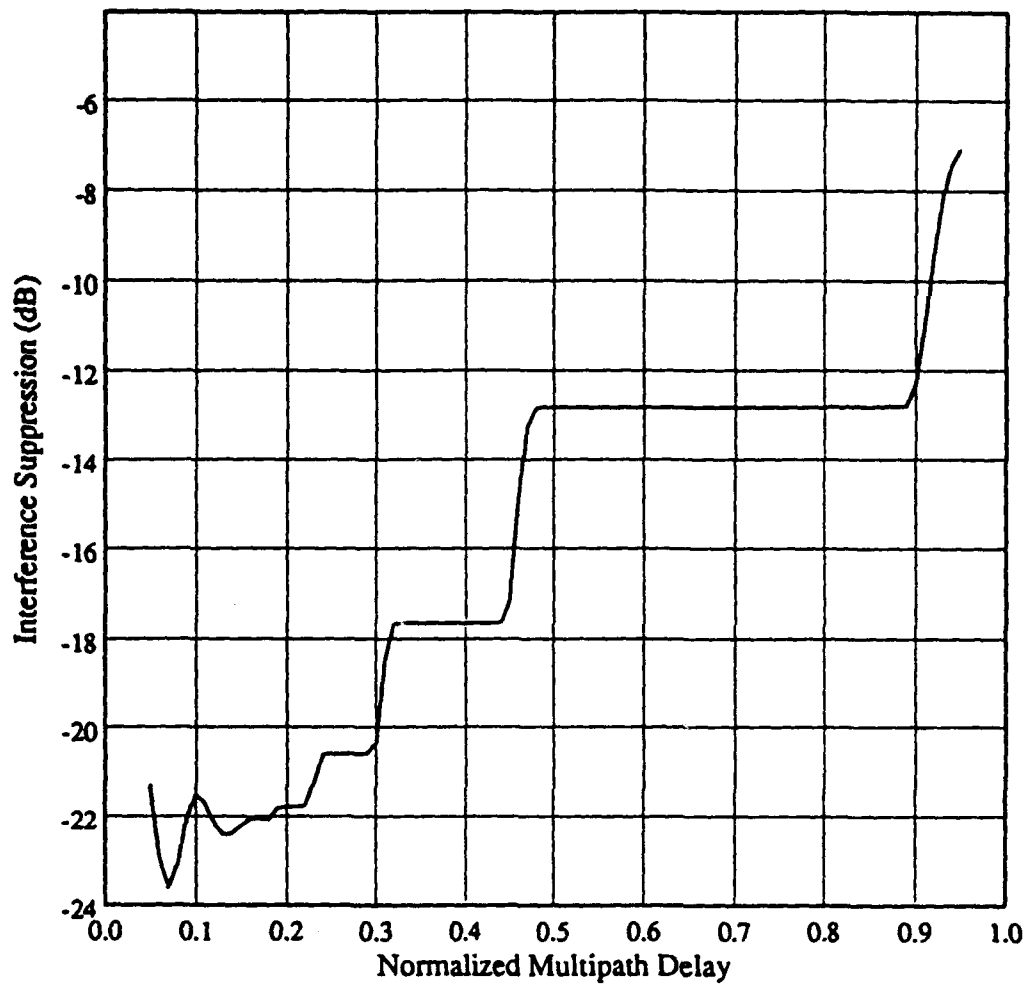
Figure 3.8.   Effect of Multipath Delay on Suppression

4.0 TIME DOMAIN SIMULATION

In order to explore the effects of amplifier limiting and loop time delay in the closed loop system a step-by-step time simulation of the system was created. The approach is a simple, brute force approach where the signal is represented as an actual time domain waveform with no complex signal representation. This method provides direct representation of signal delay and signal limiting. A time sampling grid of 8 samples per cycle at 170 MHz provides accurate signal representation. Integration is carried out by simply summing the appropriate samples to be integrated. Time delay is implemented with arrays and recirculating pointer indices.

The price paid for this simple, direct representation is a large number of computations. Even with this burden a simulation of a six-channel system with 1 µs delay lines and 500 µs simulation time consumes approximately an hour of CPU time on a 10 MIPS computer. This simulation program has proven to provide invaluable insight into the operation of the algorithm and the effects of limiting and time delay in the feedback path. There is excellent correlation between the simulated performance and the system performance.

4.1 CW Simulation Results

The parameters used throughout the simulations are the values shown in Table 4.1, unless they are explicitly stated to be otherwise. These parameters correspond closely to those in the experimental system.

Table 4.1. Parameters Used for Simulation

Photorefractive time const	3.0	ms
Center frequency	70.0	MHz
Loop time delay	12.3	ns
Loop gain	60	dB
Reference level	0	dBm at sum pt.
Signal voltage limit	-17	dBm at sum pt.
Photodetector noise	-74	dBm (1 MHz)
Samples per cycle	8	
Delay line length	1.0	µs
Number of aux. channels	6	

In the figures describing limiting and noise, the reference for the limiting, suppression, and noise is always the level of the reference component. The terms desired signal, interference, and reference are all used to describe the component which is to be cancelled. We will use the term reference for this quantity in this report. The output from the processor is referred to as the error signal. The suppression is the ratio of the mean squared value of this error signal to the reference level. The mean square value is computed broadband. That is, the mean square value is obtained by simply squaring the error signal and passing the result through a low pass filter (2 µs time constant) without filtering prior to the squaring operation. The effective noise bandwidth for this simulated system is one half the sampling rate or 280 MHz.

Figure 4.1 shows the performance with the limit set at -22 dB and with and without simulated detector noise added. Also, the effect of detecting the error signal before or after the limiter is shown. The limiter has an effect only during the time when the error level is high while the noise has an effect only when the error level is low. These curves show the suppression and time constants which are predicted by the simple theory represented by Eq. 2.12. The curve labeled "with noise" shows the result when the photodetector noise is inserted at a level of -79 dB (in 1 MHz bandwidth) relative to the reference level. This noise level is the nominal level achieved with the actual circuits in the experimental system. When noise is added the simulated broadband suppression broadband drops from 60 dB to near 53 dB. This is in good agreement with the 45-50 dB suppression obtained in the system measurements.

The noise affects the suppression in two ways. The noise is not suppressed by the adaptive filter and it shows up directly in the broadband (280 MHz) detector at a level of -79 +10 log (280) or -55 dB relative to the reference.

The second way the detector noise enters the problem is in its effect on the adaptive weights. To achieve a suppression level of sup dB the noise induced error in the weights must be less than sup relative to the actual weights. Also the error signal creating the weights is sup dB below the unsuppressed reference level. Therefore, the noise induced fluctuation and hence the noise relative to the unsuppressed reference must be twice sup in the bandwidth of the photorefractive material. To achieve 60 dB suppression the noise in a 50 Hz bandwidth (3 ms time constant) must be
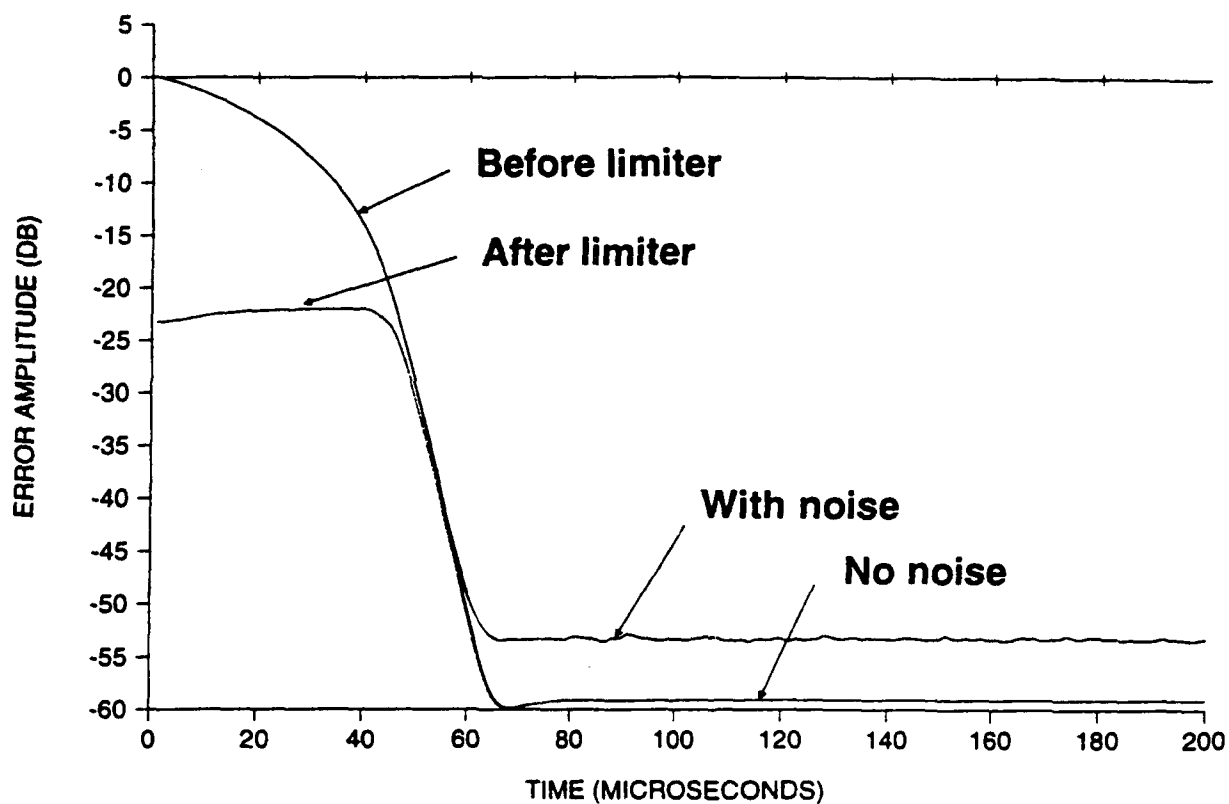
Figure 4.1. Effect of Detector Noise on CW Suppression

more than 120 dB below the reference level. The noise inserted is -79 dB in 1 MHz bandwidth or -122 dB in a 50 Hz bandwidth. Therefore the noise level on the weights is influencing the suppression at about the -60 dB suppression level where the system operates.

To separate the effect of direct noise contribution from the reference contribution to the error signal we use a narrow-band measurement of the error. In the simulation this is accomplished by performing a Fourier transform of the error signal and examining the component at the frequency of the reference input. The result of this Fourier transform procedure is shown in Figure 4.2. This result indicates that the suppression of the reference sine wave is still 60 dB even in the presence of the noise. It is the direct noise contribution to the error which reduces the broadband detected suppression to be reduced to -55 dB.

4.2 Simulation Results for Modulated Reference Signals

The first broadband simulation are made without a limiter in the system in order to provide a basis for understanding the more complex situation when the limiter is present. Broadband signals were generated by using a random binary modulation (square wave) at various bit rates. As explained in Section 3.0, this type of waveform has a sinx/x shape for its spectrum. Because of the relatively slow drop of power with frequency this is an especially difficult waveform for the LMS type processor.
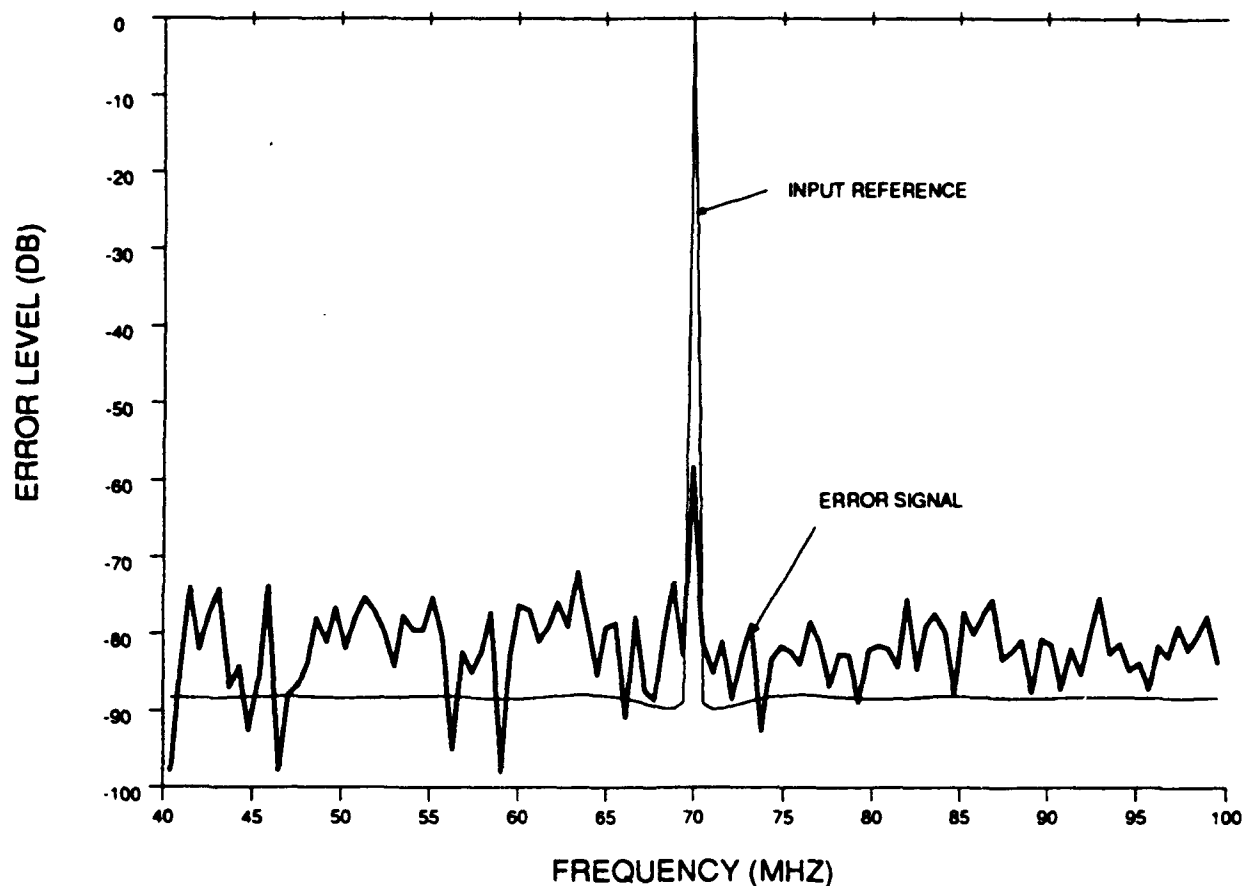
Figure 4.2. Spectrum of Suppressed CW Signal

Figure 4.3 shows the simulated transient response for a bit rate of 5 MHz, with and without limiting at -17 dB below the unsuppressed reference level. The CW suppression curve is included for comparison. The 5 Mb/s modulation reduces the suppression from 60 dB to approximately 12 dB. The limiter appears to help the suppression somewhat, but this is not the case. The rms level of the interferer is lower, but the system is in limit for significant periods of time. During these periods the desired signal will also be suppressed. In order for the cancellation system to be effective it must bring the suppressed interference level below the limiting level.

In Figure 4.3, the data is computed prior to the limiter. Figure 4.4 shows the error signal levels after the limiter for three square wave modulation rates. The limiting level is at -7 dB relative to the uncancelled reference.

The effect of data rate on suppression without limiting is shown in Figure 4.5. This set of curves provides some additional insight into the problem that the LMS algorithm has with signals which have slow rolloff spectrum. The 100 kHz data rate curve shows that the system adapts to a high rejection ratio, then a large error transient occurs when a bit transition passes over the active taps on the delay line. This effect could be reduced by softening the transition edges which is equivalent to filtering out some of the high frequency content and producing a spectrum which rolls off at a more rapid rate. If the loop gain could be increased further, then the tap weight distribution would become more peaked over a narrow delay range and the duration of this transient effect would be decreased. In that sense this effect is due to the finite loop gain. In an idealized situation these transient errors disappear entirely when a true integrator is used in the feedback path (infinite dc gain). In a realistic situation the system dynamics are such that the ideal steady-state distri-
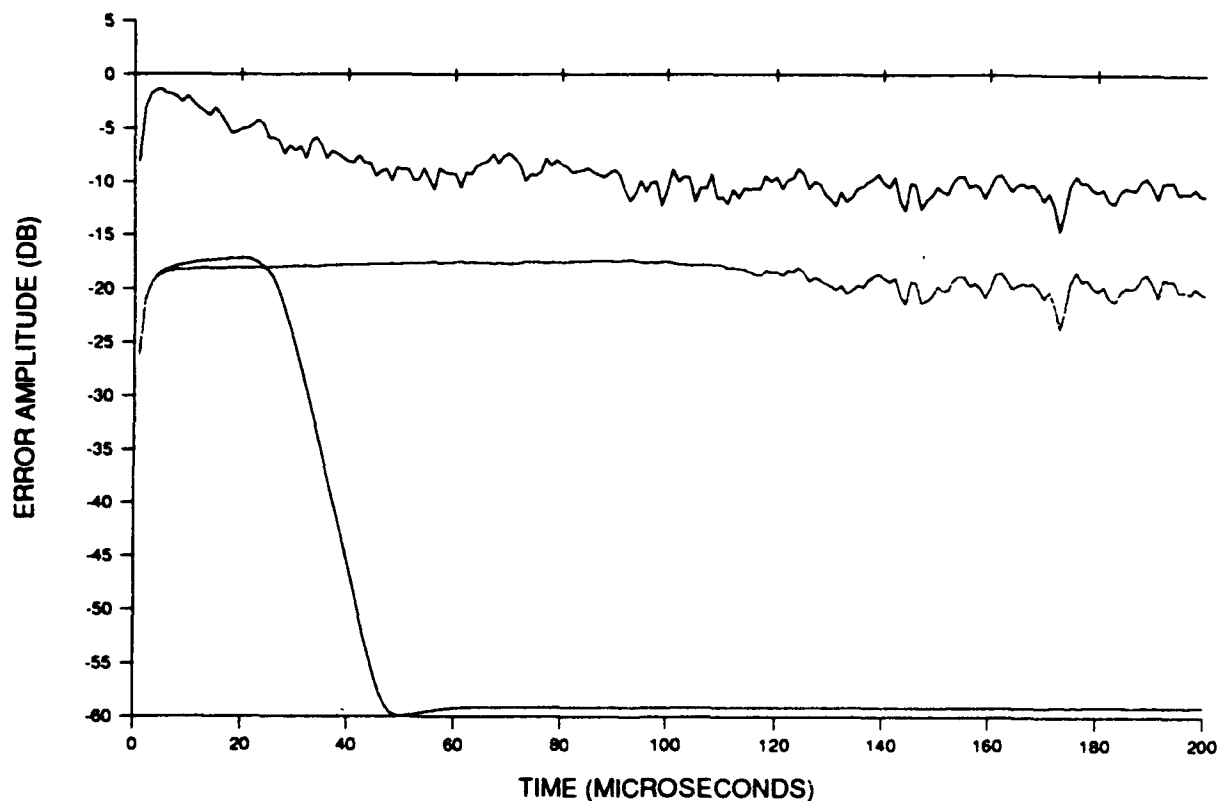
Figure 4.3. 5 MHz Suppression With and Without Limiting

- 28 -
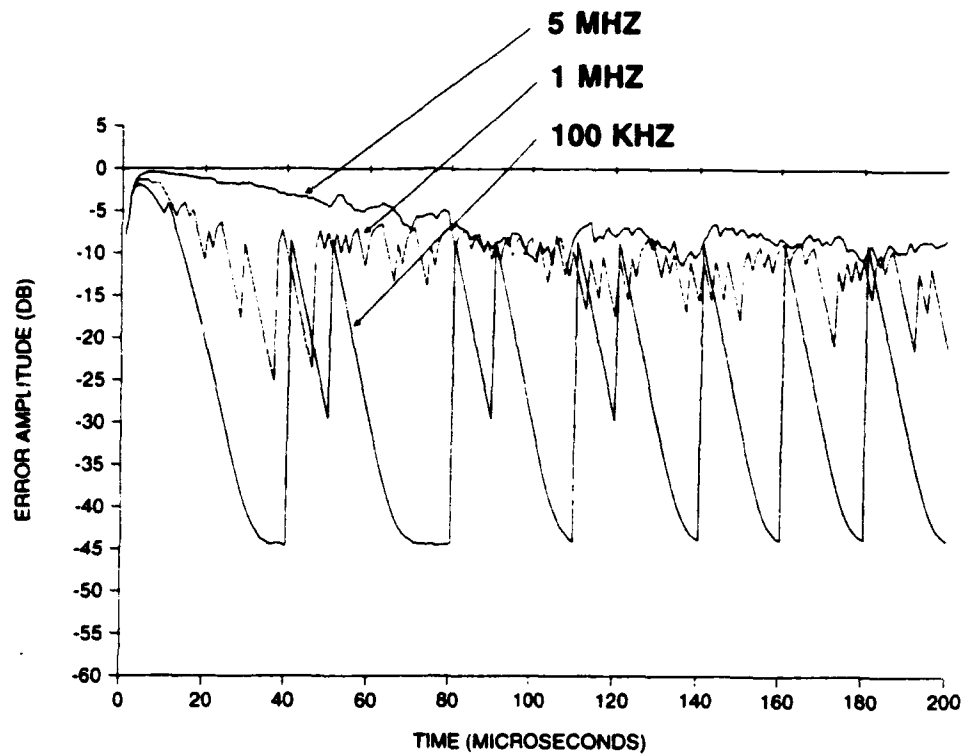
Figure 4.4. Suppression at Limiter Output for Various Modulation Rates
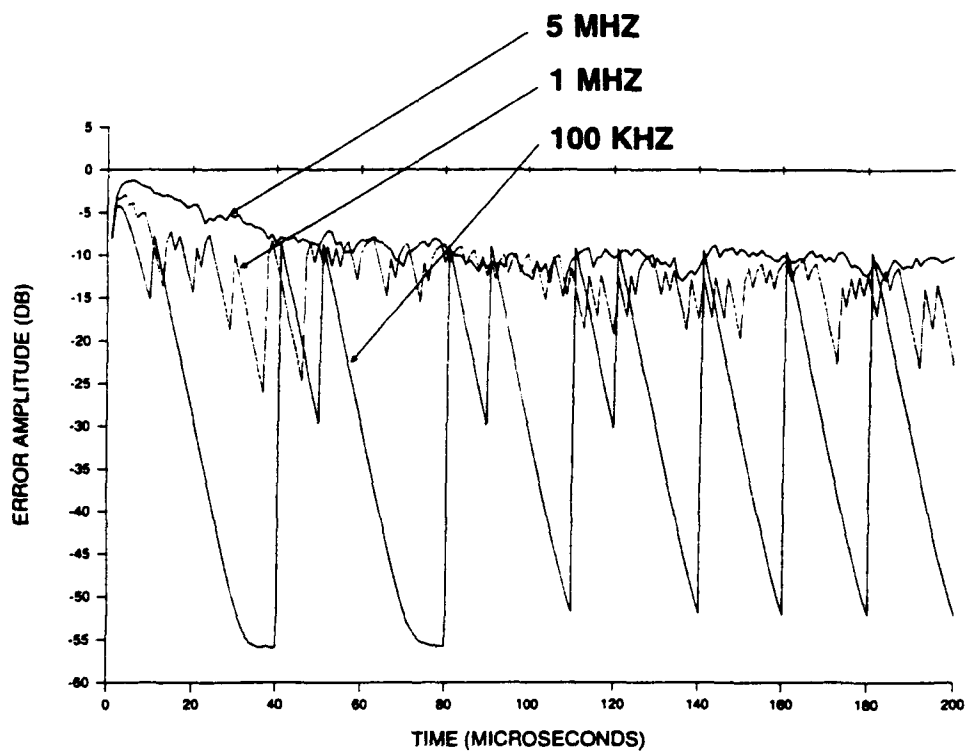
Figure 4.5. Suppression for Several Modulation Rates Without Limiting

bution would never be reached because of the dynamics of the system inputs. In mathematical terms a realistic system is not stationary.

The tap weight distributions in a single channel for 1 MHz and 5 MHz data are shown in Figures 4.6 and 4.7, respectively. For an ideal canceller with no noise both the distributions would be an impulse at the appropriate delay value where the auxiliary signal matches the reference.

The spectrum of the error signal also illustrates the nature of the problem of cancelling broadband signals. Figure 4.8 shows the spectrum of the error signal along with the spectrum of the input reference. The canceller suppresses the strong central components, but it has little effect on the weaker outlying components. The spectral components may be viewed as many independent interferers. Since the loop gain of the LMS processor is proportional to signal power the loop gain for the weaker spectral components is low and there is little suppression. The spectrum of the input and the error signal for a 5 MHz random square wave input are shown in Figure 4.8. The suppression for the strong spectral components is in the 40 dB range, but the weak components are hardly suppressed at all. The overall suppression is approximately 12 dB as shown in Figure 4.5.
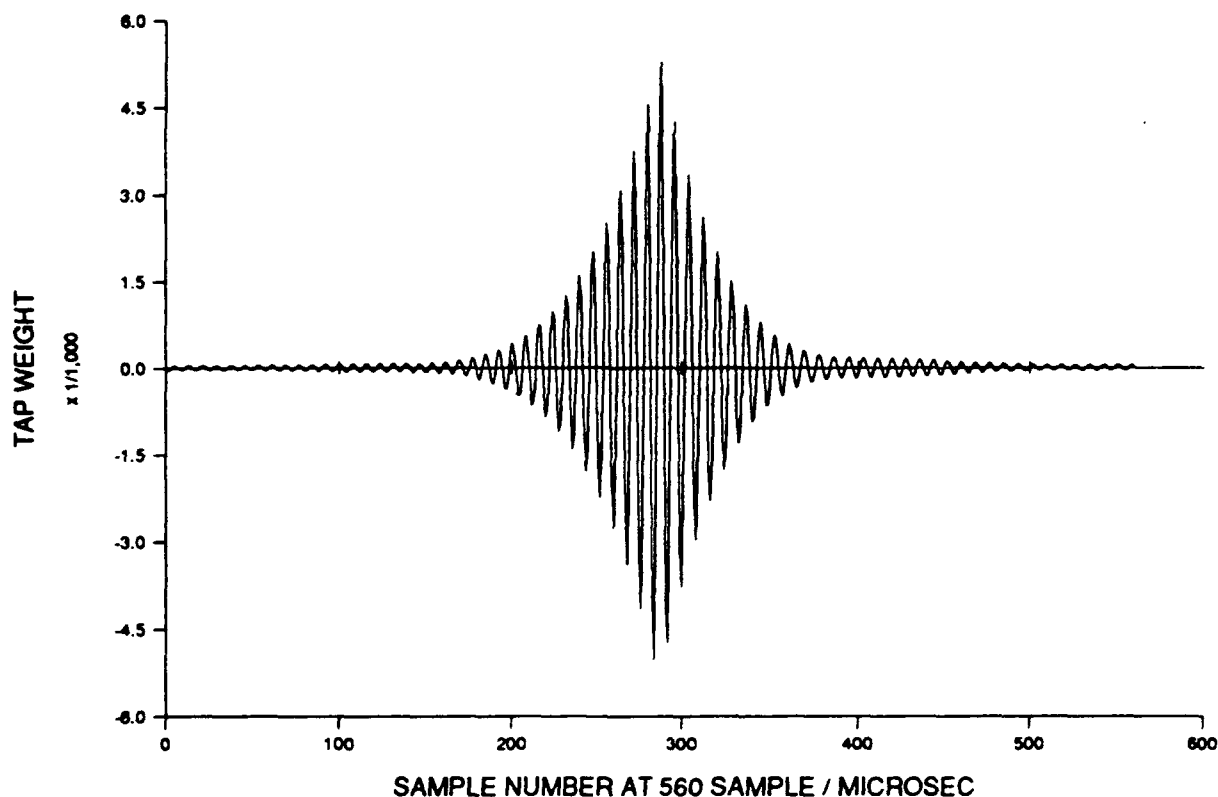
Figure 4.6. Tap Weight Distribution for 1 MHz Signal

- 30 -
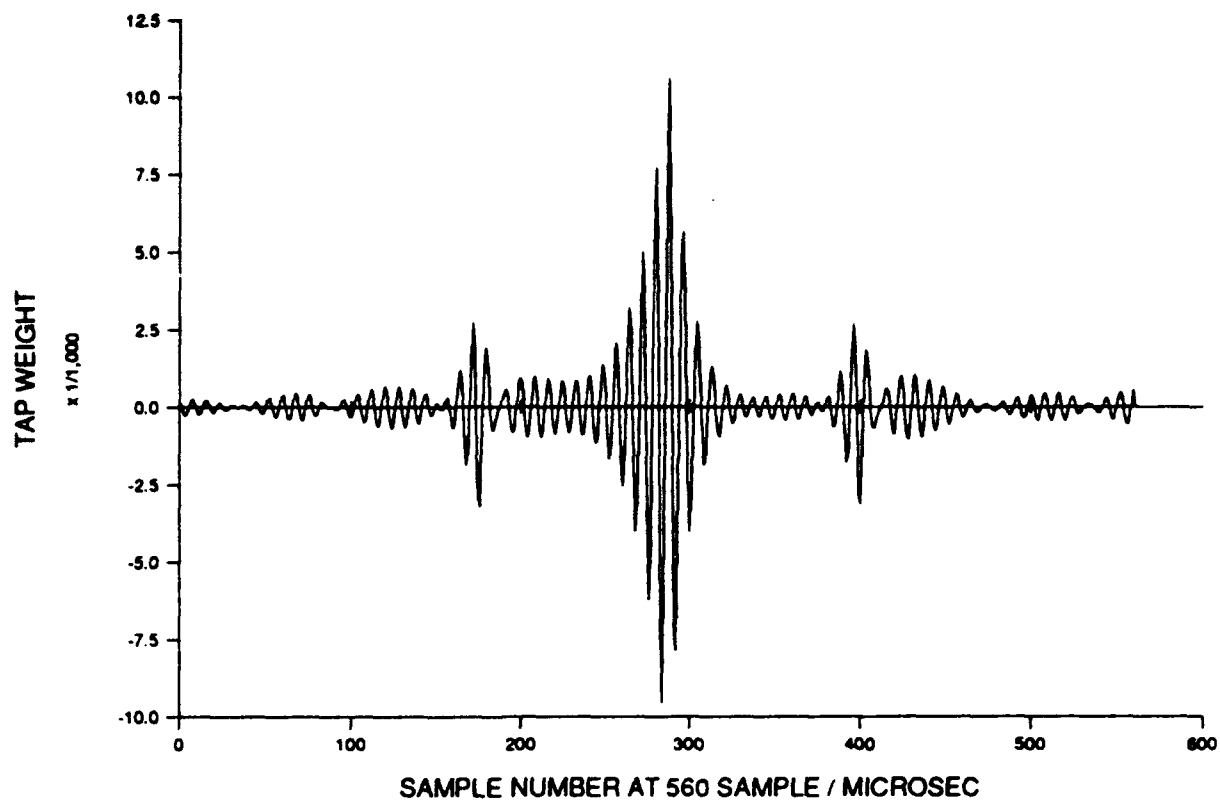
Figure 4.7. Tap Weight Distribution for 5 MHz Signal
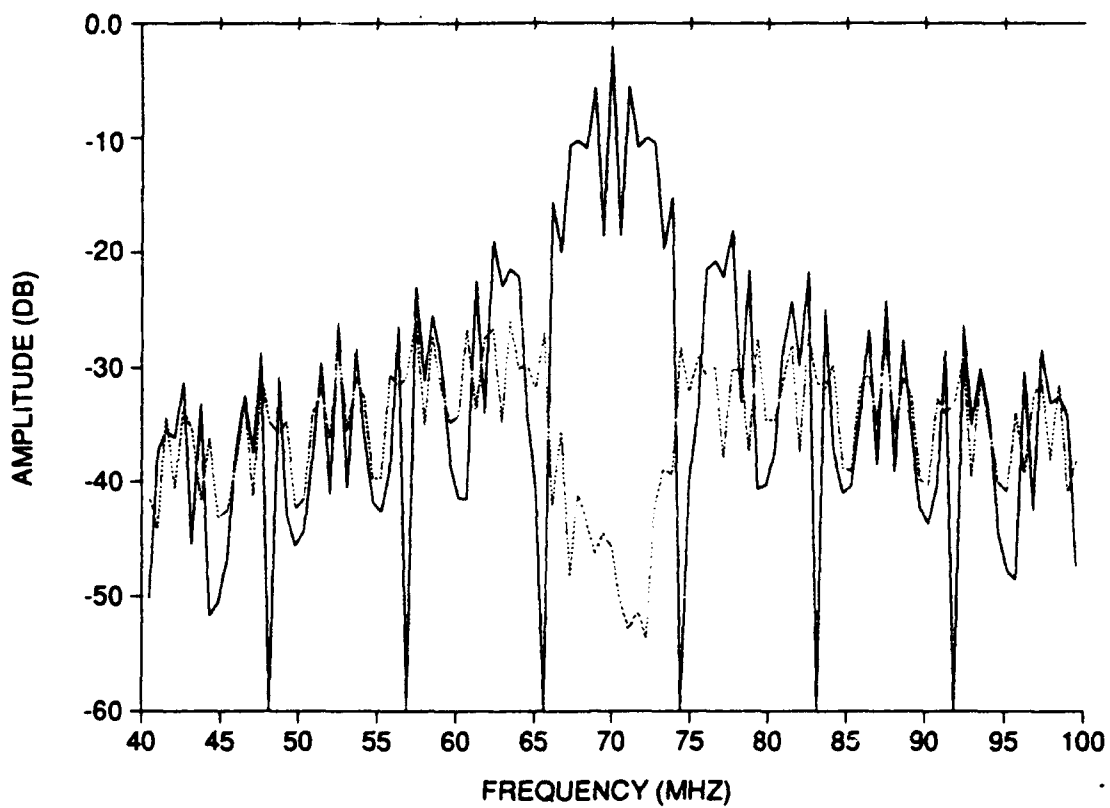
Figure 4.8. Spectrum of Input and Output for 5 MHz Biphase Modulation

- 31 -

5.0 PHOTOREFRACTIVE PROCESSOR

Implementation of the process described in Section 2.0 requires a processor which multiplies the error in the signal estimate times the signal vector components and low pass filters (integrates) the resultant products. It must also multiply the integrated products times the corresponding signal vector components and sum these results to form the estimate of the desired function, D. The system implemented on this program used an array of acousto-optic Bragg cells to generate the signal vector components. A photorefractive integrator is used in a time integrating correlator configuration to provide the multiplication and integration. The system accepts signals from each of six antenna array elements and one reference signal input. It forms an estimate of the reference signal based on a weighted linear sum of delayed signal components (taps) from each of the six-channels. A six-channel Bragg cell provides the necessary six-channel delay. The photorefractive material provides the variable tap weights and the summing is carried out by the combination of a lens and photodetector. This signal estimate is subtracted from the reference function to form an error signal which is then correlated with the delayed signal components. The tap weights are then modified to reduce the correlation to zero.

5.1 Time Integrating Bragg Cell Correlator

An acoustic Bragg cell produces an intensity pattern at its output surface which is an image of the acoustic wave. For an input signal, $S(t)\cos\omega_c t + N(t)$, this intensity is a travelling wave of the form

$$I(x,t) = I_0(t)\left[1 + 2\frac{\sqrt{\eta}}{S_0}\left(N + S\left(t - \frac{x}{v}\right)\sin\omega_c\left(t - \frac{x}{v}\right)\right)\right] \qquad \text{(Eq. 5.1)}$$

The normalizing signal S_0 is the rms signal level required to produce the diffraction efficiency η.

If time integrating element is placed in an image plane of this intensity pattern and the source producing I_0 is modulated with a reference signal to produce illumination of the form,

$$I_0(t) = P_0(1 + mR(t)\cos\omega_c t) \qquad \text{(Eq. 5.2)}$$

then the integrated exposure, $Ex(x)$, will contain the correlation function between S and R. m is the modulation parameter of the source laser. The result of substituting Eq. 5.2 in Eq. 5.1, integrating with respect to time, and ignoring high-frequency terms is

$$Ex(x) = P_0\left(1 - m\frac{\sqrt{\eta}}{S_0}\sin\left(\frac{w_c x}{v}\right)\right)\int R(t)\,S\left(t - \frac{x}{v}\right)dt. \qquad \text{(Eq. 5.3)}$$

A CCD array could, for example, be used to read this exposure function and extract the correlation values. When the integrating photodetector is a photorefractive element, a structure similar to Figure 5.1 results. In this case, the correlation can be read out optically rather than electronically. This photorefractive integrator is advantageous for implementing various tapped delay line filter architectures where it is desired to multiply delayed signals by correlation values and sum the results.
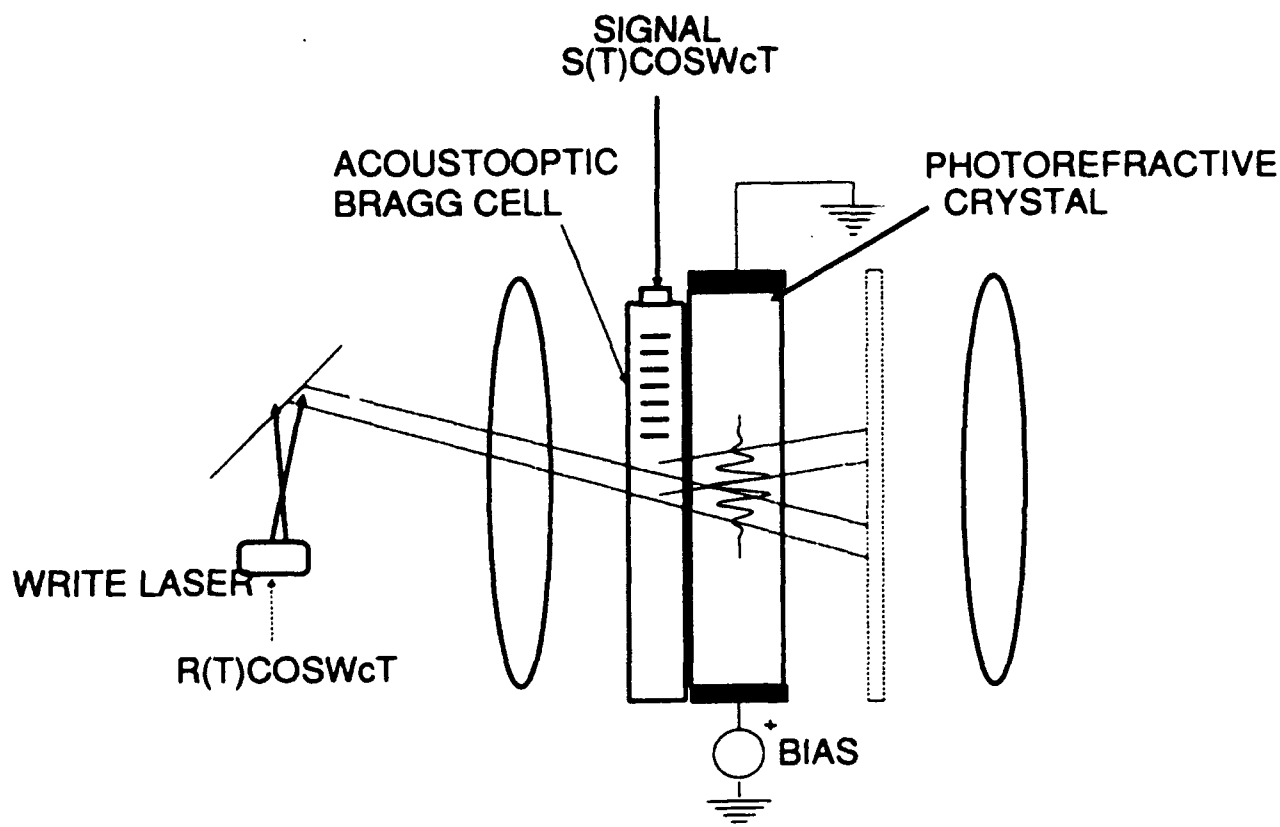
Figure 5.1. Photorefractive Correlation (Write) Process

The key to this system is the previously described action of the Bragg cell as an intensity modulator. That is, the interference of the undiffracted and diffracted light components produces an intensity pattern at the output surface of the Bragg cell. This sinusoidal intensity pattern travels at the acoustic velocity. Modulation of the source at the same frequency as the Bragg cell drive causes the fringe pattern to appear stationary on the photodetector array, producing the exposure function described by Eq. 5.3.

The photorefractive material in the present system is operating with a large, externally applied dc bias field. Under these conditions photorefractive field is equal to the applied bias field times the amplitude of the spatially varying component of intensity divided by the average intensity. For the exposure distribution given by Eq. 5.3 the resulting space charge field is

$$E_{sc}(x) = E_0 \frac{\sqrt{\eta}}{S_0} \sin\left(\frac{w_c x}{v} + \phi\right) \int R(t)\, S\left(t - \frac{x}{v}\right) dt. \qquad \text{(Eq. 5.4)}$$

The refractive index variation is proportional to this electric space charge field and the grating diffraction efficiency is proportional to the refractive index variation squared. The phase angle, ϕ, is the phase angle between the optical intensity pattern and the refractive index grating produced by that intensity. The actual value of ϕ is a complex function of the material parameters and bias conditions. Generally, for high bias, drift dominated conditions ϕ is zero. For diffusion dominated conditions ϕ is $\pi/2$.

A second laser (read laser) may be used to read the grating resulting from the combined Bragg cell and photorefractive material. This resultant effective grating varies in time as the moving acoustic grating propagates past the stationary photorefractive grating. In effect, the correlation coefficients are multiplied, point by point, by the delayed, incident signal. A lens sums the intensity components from the delay positions on the photodetector as shown in Figure 5.2.

The combination of the read and write functions forms a basic structure in which correlation coefficients are computed and multiplied with delayed signal components. This basic structure is the fundamental building block for the implementation of the LMS algorithm[13]. This algorithm, in turn, is a basic algorithm for implementing many types of adaptive filters and optimal estimators. It has application in interference cancellation, antenna beamforming, null steering, direction of arrival estimation, and frequency estimation. A symbolic block diagram of the generic correlation cancelling loop implementation of the LMS algorithm is given in Figure 5.3.

The first feature to note on this diagram is the series of delay elements of across the top of the diagram. These delays and the first row of multipliers are implemented in the time integrating correlator of Figure 5.1. The signal to be processed, S(t), which contains some desired component D(t) is input at the left side of the diagram. A locally generated replica of the desired quantity to be estimated (referred to as a reference in the present context) is input on the right. The output of the summing node is an estimate, E, of the desired component of the signal. The difference between the reference and the signal estimate is fed back to the multipliers which feed into the integrators to produce tap weights.
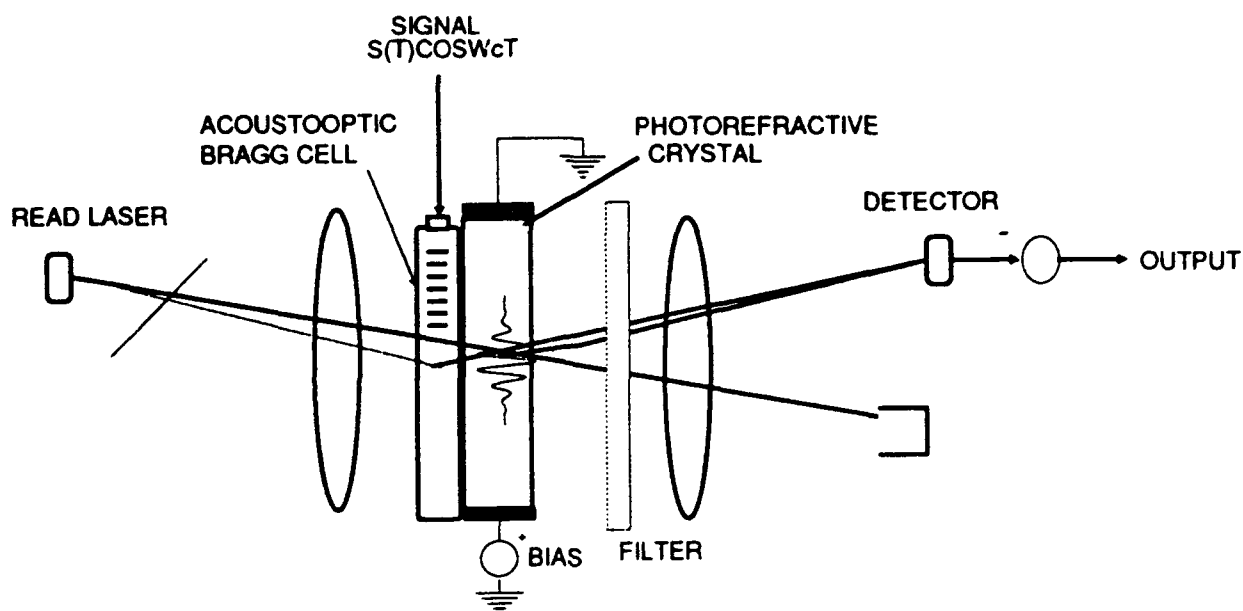
Figure 5.2.   Readout Process
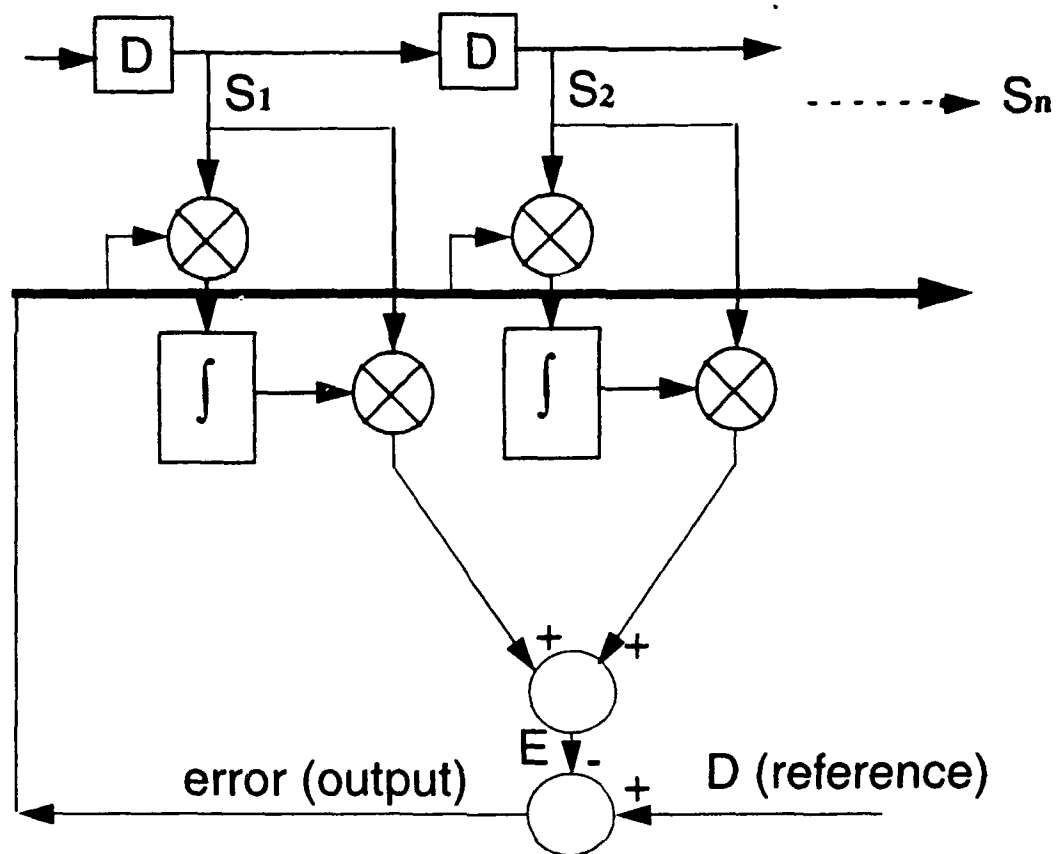
Figure 5.3. General Diagram for Correlation Cancelling Loop

There are two separate functions shown in the diagram of Figure 5.3; one is computing correlation coefficients (tap weights), and the second is the formation the signal estimate by applying the tap weights to the delayed signal components. In the photorefractive adaptive filter these functions can be separated by using a modulated laser (write laser) to implement the time integrating correlator and a second unmodulated read laser to form the signal estimate from the weighted, delayed components. The same Bragg cell serves as the delay element for both purposes. The time integrating correlator produces the correlation coefficients as a stationary refractive index grating in the photorefractive material.

5.2 Photorefractive Correlator With Optical Readout

Once this stationary grating has been formed, the readout process (using the second laser) can be considered as a completely separate process. The readout process consists of detecting the interference between the frequency shifted light diffracted by the moving acoustic signal and that diffracted by the stationary correlation coefficients. The product of the signal and tap weights can thus be taken from the cross-product term (heterodyne beat) between these two optical components.

In the acousto-optic/photorefractive combination there are two refractive index gratings. The photorefractive grating has a diffracted light field strength, η_1, proportional to Esc as expressed by Eq. 5.4. The refractive index grating propagating in the Bragg cell has a diffracted light field strength, $\sqrt{\eta_1}$, proportional to the acoustic strain. The total grating is a combination of these two. A complete solution of the diffraction from these two thick phase gratings is quite complex and very dependent on the geometry. For purposes of this discussion, and for many other practical purposes, the grating strengths can be summed. The diffracted light intensity at any given x location is then proportional to the square of the sum of these two diffracted field components. The cross-product term in this squared sum is separable because the motion of the acoustic wave causes a fluctuation at the carrier frequency ω_c. A phase shift exp $(i\omega_c T_d)$ appears in the stationary photorefractive grating and a cancelling exp $(-i\omega_c T_d)$ appears in the travelling acoustic grating. Therefore, the phase of the output intensity modulation is independent of the signal delay T_d.

In the small diffraction efficiency approximation the total light power deflected from a region of width dx at location x is

$$dP_d = I_0 (\eta_1 + \eta_2 + 2\sqrt{\eta_1 \eta_2}\sin(\omega_c t + \phi))\, dx. \qquad \text{(Eq. 5.5)}$$

The time variation in this equation is written as a sine function (90 degrees phase shift relative to the cosine source modulation) in recognition of the 90 degree phase shift between intensity and acoustic strain. This leaves the remaining phase, ϕ, as the phase shift between the intensity pattern and the resultant photorefractive grating. In this way, ϕ corresponds to the phase shift usually referred to in the literature concerning the photorefractive effect.

When a separate, unmodulated, probe beam is used, the probe power deflected to the photodetector is sinusoidally modulated at the carrier frequency with a phase which is always 90 + ϕ degrees relative to the write source modulation. This output intensity modulation is independent of the delay incurred by the signal before it enters the Bragg cell. This result provides a way to measure ϕ directly, by measuring the phase between the laser source modulation and the photodetector output.

5.3 Photorefractive Implementation of LMS Algorithm

The photorefractive adaptive antenna array processor was designed according to the foregoing analysis. The block diagram of this processor is shown in Figure 5.4. A conceptual layout diagram of this system is shown in Figure 1.1.

Based on the predicted photorefractive diffraction efficiency and the photodetector noise levels, a suppression factor of 40 dB was projected for narrow-band signals. The actual performance achieved is shown in the transient response curve of Figure 5.5. The interfering sinusoid is turned on at t=0. A reference curve for the interference level without cancellation is obtained by blocking the laser beams. This reference curve is the dashed line across the top of the figure. The two curves represent data taken with two different reference input levels. The higher reference level produces a longer response time because the amplifier stays in saturation for a longer time and the total suppression is reduced.

Figure 5.4. Photorefractive Processor Block Diagram

Figure 5.5. Measured Transient Response for Photorefractive Processor

6.0 DESCRIPTION OF THE EXPERIMENTAL SYSTEM

The system actually implemented is described by the schematic diagram shown in Figure 1.1. This figure is repeated here in Figure 6.1 for convenience.
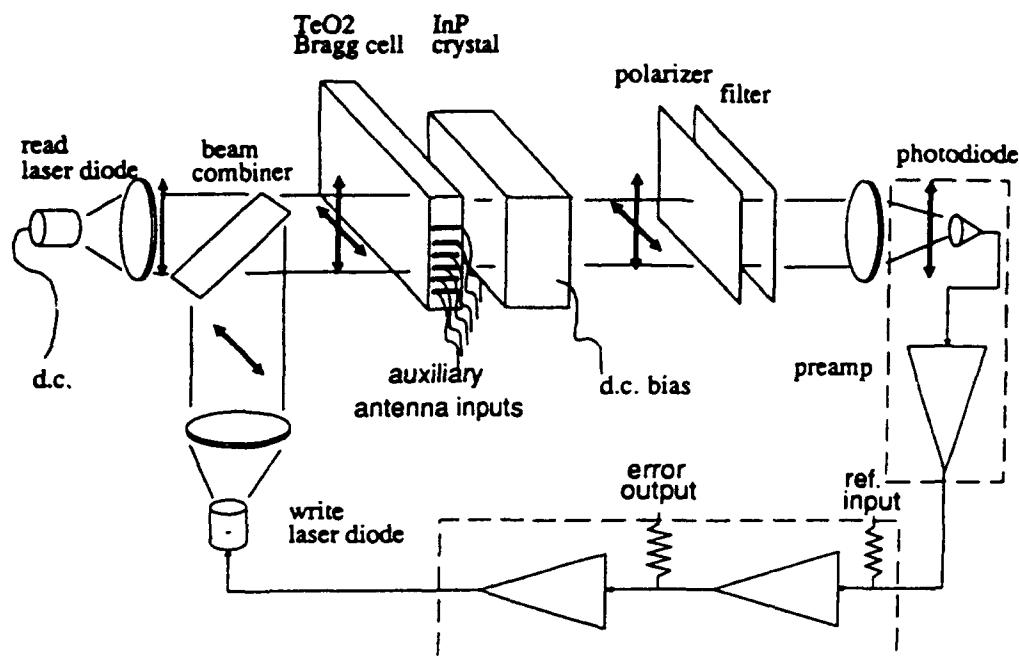
Figure 6.1. System Schematic Diagram

A photograph of the system is shown in Figure 6.2.

6.1 Description of Key Components

As a preliminary to describing the actual system built on this program the key components will first be identified and described. These key components consist of:

Semiconductor laser diodes at 1.2 and 1.3 μm wavelengths for correlation and tap weighting, respectively,

A six-channel acousto-optic Bragg cell with 1μs delay and 30 MHz bandwidth,

An InP photorefractive material operating at 3,600 volts bias (+/- 1,800) across 5 mm,

An optical system consisting of two collimating lenses for the lasers, a polarizing combiner, a polarizing filter and a wavelength filter (to eliminate the write light from the read system) and a transform lens,

A photodetector,

and a loop amplifier with ~ 90 dB of gain.

Figure 6.2. Photograph of Experimental System

6.1.1 Read and Write Lasers

The read laser beam multiplies the stored correlation weights in the photorefractive crystal by the delayed signals. The Fourier transform lens sums these weighted signals over the delay aperture. We used a 1.3 μm OKI diode laser rated at 100 mW. Figure 6.3 shows the power measured at the input surface of the Bragg cell versus drive current. The linear line is given approximately by the equation

$$P=0.165i\text{-}3.8$$

from which we can infer the optical power at the Bragg cell by monitoring the drive current. A similar plot is given in Figure 6.4 for the write laser, which is a 1.2 μm OKI laser diode rated at 50 mW. The best linear fit equation for the write laser power is

$$P=0.15i\text{-}4.7.$$

Figure 6.5 shows a typical measurement of the noise levels of the laser diodes, again in terms of drive current. The noise level of the read laser is critical to the operation of the system, as it will raise the noise of the system if greater than the shot noise of the detector. Inasmuch as the write laser is filtered out prior to detection and the noise will not correlate with the signal in the Bragg cell, its noise level is less critical to the operation of the system. For a given drive current the plot shows a large difference between the read and write laser noise levels. The RIN noise cycles through high and low noise levels as the drive current increases with an overall increase in noise due to increased shot noise. The cyclical high and low noise levels are due to changing mode
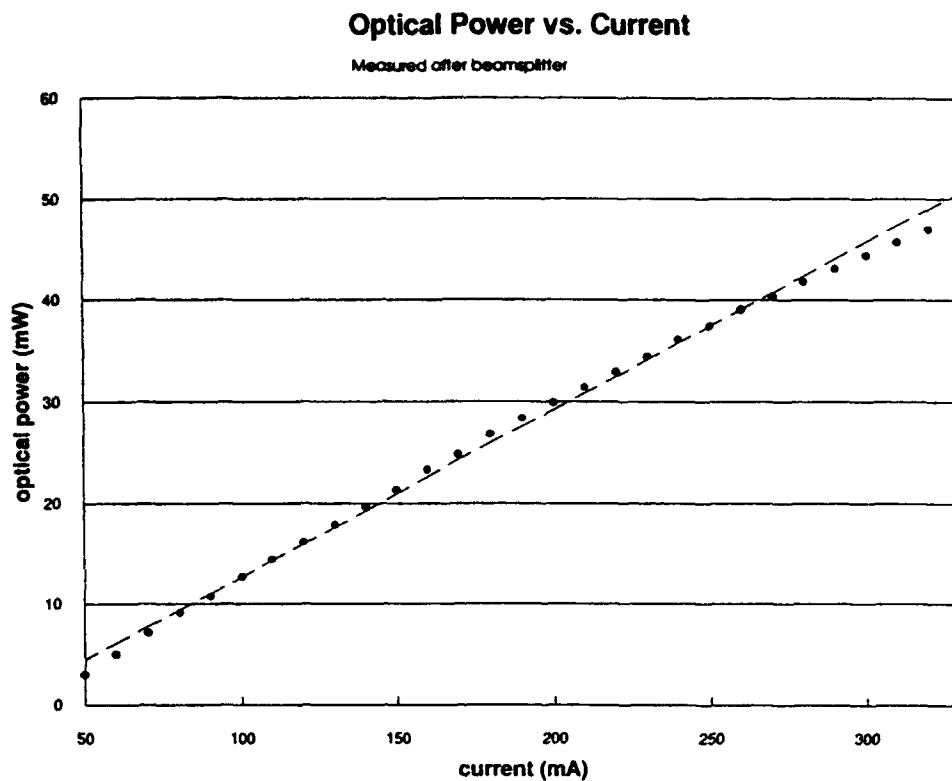
Optical Power vs. Current

Measured after beamsplitter

Figure 6.3. Read Laser Power Versus Drive Current

Optical Power vs. Current

Measured after beamsplitter
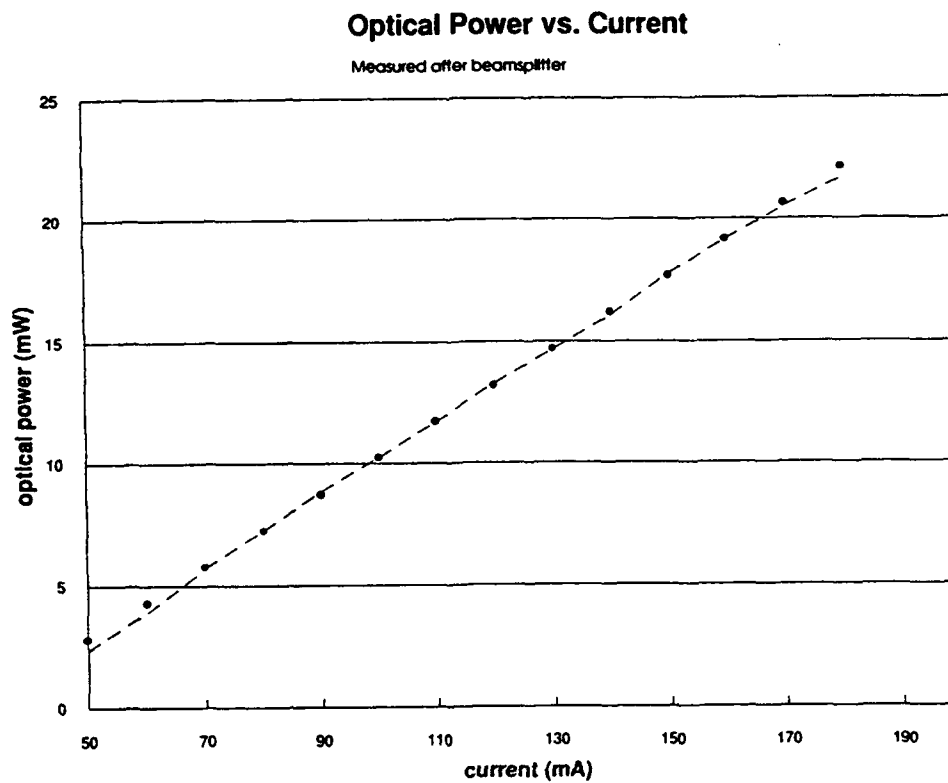
Figure 6.4. Write Laser Power Versus Drive Current
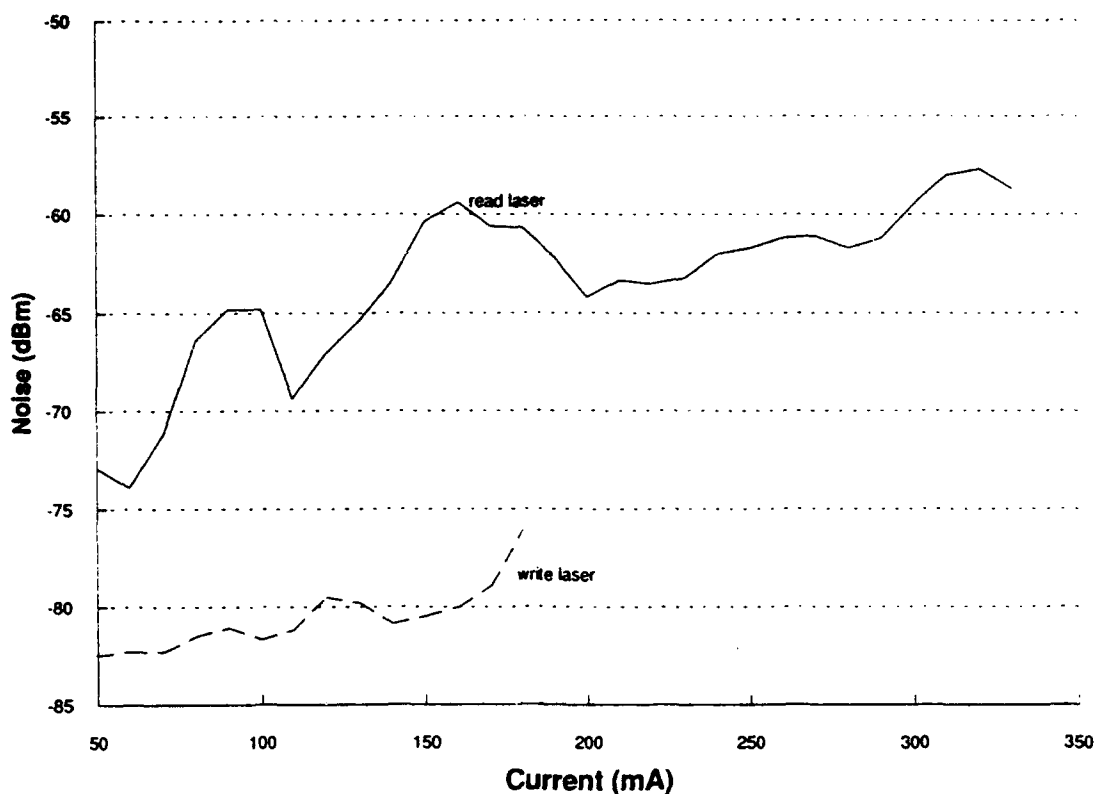
Figure 6.5. Laser Noise Level Versus Drive Current

structure of the laser, caused by either wavelength tuning due to current changes, or possibly optical reflections making the laser cavity unstable. During operation the noise level of the read laser measures between -60 and -68 dBm in a 1 MHz bandwidth at the preamplifier output. This level is dependent on optical alignment, room temperature, and laser current.

The noise of the write laser was also measured with a modulation signal driving it. Over a 40 dB modulation range the noise level changed by only 3.5 dB.

6.1.2 Bragg Cell

A six-channel Bragg cell was custom designed and constructed for the adaptive processor. Each channel has a 1 μs delay aperture and 20 MHz bandwidth centered at 70 MHz. The design is a balance of diffraction efficiency, bandwidth, and acoustic beam spreading. The material chosen for the acousto-optic interaction is tellurium dioxide operating with a longitudinal wave propagating along the [001] crystal axis. This propagation mode provides a good diffraction figure of merit and a moderate self-collimating effect due to anisotropic propagation effects. This particular propagation direction reduces beam spreading to 40 percent of that for isotropic propagation with the same geometry. Also, the chosen direction interaction has a low polarization dependence. This is an important feature since it allows the use of polarization multiplexing of the read and write beams in our system.

The channel height is chosen to correspond to the near to far field transition at the far edge of the aperture. The relation that defines this is:

$T=h^2/\Lambda$

where T = time aperture length

h = aperture height

Λ = acoustic wavelength = velocity/frequency

Λ= [4200 m/s] / [70 MHz] = 60 μm.

The propagation velocity is 4.2 mm per μs (Λ=60 μm at 70 MHz) and a 1 μs aperture is 4.2 mm long in the propagation direction (horizontal). Solving for h yields a channel height of 0.5 mm. The center-to-center spacing of the channels is 0.85 mm. Figure 6.6 shows the computed variation of acoustic power density caused by acoustic wave diffraction in the vertical direction. Since the diffraction is symmetric about the center of the cell only one half the aperture is plotted. The total acoustic power contained in the 500 μm aperture defined by the transducer drops by less than 1 dB as the aperture moves from the transducer to the 1 μs delay position. The spillover power from one aperture to an adjacent one is -20 dB at the 1 μs distance. The effect of this level of crosstalk on performance of the adaptive filter has been imperceptible.

The length of the acoustic transducer in the direction of optical propagation is L=18 mm. This provides a Bragg diffraction parameter of $Q=2\pi\lambda L/(n\Lambda^2)=18$. The computed diffraction efficiency versus frequency for this design is shown in Figure 6.7. The parameters used in this computation are:

Drive power	100 mW
Elec. to acoustic conv. eff.	0.8
Wavelength	1.3 μm
Polarization	Vertical
Time aperture	6 mm (1.4 μs)
Transducer heigth	500 μm
Transducer length	18 mm

The theoretical diffraction efficiency at the peak is 240 percent per watt and the frequency response is within 0.7 dB of the peak across the 20 MHz design band.

The acoustic transducer electrodes are connected to standard 50 ohm SMA type connectors. The transducer is designed to have the real component of its impedance close to 50 ohms in series with a capacitive reactance. The matching network consists of a simple series inductance. The VSWR is less than 1.8:1 over the 60–80 MHz band.

Figure 6.8 shows the measured diffraction efficiency versus frequency for two typical channels of the cells. The measured response from 60–80 MHz is within 1 dB of the peak as predicted by analysis. This frequency response curve is somewhat alignment dependent and the peak response frequency can be shifted by rotating the Bragg cell. In this way the peak frequency can be shifted

Bragg Cell Acoustic Intensity
Varying aperture position @ 70 MHz

Figure depicting dBr versus Channel Height (um), with curves labeled "1 us", "1/4 us", "Near transducer", and regions "channel width" and "neighbor".
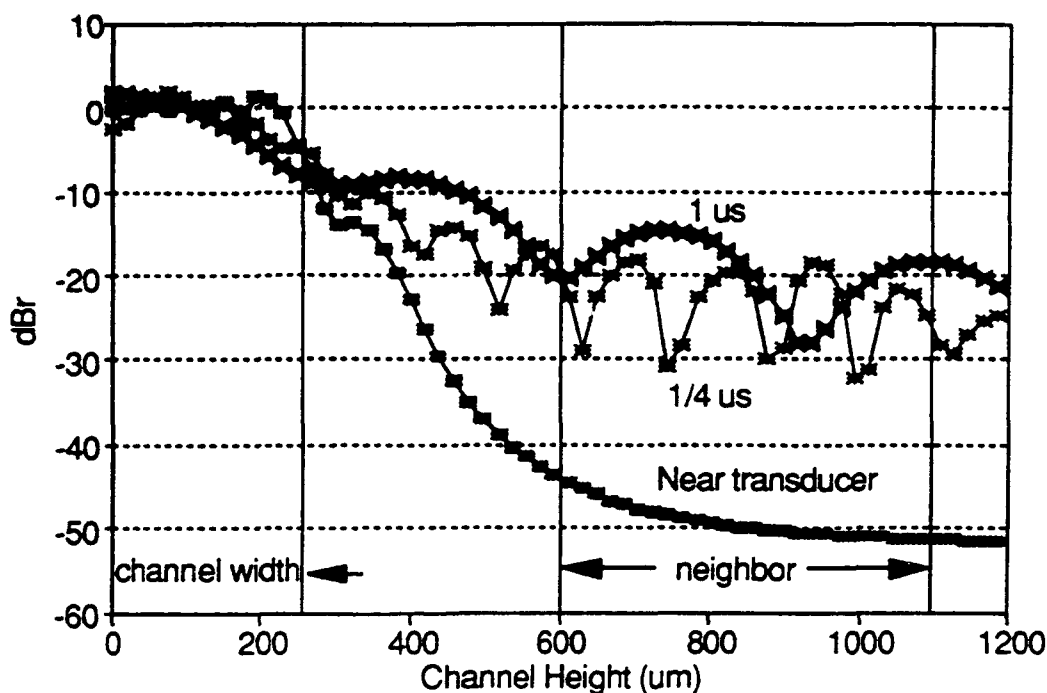
Figure 6.6. Acoustic Power Distribution in Aperture

TE02 LONG   OPT APERTURE   .10mm Start   6.00mm Width

Plot of DIFF EFF versus FREQ (Mhz).

SIMPLE TRANS 500.u Ht 18.00mm LEN   100.mW .80cls

ILLUMINATION: 1.300u   4.8mrad Gctr= 3.00mm Gdia= 10.00mm

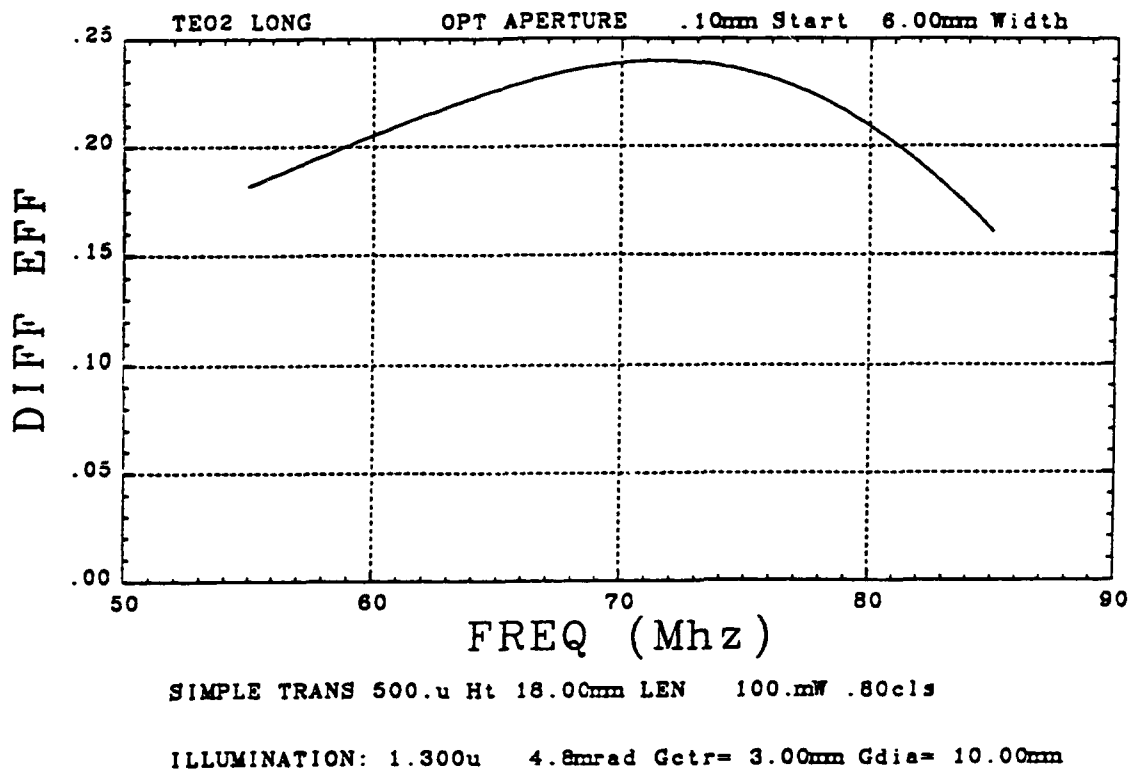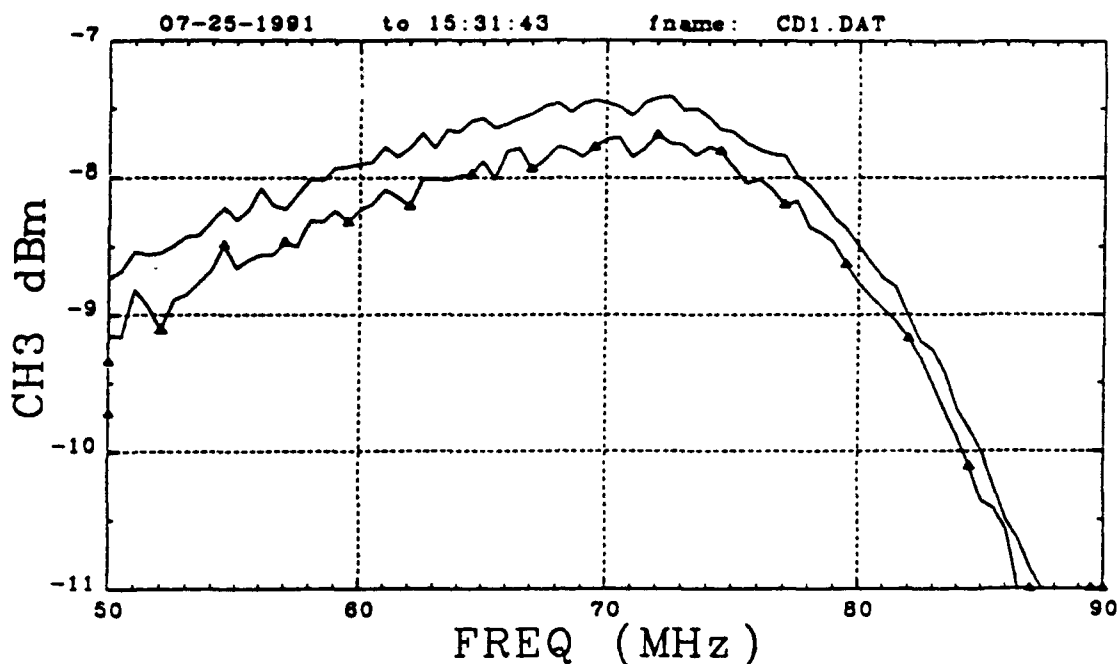*Figure 6.7. Computed Bragg Cell Diffraction Efficiency Versus Frequency*

Figure 6.8. Measured Bragg Cell Diffraction Efficiency Versus Frequency

above 70 MHz and the bandshape can be adjusted for equal response loss at the upper and lower band edges (60 and 80 MHz).

The Bragg cell is used twice in the adaptive filter processor. During the write operation, the 1.2 μm wavelength incoming light is horizontally polarized and the diffracted light forms a fringe pattern in the photorefractive crystal. For readout, illumination is a vertically polarized 1.3 μm beam. The cell operation optimizes differently for the different wavelengths. A balanced band-shape corresponds to an input illumination at 4.4 mrad for the 1.2 μm beam and 4.8 mrad for the 1.3 μm beam. The figure of merit for the acousto-optic substrate also differs with input polarization. Figure 6.9 illustrates a 4.6 mrad illumination angle and its effect on the two light wavelength responses during simultaneous read and write. The bold curve is the geometric mean and represents the net system transfer including both interactions. The product response varies about 1.2 dB across the 60 to 80 MHz band of interest.

The bandwidth and diffraction efficiency characterize the operation of the Bragg cell. Since we fully illuminate the cell with a large optical beam (light incident between channels as well), we defined two diffraction efficiencies. We define the local diffraction efficiency as the percentage of light diffracted within the regions of acoustic activity, that is inside each channel. The global efficiency is defined to be the total percentage of light diffracted with all channels diffracting versus total light illuminating the cell. The global efficiency includes the illumination losses and it is appropriate for use in the loop gain calculation while the local diffraction efficiency is used to design the cell and to evaluate the acoustic transducers.

The local diffraction efficiency is measured by placing a slit in the optical beam positioned such that only the light incident on an acoustic column is passed. The slit dimensions are such that the illumination covers the entire time (horizontal) aperture, but only a fraction of the acoustic height.
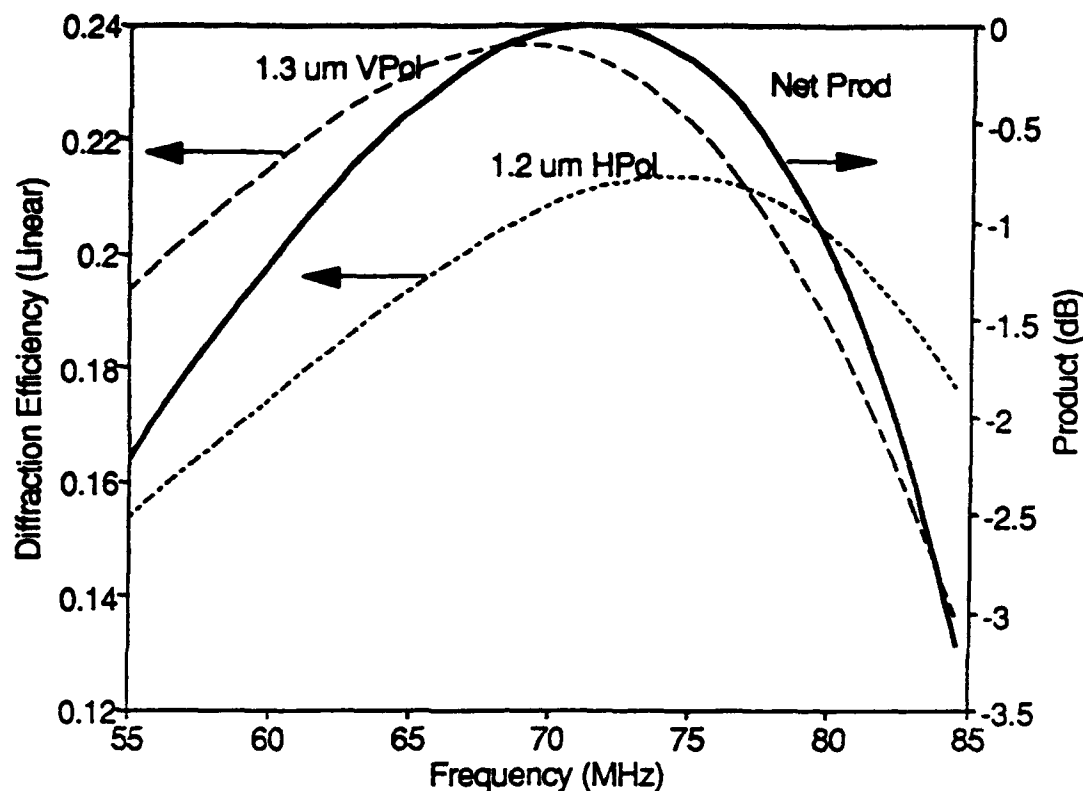
Figure 6.9. Measured Frequency Response of Simultaneous Read and Write

When illuminated in this way, the diffraction efficiency of the cell measured 128%/W for a single transducer (21%/W when all six transducers are powered) at 1.3 m wavelength.

To measure the global diffraction efficiency the optical beam illuminates the entire window of the acoustic cell. The beam is diffracted at a rate of 21%/W in the regions of acoustic energy (local diffraction efficiency) and not diffracted at all between acoustic columns. This results in an overall loss of efficiency for the device. The global diffraction efficiency of the cell, measured at 1.3 m wavelength, is 5%/1.2 W (5% diffracted power when each channel is driven by 200 mW). This suggests that the overall illumination efficiency is approximately 20%. This is close to the estimated value of 22.5% resulting from a 60% fill ratio of the aperture (0.5 mm/0.85 mm), a 50% illumination spillover loss and 10% loss from optical surfaces.

6.1.3 Photorefractive Integrator

Photorefractive technology involves a nonlinear optic effect in materials in which the index of refraction is related to the intensity of light incident on a material. In the particular context here an index grating forms via photoconductive charge transport due to the spatial content of the incident beams. This process is slow compared to the frequency of light since it involves charge transport. It is also slow compared to the frequency of information, in the applications here, and thus acts as an integrator of the information over time.

The role of the photorefractive material here is as a beam combiner and a time integrator. Both of these processes are inherent to the nature of photorefractive materials when light with a spatial frequency component is incident upon them.

The time scale of the integration depends on the response time of the charge transport. This time scale is related to the time scale of the system adaptation through the gain of the feedback loop of the system. In general, the time constant for the intended applications should be on the order of milliseconds.

The materials chosen for this program are semiconductor materials because the response time of the charge redistribution is much faster than in most nonconductive materials. Several such materials were investigated on IR&D and indium phosphide was shown to be well suited for this application.

A couple of the oxide insulators have shown promise for high-speed signal processing applications, but have not as yet been thoroughly investigated. Iron-doped potassium niobate and bismuth silicon oxide are two of these materials.

Another factor which influences the choice of semiconductor materials over other crystals is the wavelength of light required to generate the interaction. Once again the energy structure of the crystal and its impurities and defects govern which wavelength is applicable. It is desirable in most applications to use compact efficient laser sources such as injection laser diodes. The small band gap and shallow trap levels of semiconductors allows photo-ionization of charge carriers with the relatively small photon energies available from laser diodes.

The photorefractive material has a time constant which, according to presently published theories, varies with the incident illumination level, spatial frequency, and bias level. The time response for the indium phosphide material used was computed. The results of this computation are shown in Figure 6.10. The corresponding measured time response curves are shown in Figure 6.11. The correspondence is adequate for rough computation of performance, but there are clearly discrepancies in many details of the curves.

From the experimental time response curve, it is seen that the material response time constant is approximately 2 ms with an optical power density of 0.2 W/cm^2. With a loop gain equal to 100 (40 dB) the closed loop time constant should be 20 μs. A closed loop time constant of 70 μs was observed. The discrepancy is attributed to the effect of amplifier limiting due to the large error signal in the early stage of adaptation.

Photorefractive Device Configuration

The crystals that were investigated for the current application have cubic 4-bar3m symmetries (in point group notation) so two possible orientations for polarization preserving interactions can occur. The two orientations are shown in Figure 6.12. The first one, the [001], has been utilized most commonly in photorefractive experiments and is the one that has been used in IR&D experiments here. The second orientation, the [111], demonstrates a slightly higher figure of merit and has not yet been investigated. It is in the IR&D plan to investigate the advantages of this cut of crystal. The orientation baseline selected for the experimental device is the 001.

In this orientation the electric bias field is applied in the 001 direction. The optical beam propagates in the -110 direction with the light polarized in the 110 direction. This gives an interaction

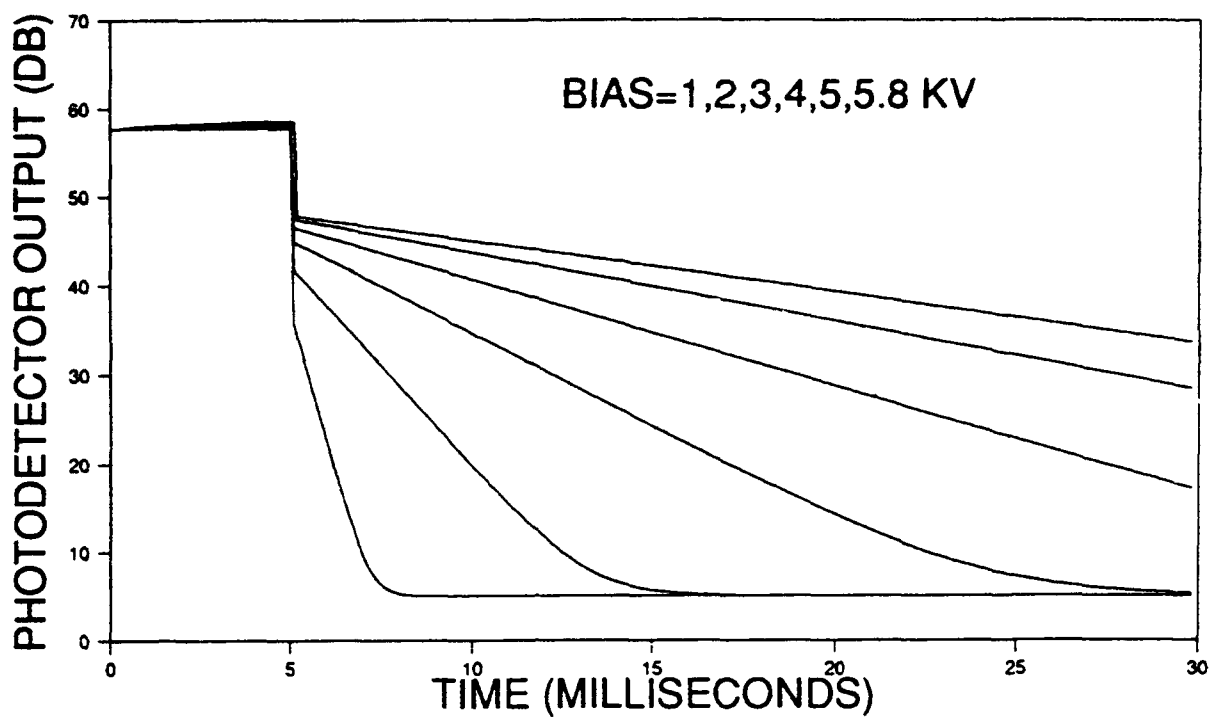## COMPUTED AMPLITUDE AT I=.2W/SQ. CM.

Figure 6.10. Computed Photorefractive Time Response for InP
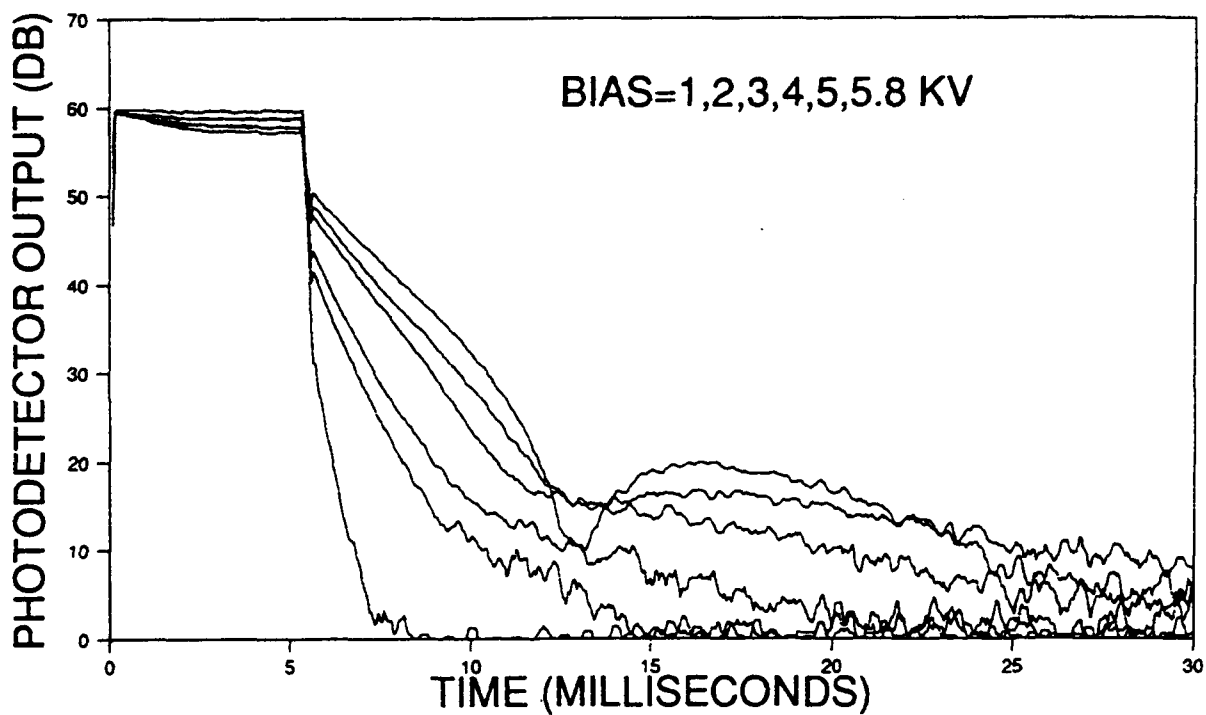
AMPLITUDE AT 60 MA CURRENT

Figure 6.11. Measured Photorefractive Time Response for InP

with no polarization rotation so that the transmitted and diffracted beams will interfere on the photodetector for heterodyne detection of the desired signal.

The photorefractive crystal, as with the Bragg cell, is characterized by its diffraction efficiency. The diffraction efficiency is dependent on voltage, wavelength, polarization, laser power, and a host of other variables. The efficiency is then dependent on the system operating parameters. To determine the operating efficiency, the system was first optimized for closed loop, single tone suppression. We measured the diffraction efficiency of the Bragg cell with the photorefractive crystal voltage turned off. The voltage was then returned to the photorefractive crystal and the global diffraction efficiency measured again. This time the measurement includes the light diffracted from the Bragg cell and the light diffracted due to the photorefractive crystal grating. The photorefractive grating efficiency accounts for the difference between the two measurements. This method yielded a diffraction efficiency of 1.5 percent.

6.1.4 Wavelength Filter

The write laser beam passes through both the Bragg cell and the photorefractive crystal and must be filtered out of the optical path prior to the detector. The beam has the signal imparted on it by the Bragg cell and if detected the signal could not be suppressed. A wavelength filter that blocks the 1.2 m wavelength and passes the 1.3 m wavelength performs the filtering function. The filter attenuates the 1.2 m wavelength by 25 dB, while attenuating the 1.3 m beam by only 1.5 dB.

6.1.5 Photodetector and Feedback Loop Electronics

The feedback loop electronics provides over 90 dB of gain and subtracts the estimate from the reference signal. As these take place within the loop, delay time must be minimized to achieve max-
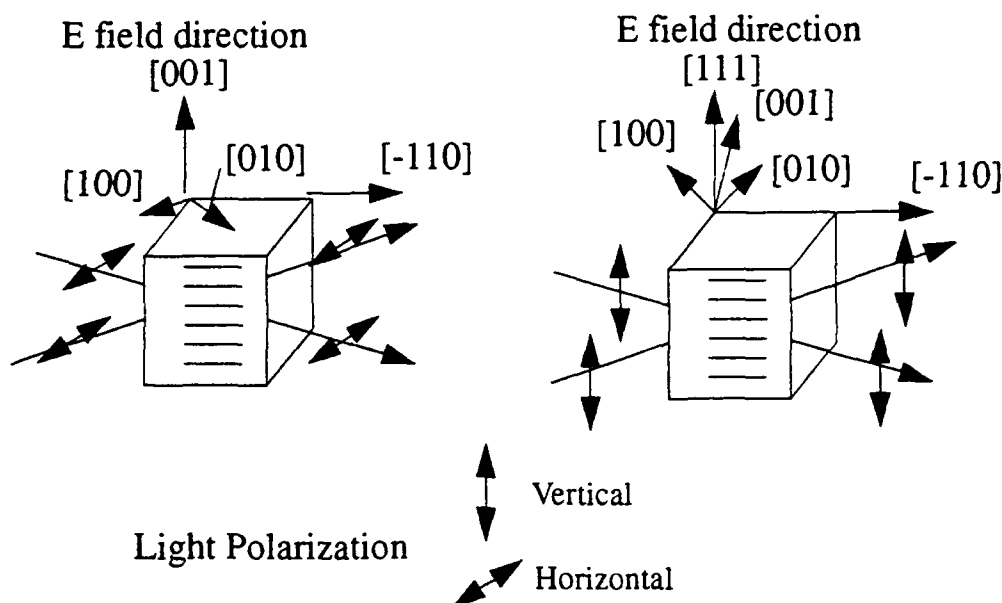

Figure 6.12. InP Orientations for Photorefractive Interaction

- 48 -

imize operating bandwidth. Implementation is in two separate blocks: the detector preamplifier and the loop amplifier.

The loop amplifier designed for this program features high gain and low time delay. The measured gain of the amplifier is +75 dB. The delay time, minimized by excluding interstage filtering, measured 7 ns. The output power saturated at +26 dBm.

A second amplifier assembled for the program consisted of four discrete amplifier stages. These stages were commercially available packaged amplifiers. By placing these amplifiers in series, enough gain could be obtained to operate the system. This amplifier package demonstrated 72 dB of gain. The delay time through the amplifier however is much larger, ~16 ns, which limited the suppression bandwidth achievable by the system.

A PIN in GaAs photodiode (RCA C30619) is used as our single point, wide area detector. Its responsivity is 0.8 A/W with an operating bias voltage of 5 volts. The 0.5 mm diameter provides a useful area of 0.2 mm^2. As indicated in the schematic in Figure 6.13, a termination of 50 ohms is followed by a pair of Watkins Johnson amplifiers separated by a resistive pad. The reference and estimate signal subtraction is done in the preamplifier block by injecting the reference through a summing network. The gain of this preamplifier is measured as 26 dB. The signal of interest (reference) and the detected signal are compared at the sum port. The difference signal (error) is then amplified and measured at the output port. At this output port the measured noise level in a 1 MHz bandwidth is -77 dBm. The noise of the preamplifier is below the RIN of the semiconductor diode
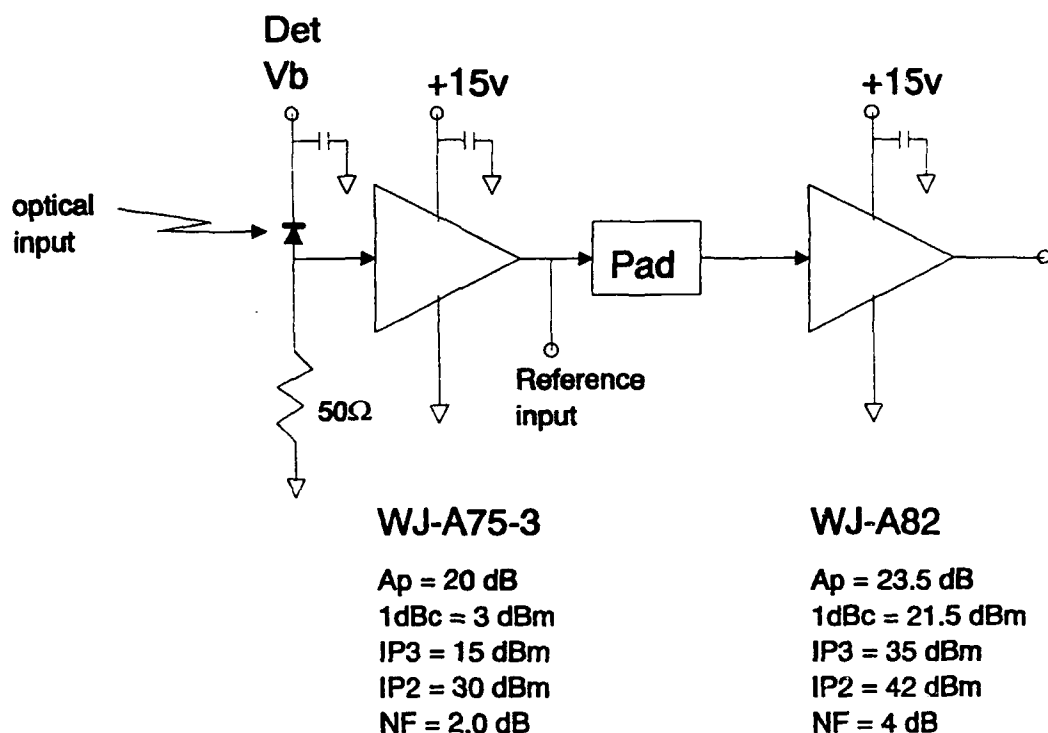

WJ-A75-3

Ap = 20 dB
1dBc = 3 dBm
IP3 = 15 dBm
IP2 = 30 dBm
NF = 2.0 dB

WJ-A82

Ap = 23.5 dB
1dBc = 21.5 dBm
IP3 = 35 dBm
IP2 = 42 dBm
NF = 4 dB

Figure 6.13. Detector Preamplifier Schematic Diagram

read laser. A lower noise floor may be achievable by using a transimpedance configuration in conjunction with a lower noise laser.

The majority of the feedback gain is obtained with the loop amplifier diagrammed in Figure 6.14. This five element block must provide a high level (70 dB) of gain with a minimal time delay (6 ns). The small time delay specification precludes the use of interstage filtering typically used to help prevent oscillation. The breadboard relies on extensive shielding and careful ground plane management to help stabilize operation. Even with these precautions the loop amplifier tends to be sensitive to thermal warm-up and requires daily confirmation to ensure it is functioning properly. An alternate loop amplifier assembled from individually packaged stages interconnected with standard SMA connectors is included with the residual hardware. While exhibiting a longer delay (16 ns) it is more stable. Its gain can be easily reconfigured by changing the number of stages. The processed signal is recovered through a resistive divider at the sum port or alternatively at the monitor port in the breadboard loop amplifier. The monitor port provides additional amplification to increase the processed signal level, but can be in saturation before suppression has been achieved. The staged loop amplifier has an RF splitter at its input to monitor the processed signal.

The loop amplifier must also protect the write laser from excessive modulation current. The write laser drive circuit consists of a 50 ohm resistor in series with the laser and a reverse bias protection diode in parallel with the laser. The reverse bias diode prevents the laser from exposure to voltages above its reverse breakdown level during any harmful current surges from power supply transients or excessive modulation. Our write laser is rated for up to 176 mA; this corresponds to +23 dBm
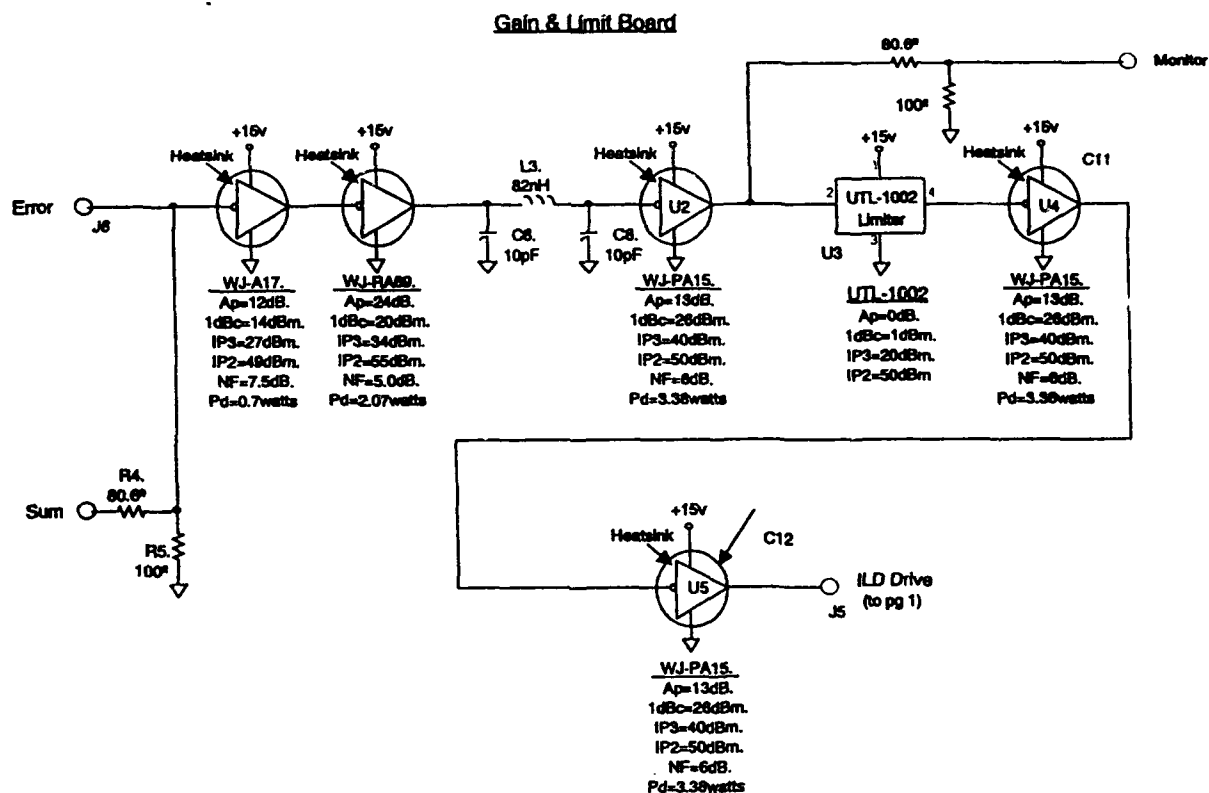

Figure 6.14. Loop Amplifier Functional Diagram

into the 50 ohm load. The loop amplifier saturates at +26 dBm; thus, we use an external 3 dB pad before connecting to the write laser.

An additional filter is used between the preamp and loop amplifier to suppress 2nd harmonic tones generated by acoustic standing waves resulting from echoes off the back of the Bragg cell. A custom design procured from Anatech (PN L7249) specified for minimal delay within the pass-band, 60 to 80 MHz, and maximal rejection across the 2nd harmonics, 120 to 160 MHz, achieves better than 20 dB of rejection with less than 10 ns of delay. Without this filter the CW suppression, when swept from 60 to 80 MHz, produces a lobed response with some regions of suppression limited to less than 35 dB. Placing the filter within the feedback loop trades bandwidth (from greater than 30 MHz to 20 MHz) for improved suppression levels.

6.1.6 Signal Generation Subsystem

The signal generation support electronics amplifies input signals to the proper Bragg cell level, simulates antenna array delays, provides mixers for modulation of test tones, and produces an internal pseudorandom (PN) modulation source.

The antenna array simulator front panel is shown in Figure 6.15.

A functional schematic is shown in Figure 6.16. Six output channels provide a signal path corresponding to each element of an antenna array. The output amplifiers (far right of both figures) provide +26 dBm of output, but operation at a maximum level of +23 dBm is recommended to
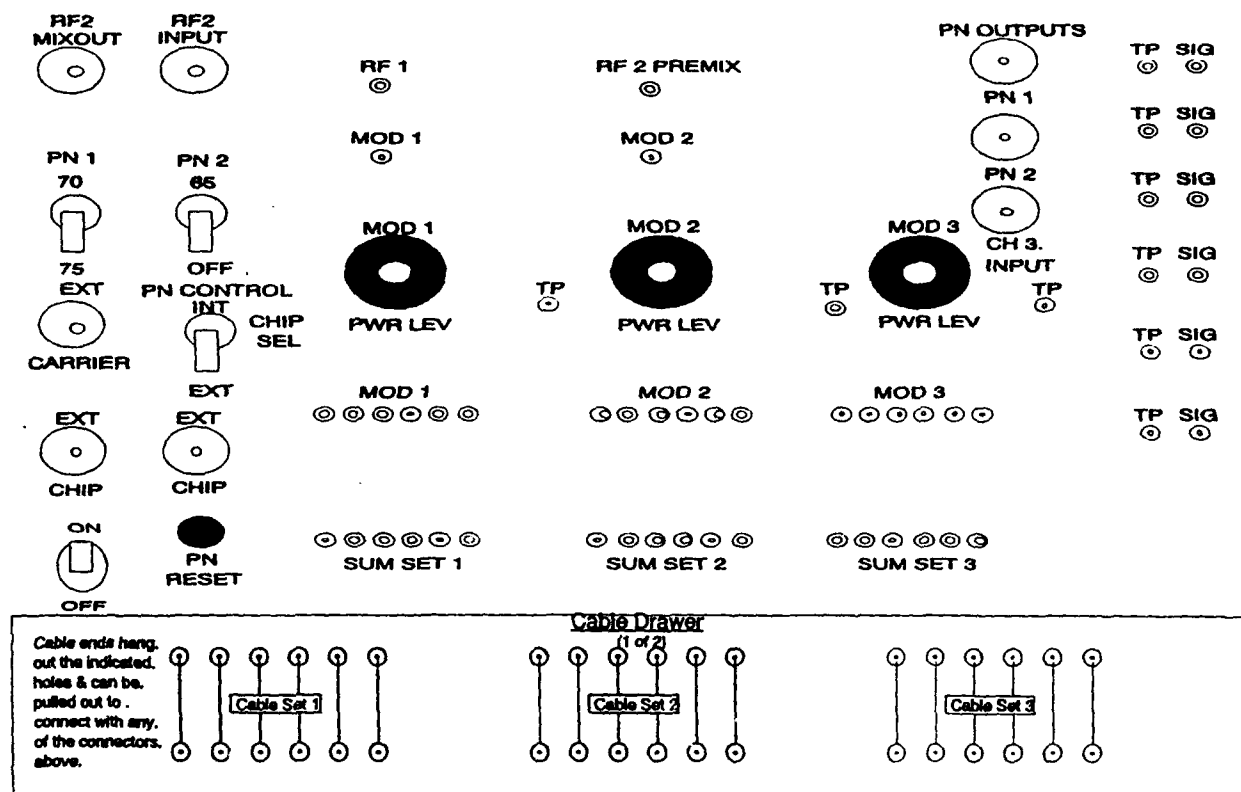

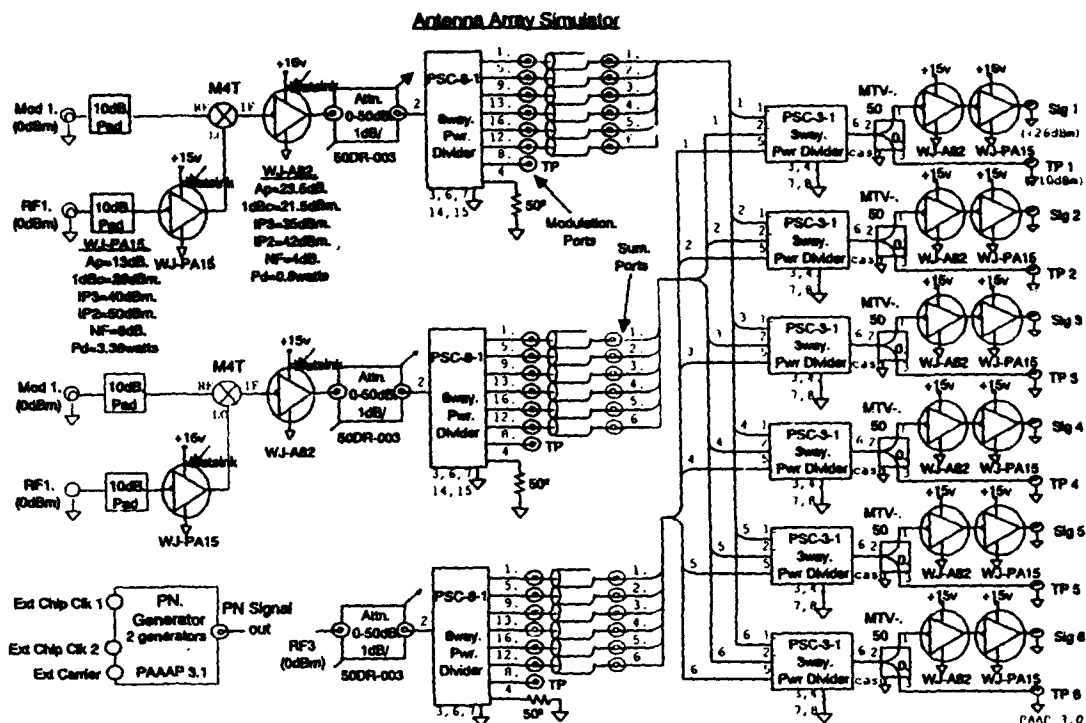*Figure 6.15. Array Signal Source Front Panel Layout*

Figure 6.16. Functional Schematic of Array Signal Source

maintain acceptable thermal wavefront distortion across the Bragg cell aperture. Inputs are derived from any combination of three signal paths. Each of the six channels of the three banks of connectors adjacent to the power level attenuators connect through a set of cables to the Bragg cells. By varying the cable lengths across the six channels each of the 3 inputs may simulate a different angle of incidence to an antenna array. Input RF 3 allows direct input of a test tone. This is the usual port to input the CW evaluation tests. Input 2 may be jumpered for direct input tone or alternately routed through its mixer for modulated input evaluation. Input 1 must have a modulation input to reach the Bragg cell.

An internally generated PN signal may be used for the modulation source. Internal carriers of 65, 70, and 75 MHz or an external reference may be used. Signal #1 is switch selectable between 70 or 75 MHz. Signal #2 is the internal 65 MHz or the externally provided reference. The clock rate for the bit sequence can be the internal 10 MHz or an externally provided rate. The nominal input levels are 0 dBm with the levels reaching the Bragg cells adjustable by the front panel attenuators.

The reference signal must be delayed relative to the Bragg cell inputs for optimal spread tone suppression. The proper delay will cause the correlation of the reference and the Bragg cell inputs to occur near the center of the Bragg cell instead of at the transducer (the zero delay case). Coaxial delay lines of length 1/2 μs were used for the experimental evaluation. Alternate methods to offset the reference may be more attractive for a fielded implementation.

6.1.7 Breadboard Signal Flow

Figure 6.17 shows the signal paths in the experimental system. The setup illustrated utilizes two input paths. The reference input is summed from a tap off of each source and routed through a

1/2 µs delay line. The ENI amplifier following the network analyzer is used to increase the level reaching CH3 to 0 dBm. The processed output viewed through the sum port of the loop amplifier is low level, but does not saturate in the open loop condition. This allows straightforward measurement of suppression amplitude and transient response. Nominal levels for the write laser drive and detector preamplifier are indicated. Open loop alignment is done by breaking the feedback loop at the detector preamplifier output, injecting the reference into the loop amplifier sum port, and observing the preamplifier output. Any unused ports should be terminated with a 50 ohm load.
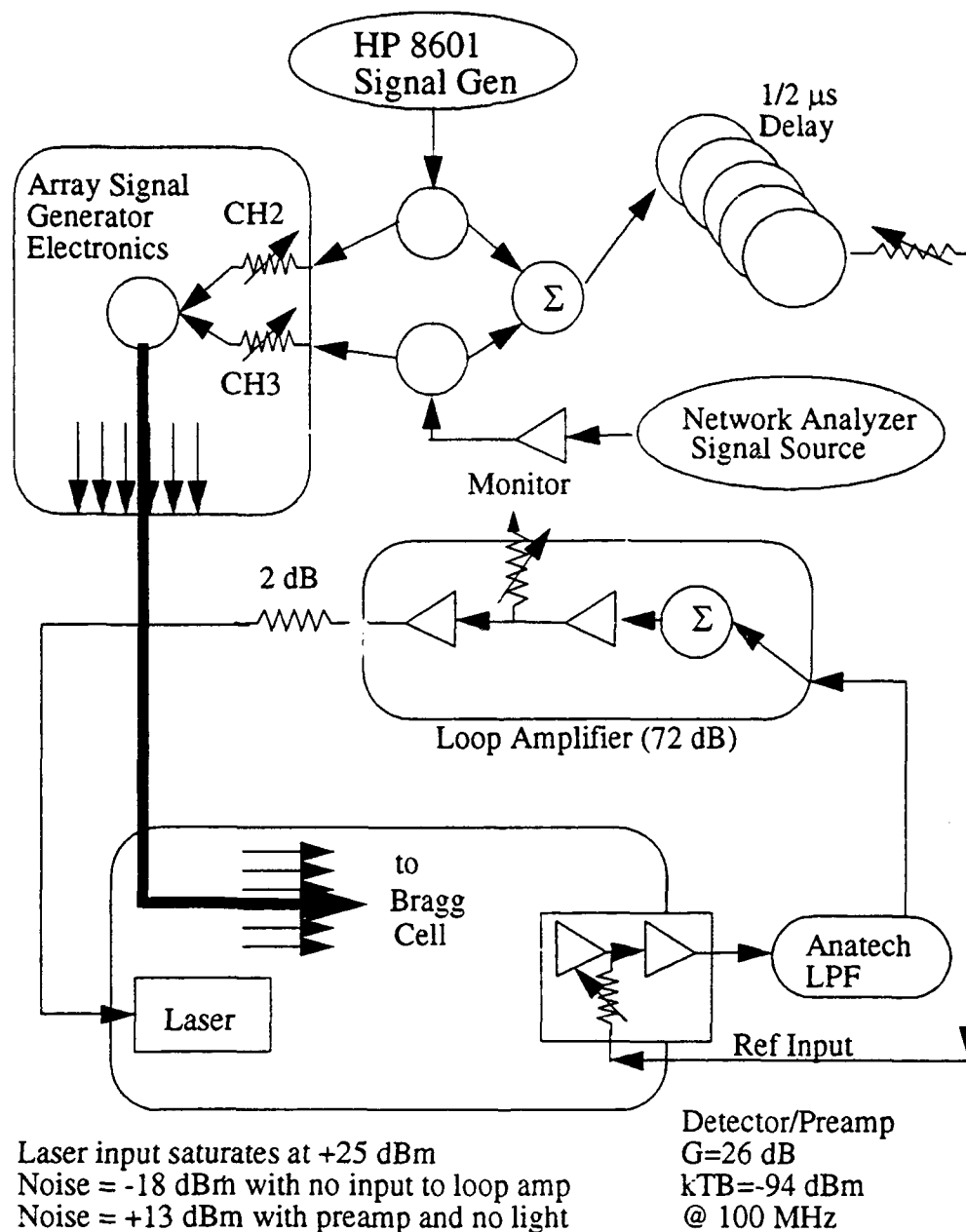
Laser input saturates at +25 dBm
Noise = -18 dBm with no input to loop amp
Noise = +13 dBm with preamp and no light

Detector/Preamp
G=26 dB
kTB=-94 dBm
@ 100 MHz

Figure 6.17. Signal Paths in the Experimental System

7.0 SYSTEM OPERATION AND TEST

To demonstrate the principles discussed in the previous sections we built and tested a breadboard optical system, along with an electronics simulator chassis. The simulator chassis provides for the modulation of three simultaneous signals and the capability to insert delay cables between individual outputs to simulate different angles of arrival. Figure 7.1 is a block diagram of the experimental system, showing all the optical components necessary for the system, and the signal path around the feedback loop.

7.1 Open Loop System Performance

Operating the system in the "open loop" configuration, shown in Figure 7.2, allows direct measurement of the loop gain and saturation levels of the system. Also the alignment in this mode serves as a course alignment for optimizing the performance of the system. The open loop configuration consists of supplying a signal to the loop amplifier that drives the write laser, and measuring the signal out of the detector assembly. No feedback path is established. The difference of input signal level to output signal level defines the total available loop gain (when the system is not in saturation). The maximum output signal level is the saturation level of the system.

A coarse alignment and optimization of the system for maximum loop gain and flatness across the band can be made using a network analyzer as a signal source and sweeping the signal across the band of interest. When optimized, we directly measure the loop gain and saturation levels. A signal of known power is inserted into the loop amplifier. The amplified signal then modulates the
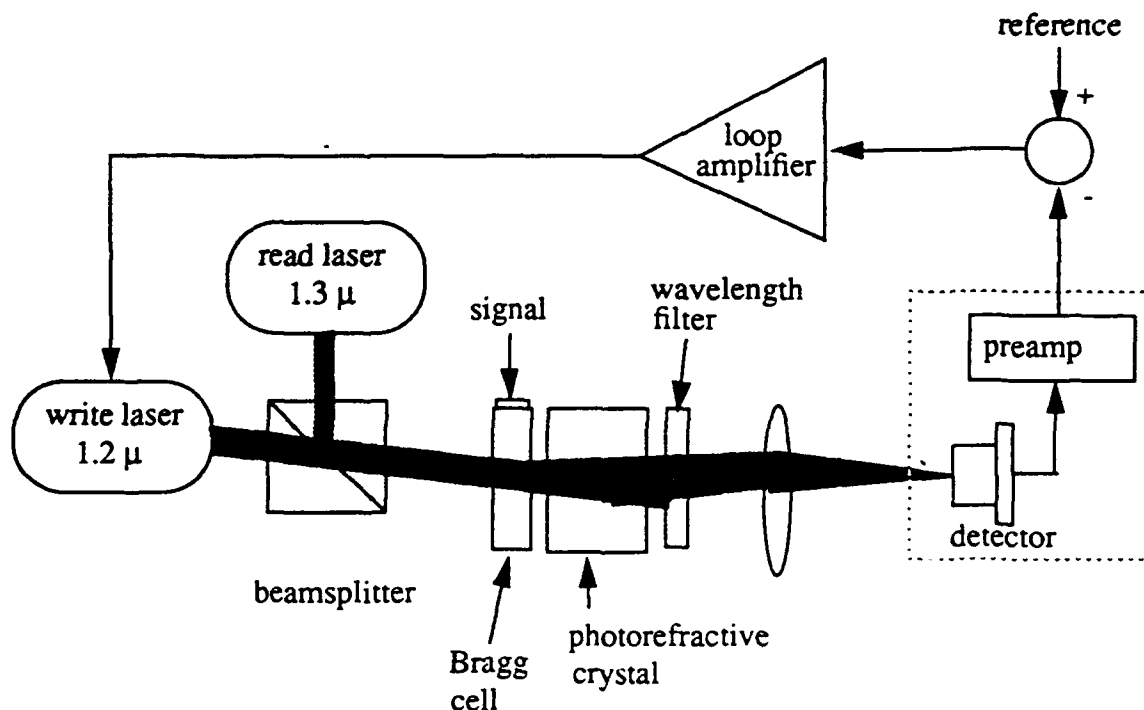

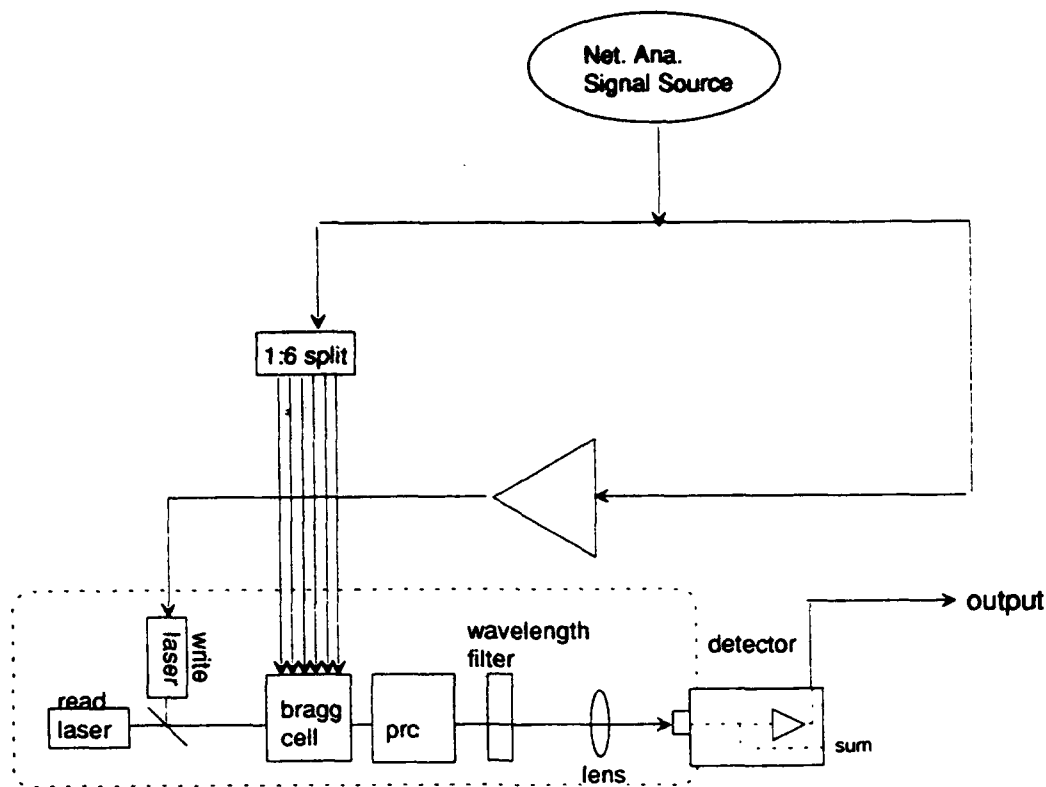*Figure 7.1. Block Diagram of Experimental System*

- 54 -

Figure 7.2. Diagram of Open Loop System Configuration

write laser. The same signal drives the Bragg cell, and the photorefractive cell records the correlation between the two signals. The read laser reads the correlation, applies it to the signal in the Bragg cell, and the detector measures the result. The detector assembly amplifies the result. If the signal is of sufficiently small power that the saturation level is not reached, the difference in input power level to output power level equals the loop gain of the system. The total loop gain measured is +65 dB. The saturation level of the system as measured at the output of the detector assembly is +8 dBm.

7.2 Closed Loop System Performance

The closed loop configuration of the system allows the suppression of signals. All system performance measurements use this configuration. We report on single tone suppression, two tone suppression, and spread spectrum suppression measurements.

7.2.1 Single Tone Suppression

The loop gain of the system fundamentally limits the suppression achievable on a single tone signal. The comparison of the signal to suppress (reference) and the signal estimate (detected optical signal) generates a residual signal (error). The system amplifies the error to create a new estimate. As shown in Figure 7.3, the error level is amplified through the loop to the level of the reference. This sets the minimum error level to be equal to the reference level less the loop gain. If the error signal drops below this minimum, the estimate will not be amplified to the level of the signal causing the error signal to increase.

Several conditions can cause the minimum error signal level to change. If the notch bandwidth noise level of the system is higher than the fundamental minimum, the error level will only drop to
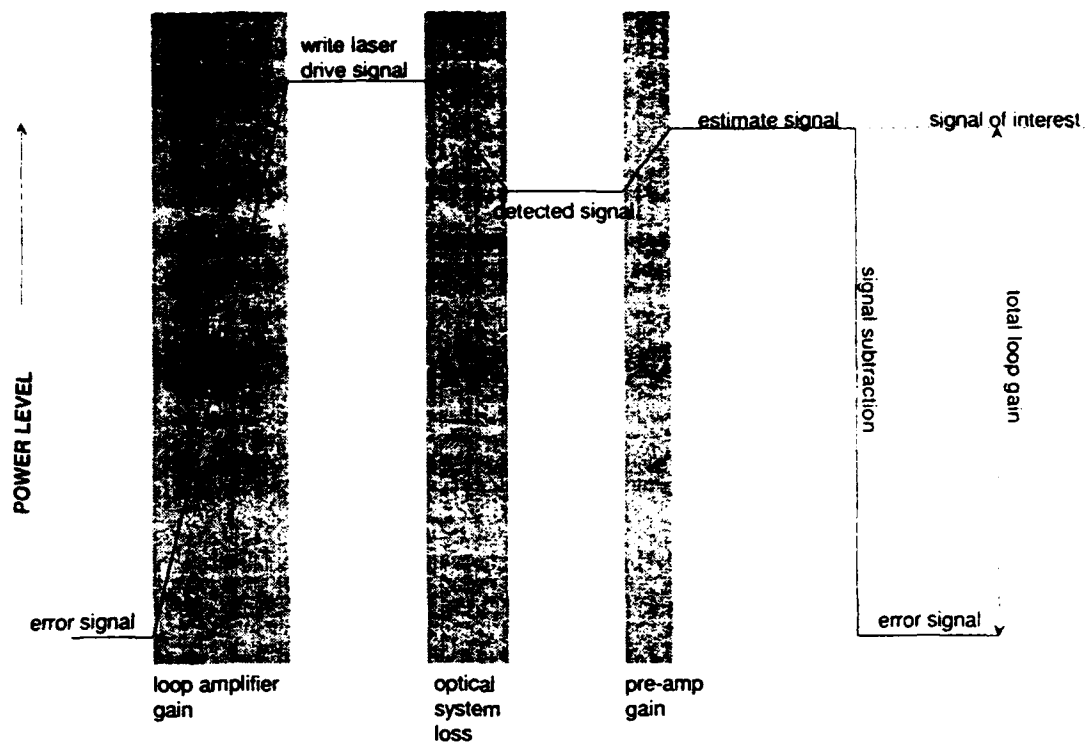
Figure 7.3. Error Output in Open Loop Configuration

this noise level. In this case, the system does not use the full loop gain available, and subsequently the suppression will be less than the loop gain. Another case is when the loop amplifier output saturates and the loop gain decreases due to a smaller gain achieved by the amplifier. This happens when either the reference is sufficiently large that the minimum error signal achievable causes the amplifier output to saturate, or if the amplifier is oscillating either in or out of band, robbing the error signal of amplifier gain. Again, in this condition the minimum error level achieved is more than the fundamental minimum available. Less signal suppression is the result.

To measure single tone suppression the system is arranged as shown in Figure 7.4. A network analyzer acts as the signal source. The source sweeps over the frequency band from 60 to 80 MHz. The signal is split into two paths. One path enters the signal generation system where it is split equally into six ports and amplified so that each port produces nominally 200 mW of RF power. These ports drive the Bragg cell channels. The second signal path passes through a variable attenuator and feeds the signal to suppress port at the detector preamp. The detector output connects to the loop amplifier input with the proper delay length to set the center of suppression band at 70 MHz. The amplifier output then drives the write laser modulation port.

With the lasers turned on and the photorefractive voltage applied, the photodetector detects an optical signal. Comparing this signal with the reference generates an error signal. The detected signal estimate converges to simulate the reference. The suppressed signal environment is monitored at the input to the loop amplifier, where a monitor port has been installed. The signal tapped at this port is 20 dB below the signal level that passes through the loop amplifier. The signal at this port feeds back to the network analyzer where a plot of suppression versus frequency is created. Figure 7.5 shows a typical single tone suppression plot with the reference power level optimized to give the best suppression. Figure 7.6 shows a plot of suppression depth as the reference power level varies. The loop amplifier output saturation limits the maximum power of the estimate signal
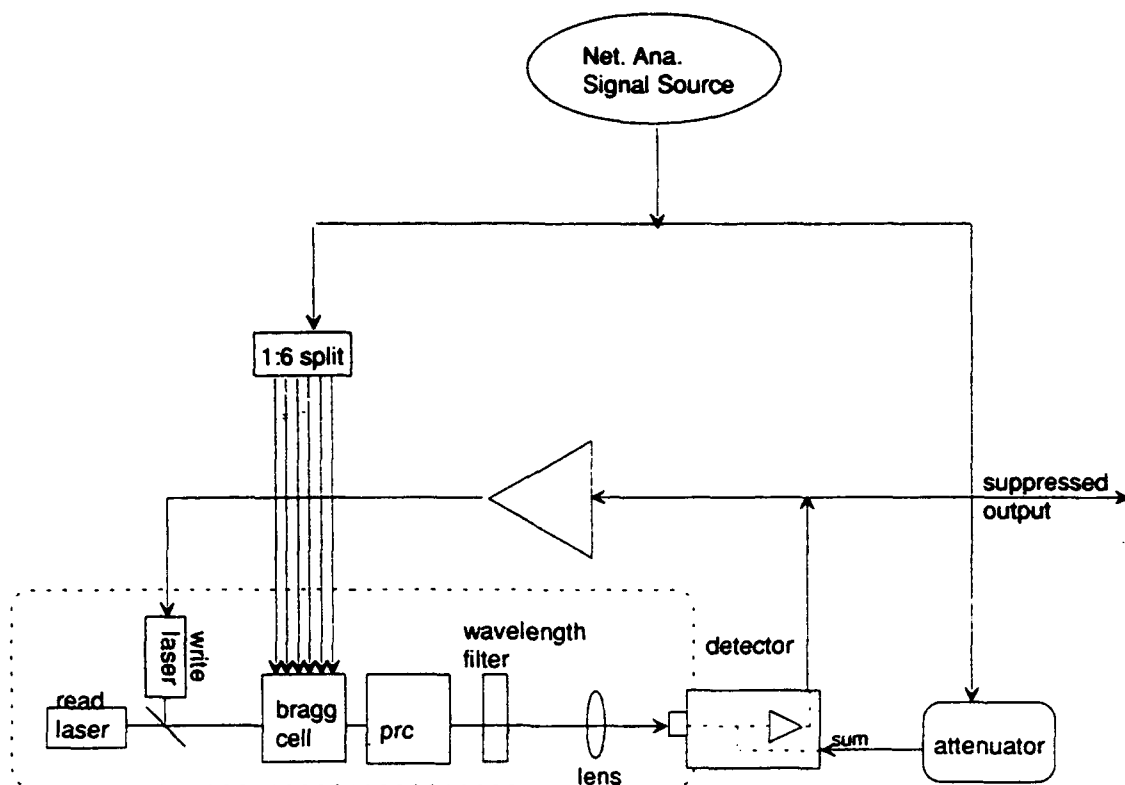
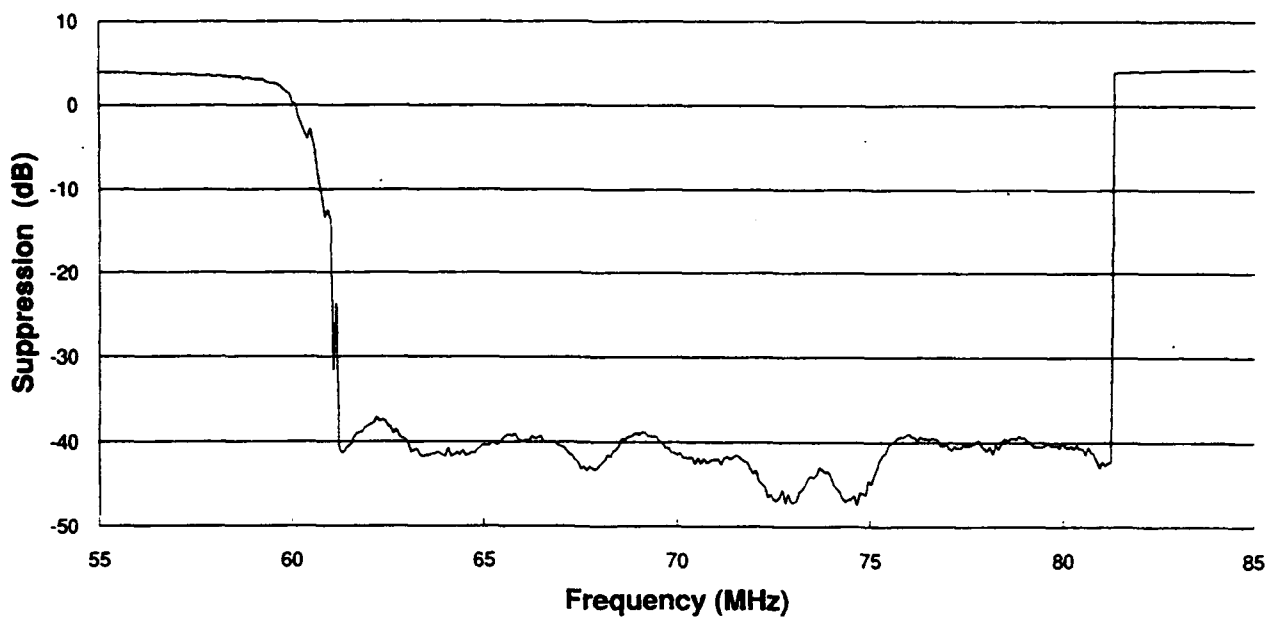*Figure 7.4. Configuration for Single Tone Suppression Measurement*

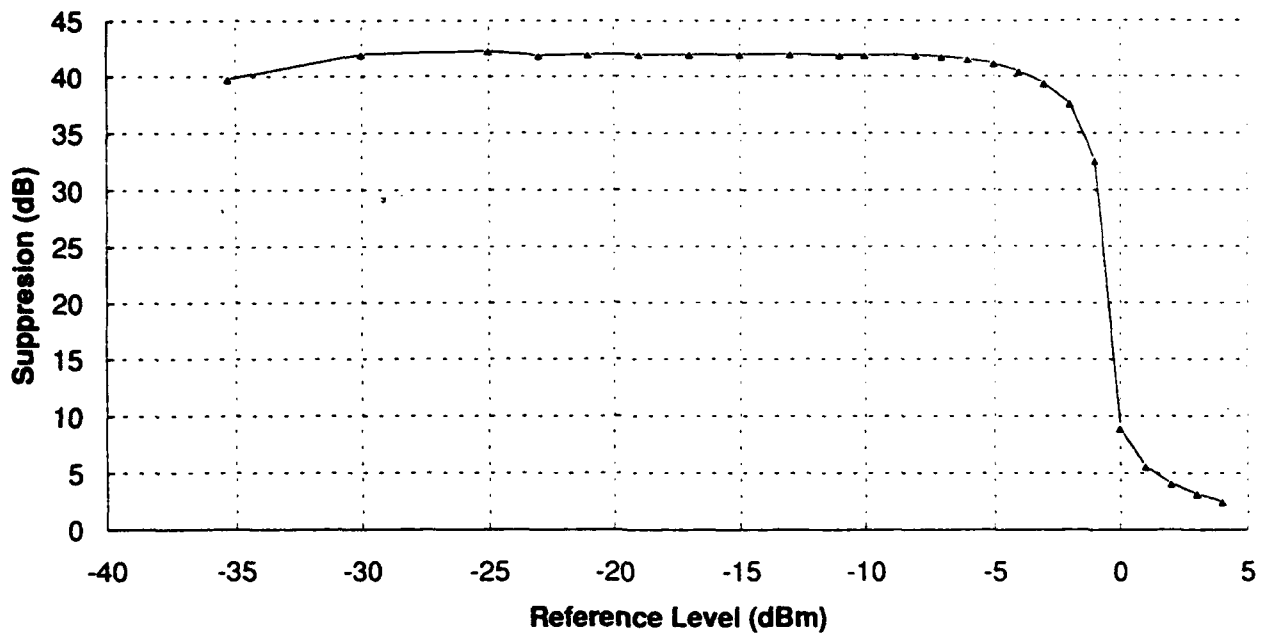*Figure 7.5. Typical Measured Single Tone Suppression*

- 57 -

Figure 7.6. Single Tone Suppression Versus Reference Level

to about 0 dBm. Above 0 dBm the estimate cannot match the reference and no suppression is possible. Below 0 dBm the estimate signal can be amplified to match the reference, producing a 42 dB decrease in signal strength. For signal levels below -30 dBm the suppression begins to drop as the error signal reaches the noise floor of the system and limits the loop gain.

7.2.2 Two Tone Suppression

To measure the two tone suppression the system is modified as shown in Figure 7.7. A second signal generator is used as the source of the second tone. This tone splits into two paths as does the first tone. The signal feeds the signal generation chassis through port RF2. The other signal path is summed with the first tone as the reference. The two tones are set to equal amplitudes using a spectrum analyzer. The second tone remains at a constant frequency while the first tone sweeps across the frequency band. The result is shown in Figure 7.8. The power of the second tone is then decreased by 10 dB, 20 dB, 30 dB, and 40 dB relative to the first tone. Figures 7.9–7.12 show the resulting suppression achieved.

7.2.3 Spread Spectrum Suppression

To measure the suppression of a spread spectrum signal the network analyzer output is phase modulated by a digital sequence of 64 bits in length approximating a 63 bit p-n sequence. This particular spread spectrum tone is chosen due to its narrow autocorrelation peak. This will represent a near worst-case scenario, as the narrow correlation peak reduces the loop gain available in the system. Figure 7.13 shows the system diagram for making these measurements.
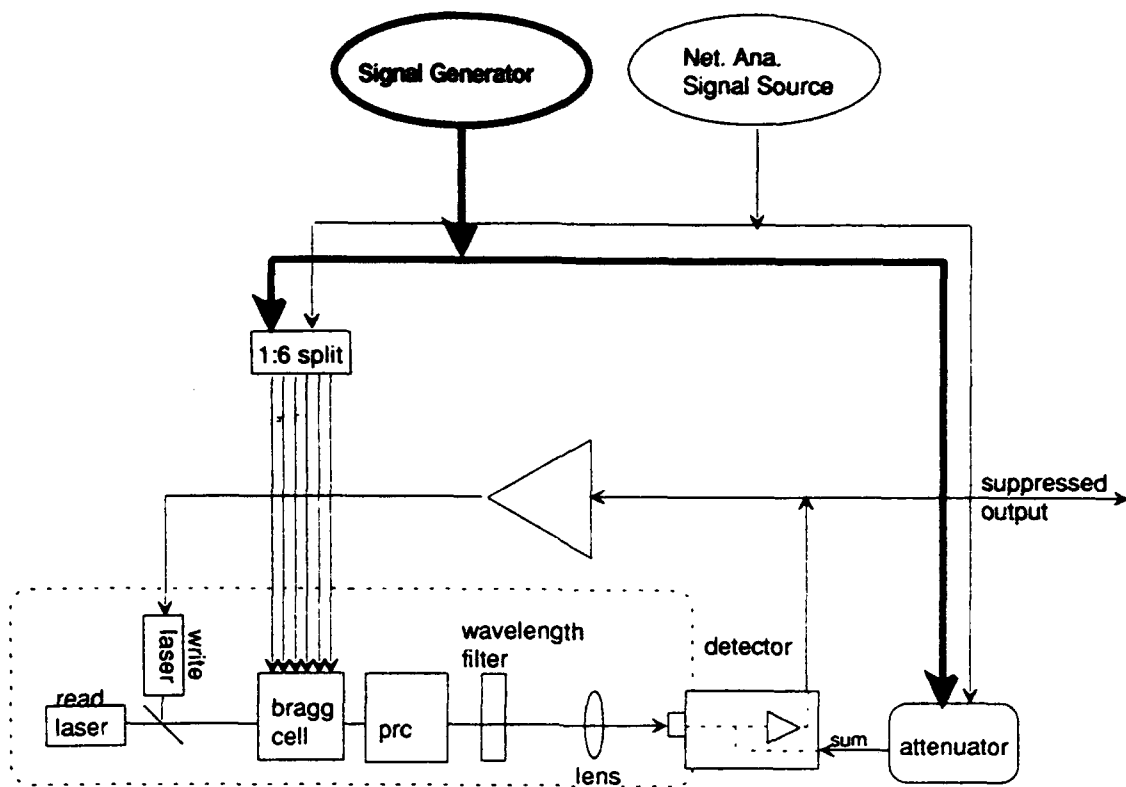
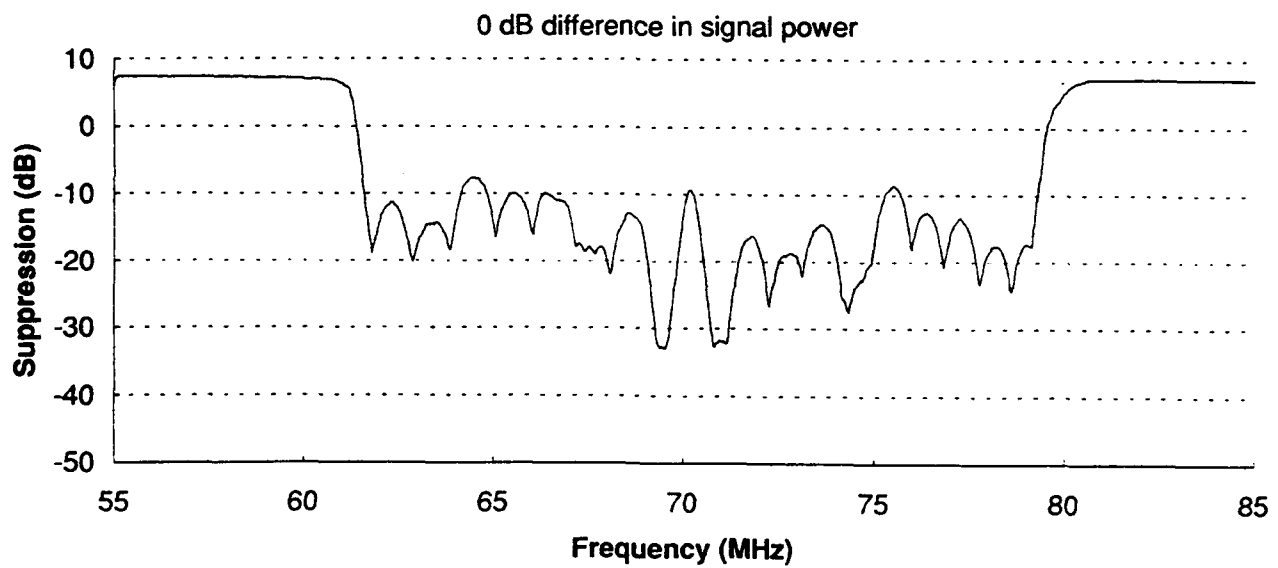*Figure 7.7. Configuration for Two Tone Suppression Measurement*

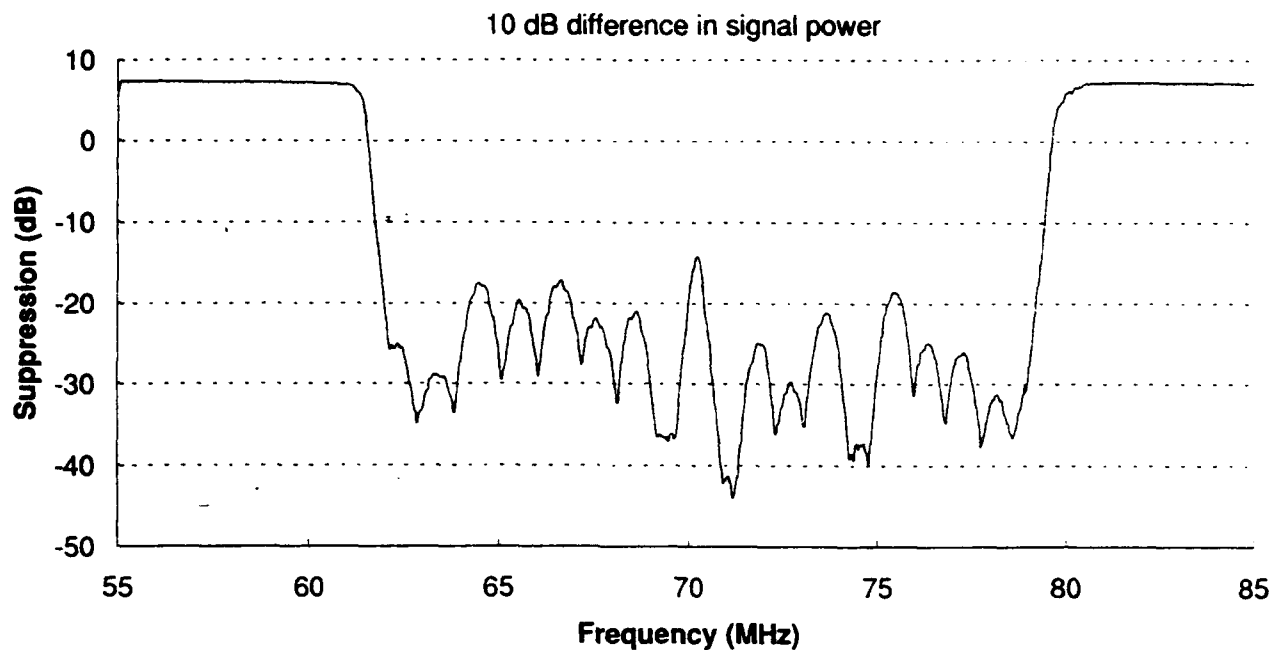*Figure 7.8. Suppression for Swept Two Tone Measurement*

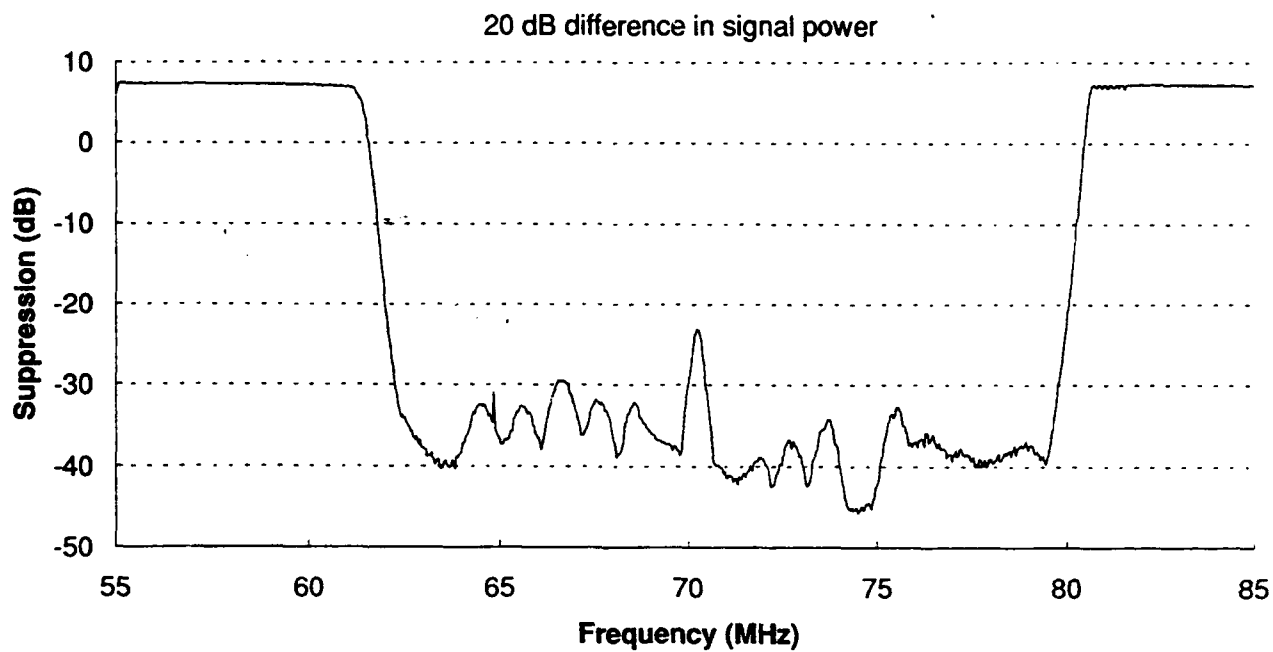*Figure 7.9.   Suppression With Second Tone Reduced 10 dB*

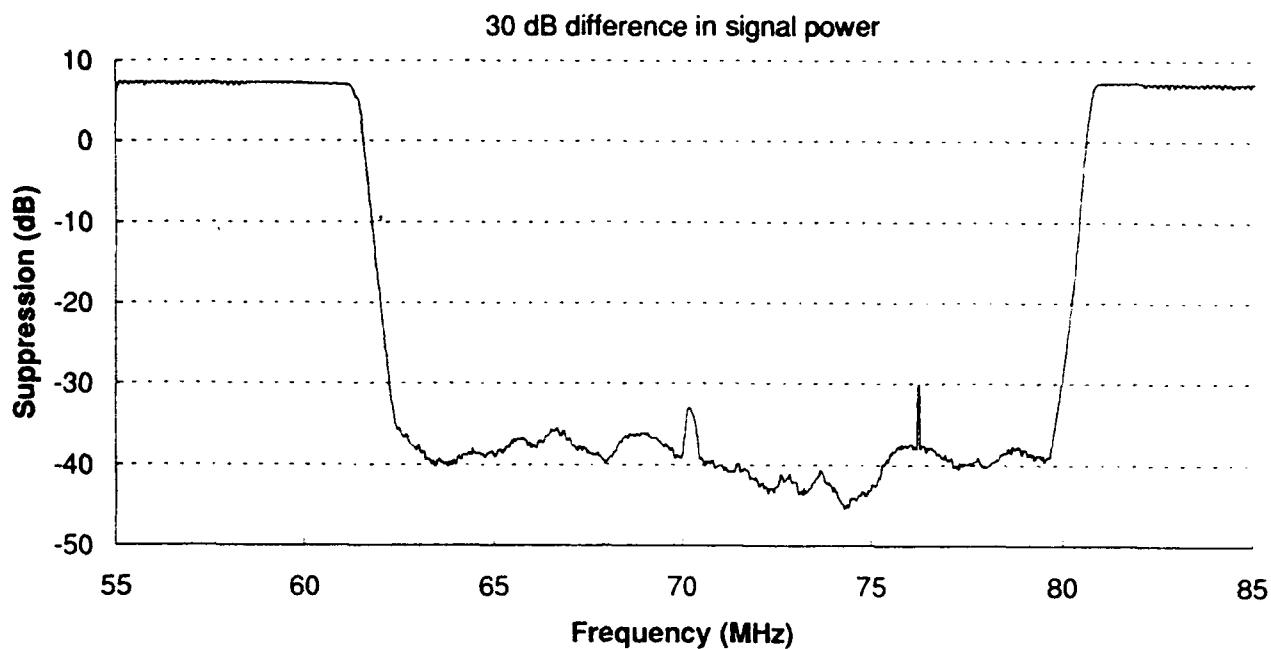*Figure 7.10.   Suppression With Second Tone Reduced 20 dB*

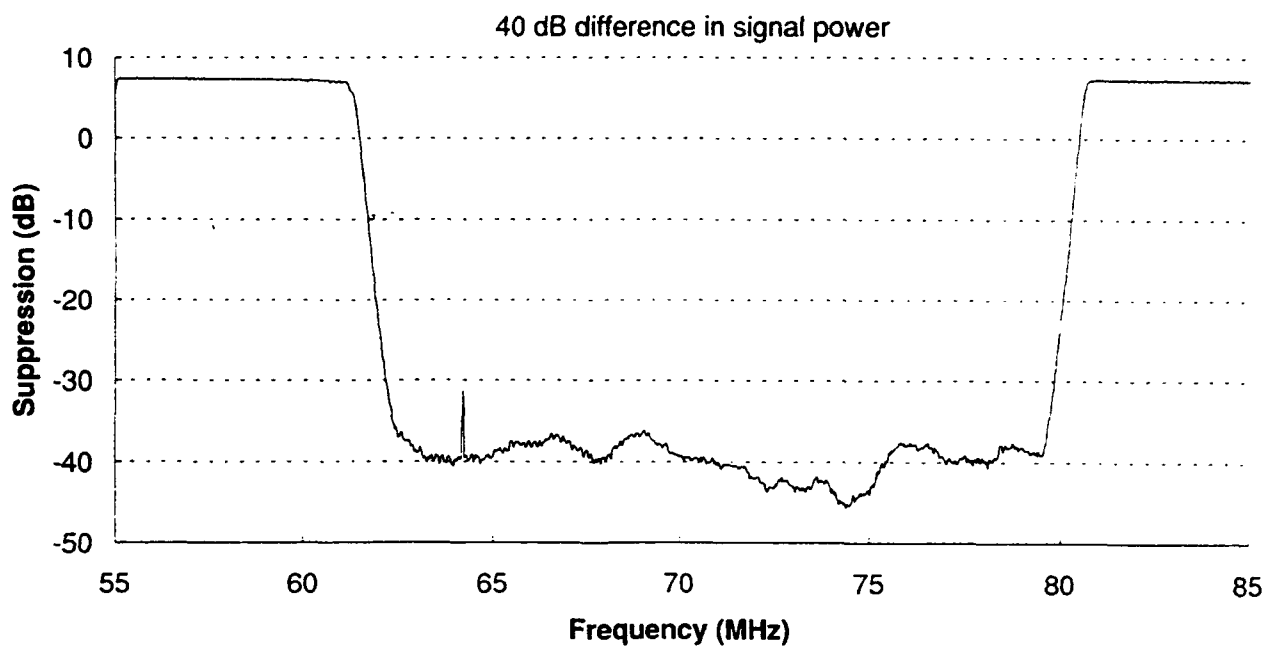*Figure 7.11. Suppression With Second Tone Reduced 30 dB*

Figure 7.12. Suppression With Second Tone Reduced 40 dB

The signal from the network analyzer is mixed with a p-n sequence generator, and the result is fed to the signal input of the signal generation electronics. The suppressed signal port connects to a spectrum analyzer. The signal spectrum is then monitored as the signal is suppressed. Quantitative results are made by measuring the total power with a RF power meter. The spread spectrum suppression is defined as the difference of RF power measured under suppression and without suppression as measured by a RF power meter. We measured spread spectrum suppression for p-n clock rates of 1 MHz to 10 MHz. Figures 7.14–7.17 show spectrum analyzer traces of suppressed and unsuppressed spread spectrum signals.

To increase the suppression of spread spectrum signals, we added a bandpass filter in the signal path with a pass band of the same width as the signal spectrum.

The analytical basis for using a filter in the reference path was presented in Paragraph 3.3.1. One argument to explain the improved performance obtained by this approach is that the tapped delay line filter is creating a replica of the reference waveform and subtracting the replica from the actual. The adaptive system can create a better replica for the filtered waveform than it can for a broadband waveform. This is especially true for any real system which has bandwidth limiting components in the tapped delay line itself. Figure 7.18 is a plot of suppression versus signal bandwidth for various reference channel filter bandwidths. A plot of suppression versus signal strength for a 5 MHz signal is shown in Figure 7.19. The saturation effect seen as the reference power level increases is a more gradual effect than the same phenomenon seen in Figure 7.6. This occurs because the signal power spreads among many frequencies with different amplitudes, rather than a signal with all its power in a single frequency. The noise level of the system affects the response
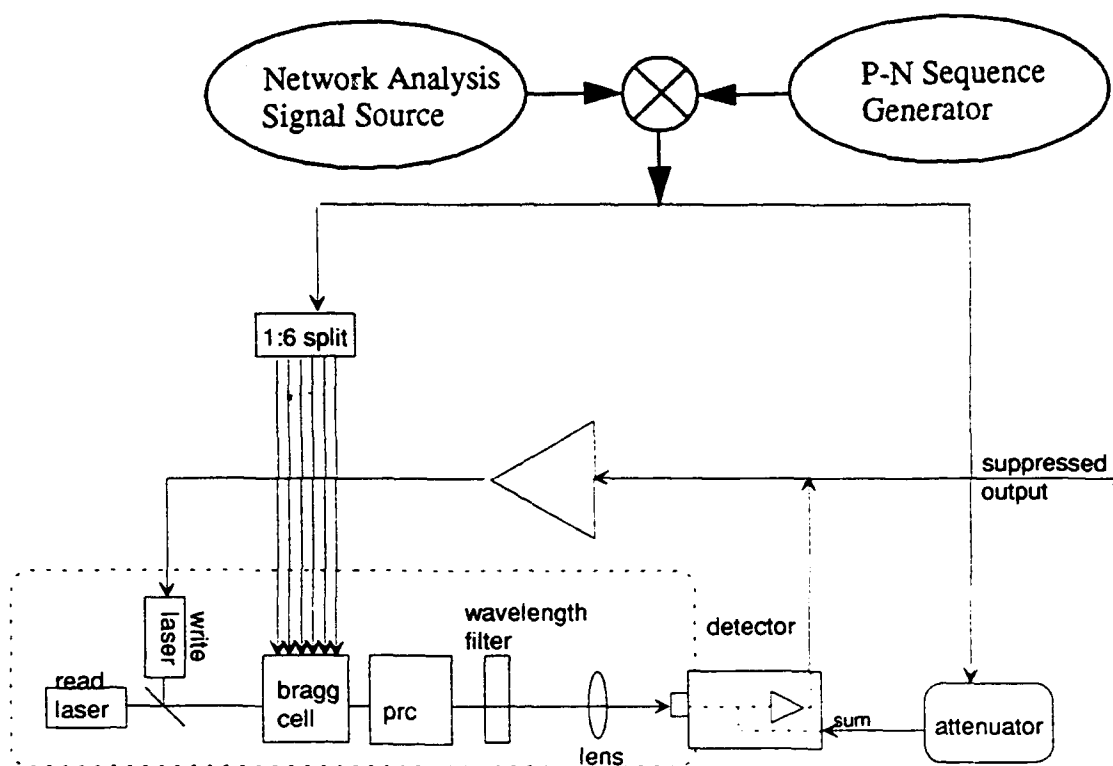
Figure 7.13. System Diagram for Broadband Measurements

- 62 -
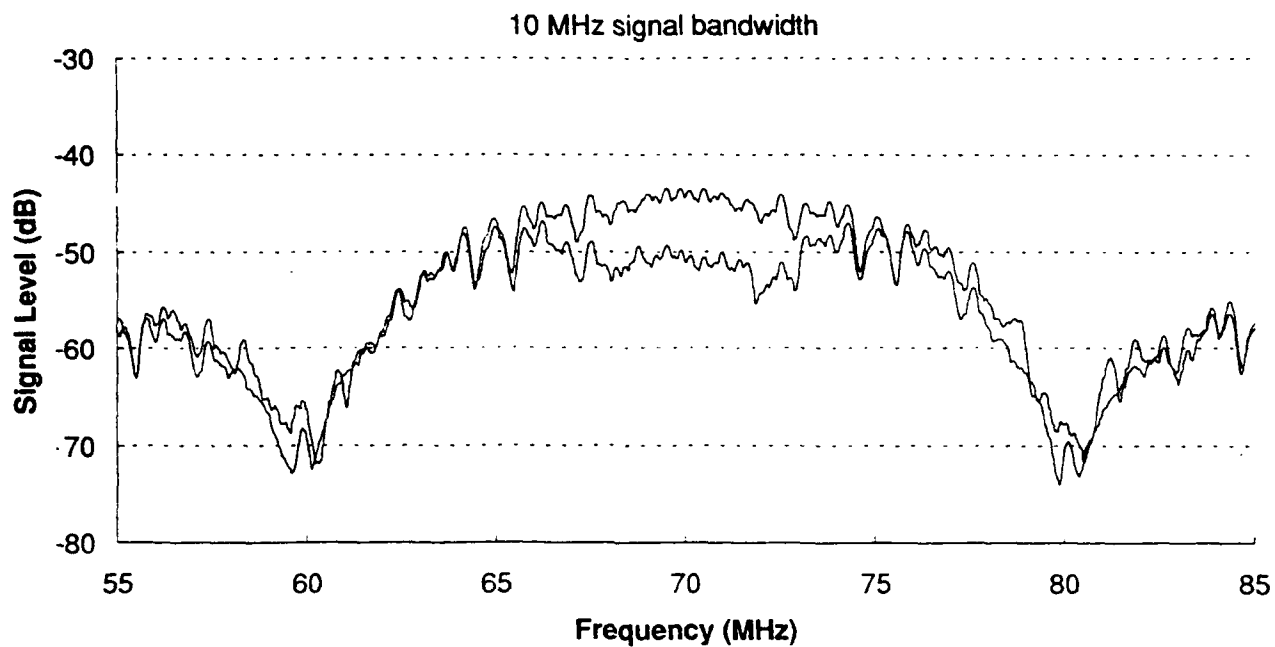
Figure 7.14. Spectrum of Suppressed and Unsuppressed Signals (10 MHz)
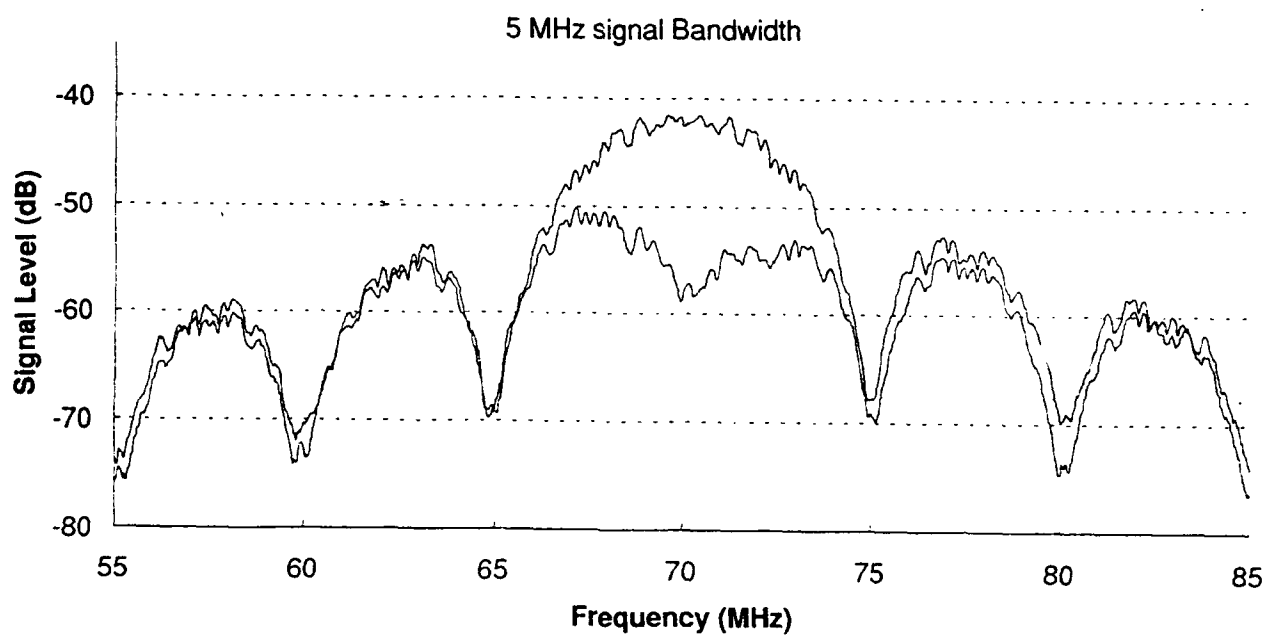
Figure 7.15. Spectrum of Suppressed and Unsuppressed Signals (5 MHz)

2 MHz signal bandwidth
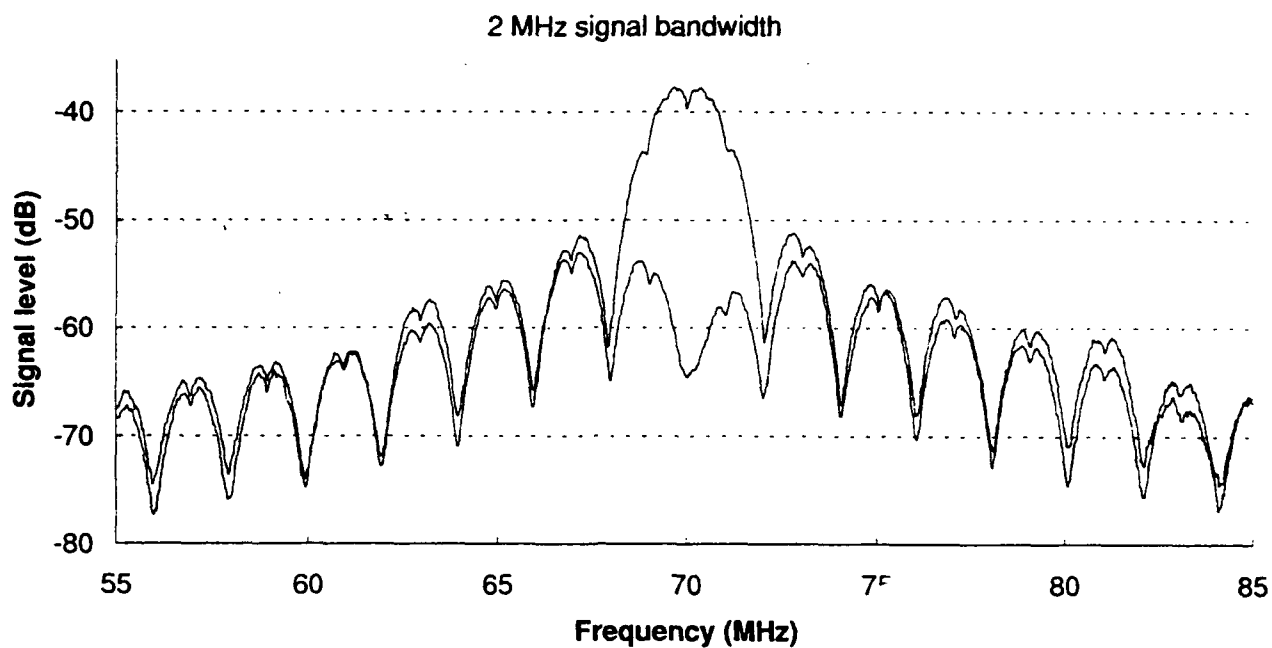
Figure 7.16.   Spectrum of Suppressed and Unsuppressed Signals (2 MHz)
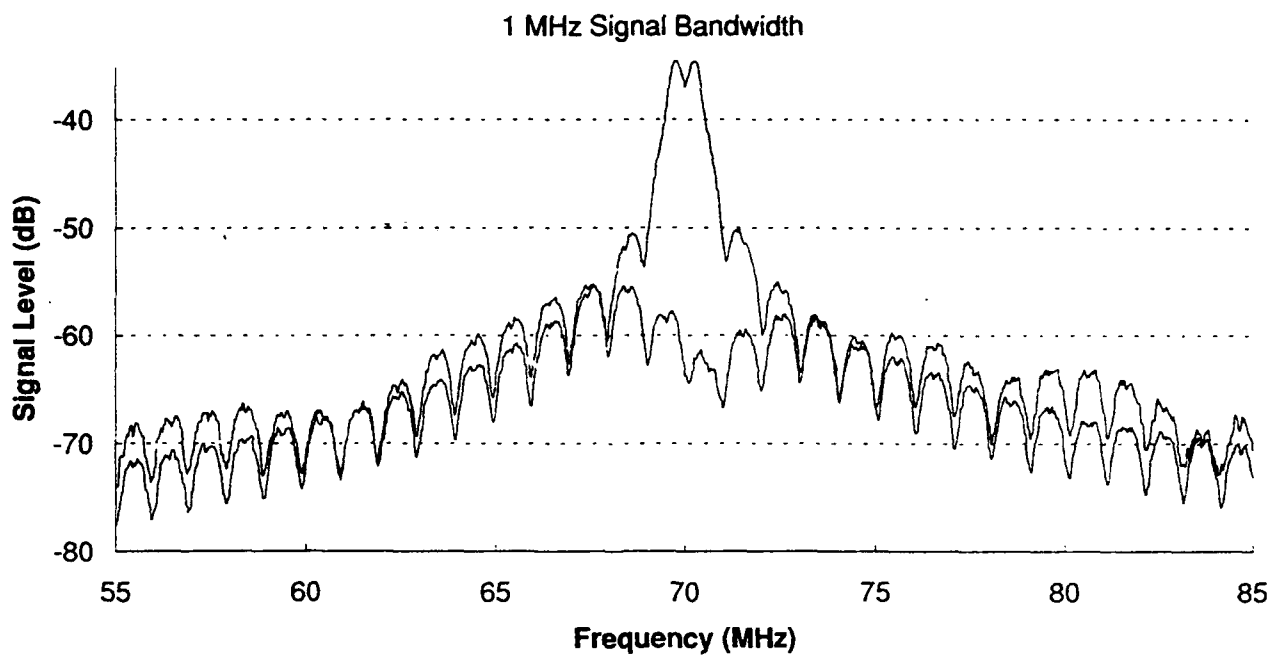
1 MHz Signal Bandwidth

Figure 7.17.   Spectrum of Suppressed and Unsuppressed Signals (1 MHz)
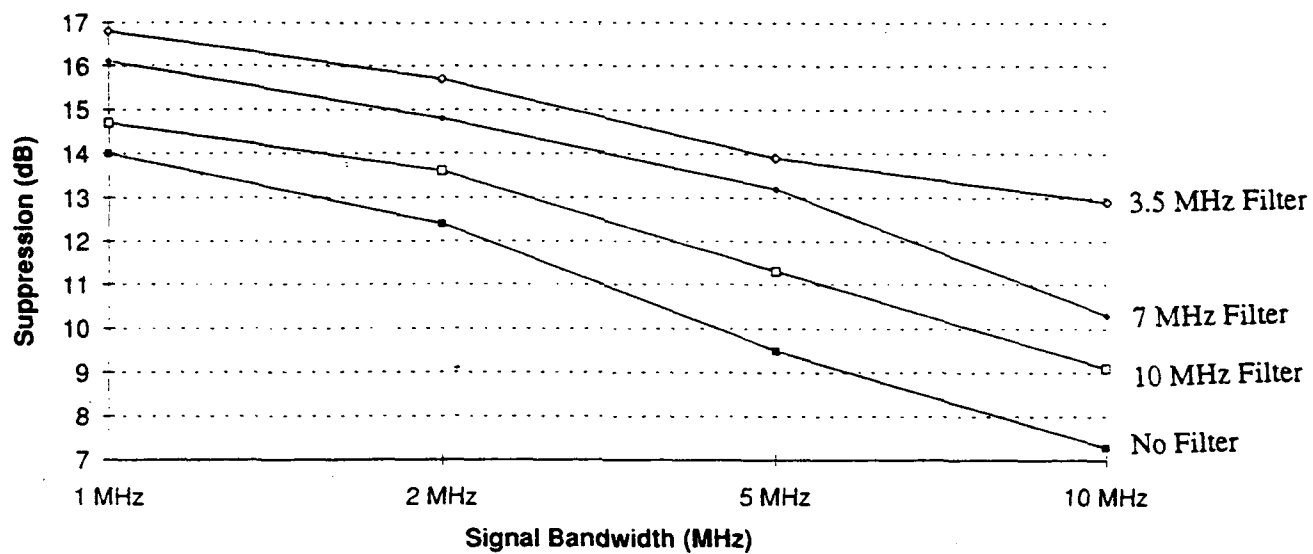
Figure 7.18. Suppression Versus Signal Bandwidth
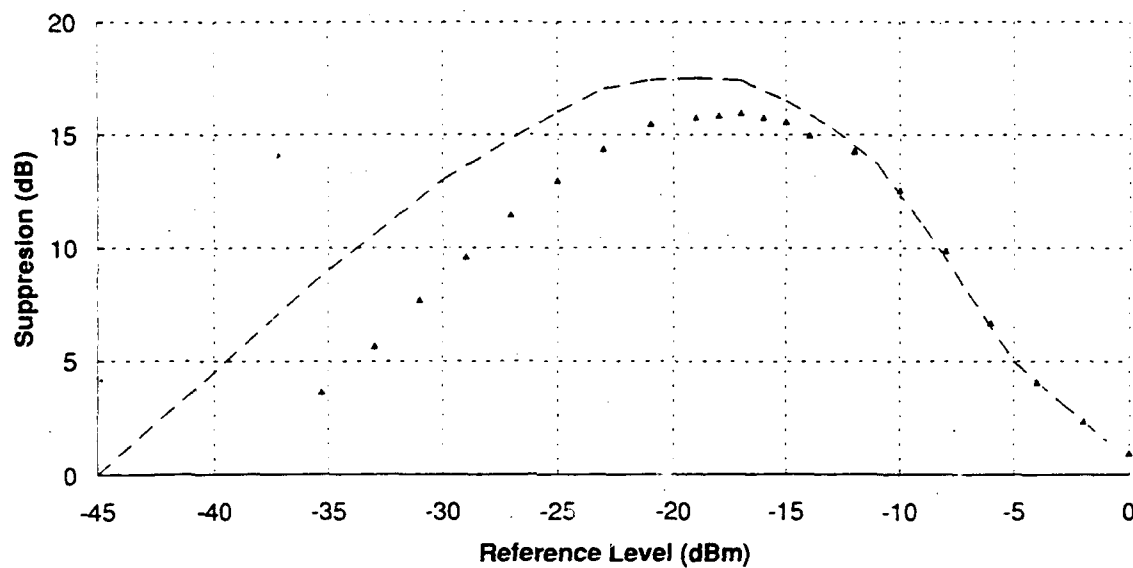
Figure 7.19. Suppression Versus Reference Level at 5 MHz Bandwidth

of the system at higher reference levels than shown in the single tone measurements. Since the curve does not reach a plateau at its peak, it can be argued that the maximum possible suppression for spread spectrum signals is greater than the 22 dB indicated on the graph. A lower system noise level shifts the positive sloped portion of the curve to the left on the graph, allowing the curve to peak at a higher value before saturation effects dominate, as indicated by the dashed line.

7.2.4 Measurements Performed With a Low Noise Read Laser

Since the read laser exhibits a high level of RIN noise, we believed that this noise level was limiting the system performance. To test this hypothesis we removed the 1.3 m laser diode and replaced it with a Nd:YAG ring laser oscillating at 1.319 m. This laser has exceptionally narrow spectral linewidth (~5 kHz) and a correspondingly low RIN level.

A lens system expanded the beam size to the same size as the laser diode beam. A variable neutral density filter wheel placed in the beam path allows for adjustment of the read laser power level. Measurements of noise levels in the system indicate that the noise floor of the preamplifier housed in the detector assembly now limits the system, rather than optical noise sources.

Measurements made of single tone suppression in the same manner as described in Paragraph 7.2.1 are shown in Figure 7.20. This plot shows a suppression of 40 dB over 23 MHz, and 45–50 dB suppression over 20 MHz an improvement of some 7–10 dB over previous measurements. An alternate optical alignment produced the data shown in Figure 7.21. It shows greater than 50 dB of suppression over a smaller bandwidth of 9 MHz. Two tone measurements as described in Para-
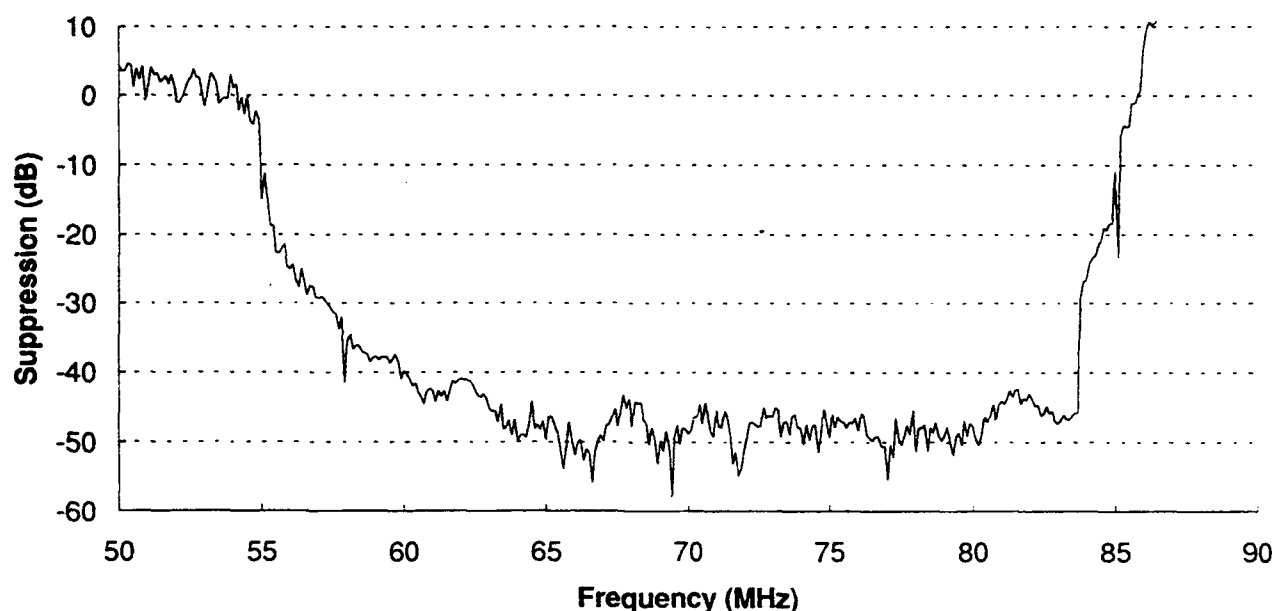
Figure 7.20.   Single Tone Suppression With Low Noise Read Laser
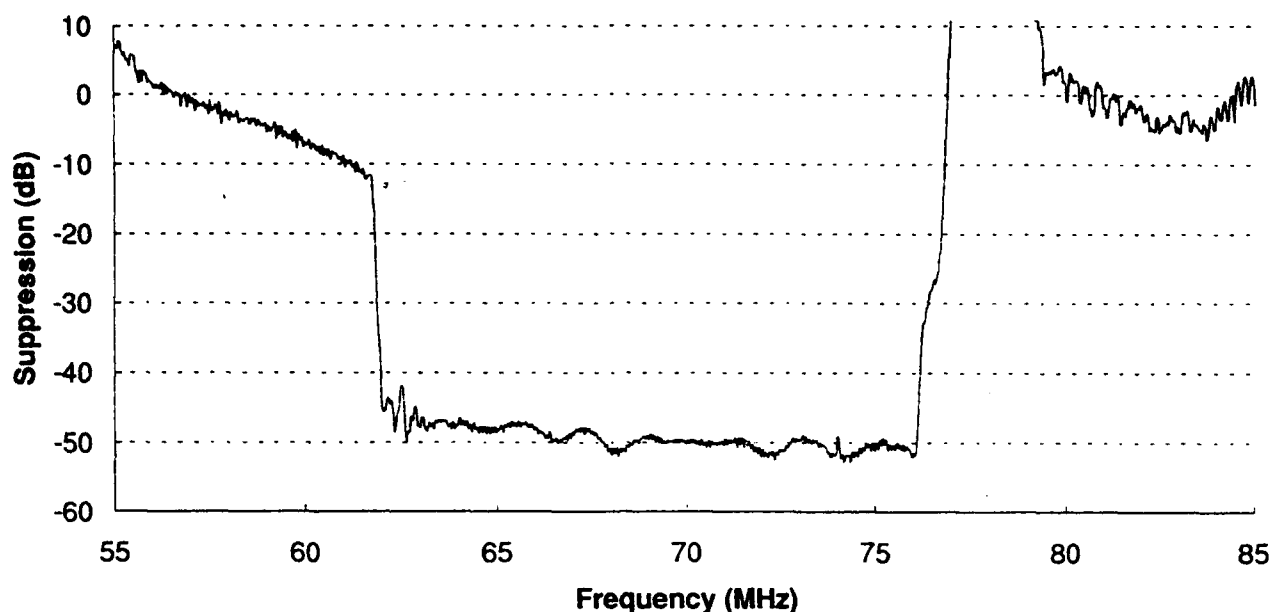
Figure 7.21. Demonstration of 50 dB CW Suppression

graph 7.2.2 showed little improvement over data taken with the laser diode read beam. The results are shown in Figures 7.22–7.25.

Spread spectrum measurements as described in Paragraph 7.2.3 were made and the results are shown in Figure 7.26. This data reflects measurements made with a RF power meter. The signal was first passed through a filter before being detected with the power meter. For measurements using 3.5 MHz filter in the reference path, the RF meter was filtered with a 7 MHz wide filter. Similarly, the 7 MHz filter in the reference path was coupled with a 10 MHz filter on the RF power meter. Measurements with a 10 MHz filter in the reference path was made with a 8 MHz filter on the power meter because no filter was available with wider bandwidth. This system suppresses a 10 MHz bandwidth signal by a total of 20 dB. However, suppression of the peak signal strength is much greater. This is seen in Figure 7.27, a spectrum analyzer trace of a 7 MHz bandwidth signal with and without suppression. Figure 7.26 indicates that the maximum suppression is on the broadband power meter is 23 dB. However, from the spectrum analyzer we see that the peak frequencies suppress more than 30 dB.

Returning to the two tone measurements, we studied the effect of a second signal incident from a different angle than the first. The first signal was inserted into the system at "boresight," that is with no relative phase shifts between array elements. The second signal was inserted into the system such that each element was shifted relative to its neighbor by 45, 90, and 127. To do this, we used the cables inside the signal generating electronics chassis. These cables provide the necessary time delay to simulate the off-axis signal. The results of these measurements are shown in Figures 7.28–7.30.
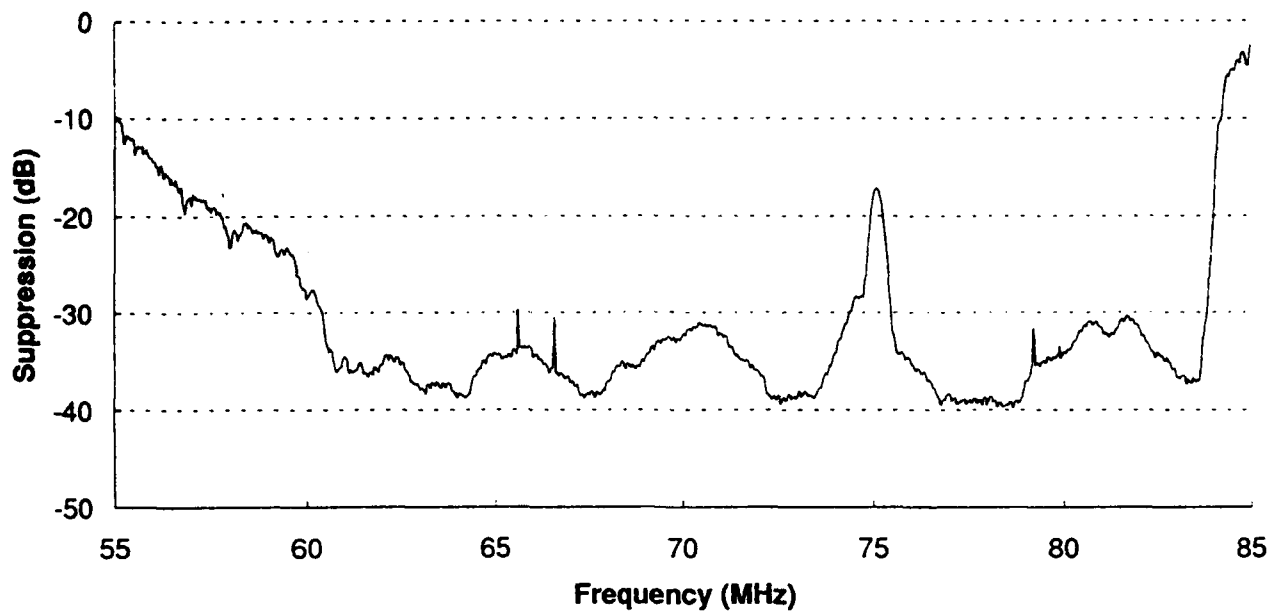
Figure 7.22.   Two Tone (0, -30 dB) Suppression With Low Noise Read Laser
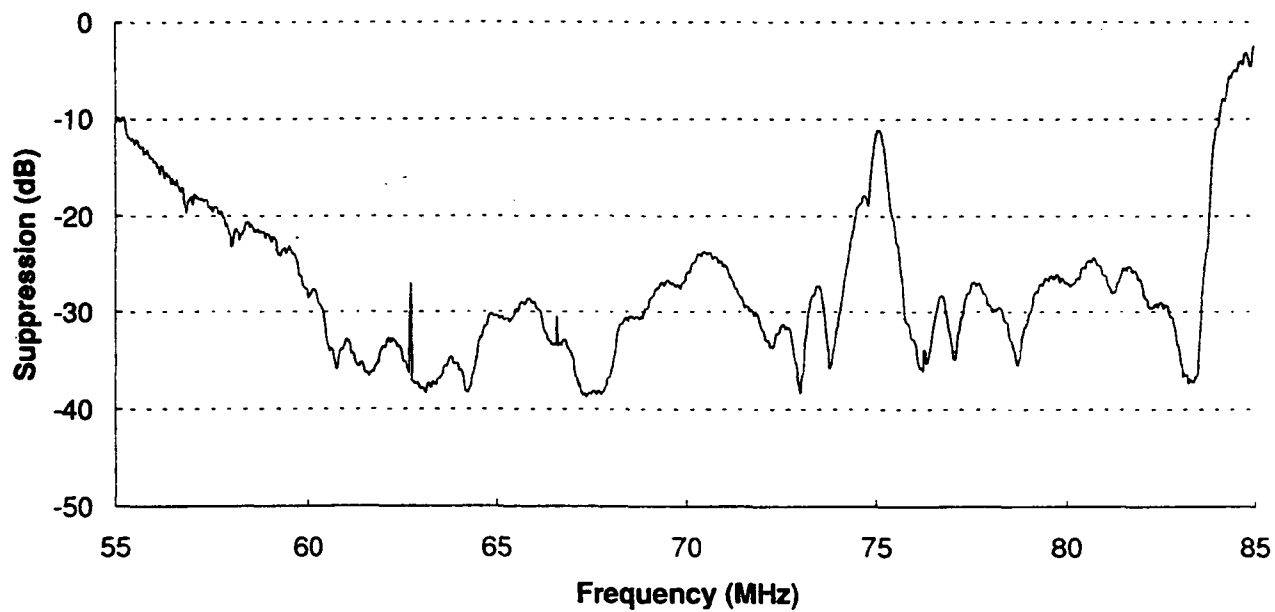
Figure 7.23.   Two Tone (0, -20 dB) Suppression
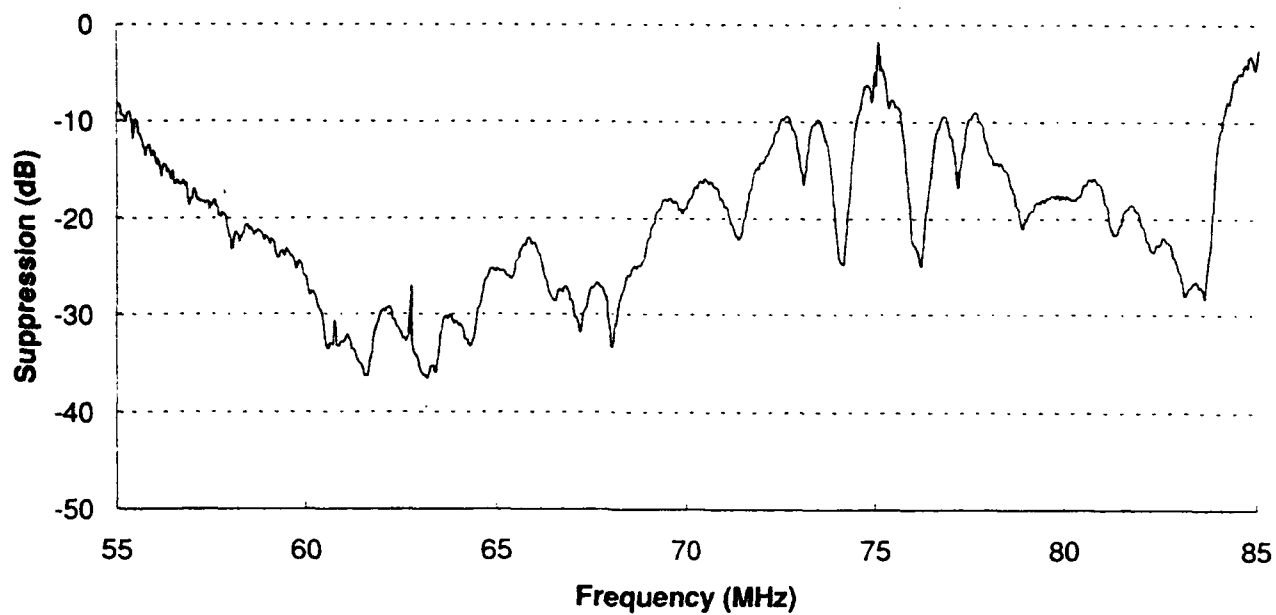
Figure 7.24. Two Tone (0, -10 dB) Suppression
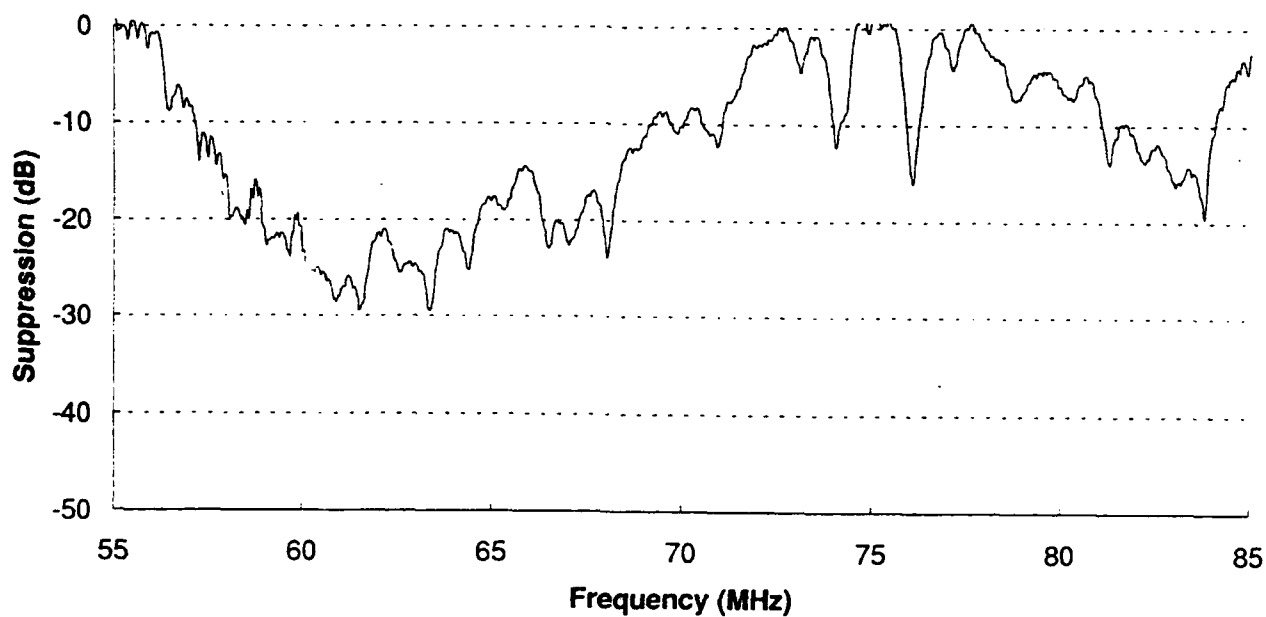
Figure 7.25. Two Tone (0, 0 dB) Suppression
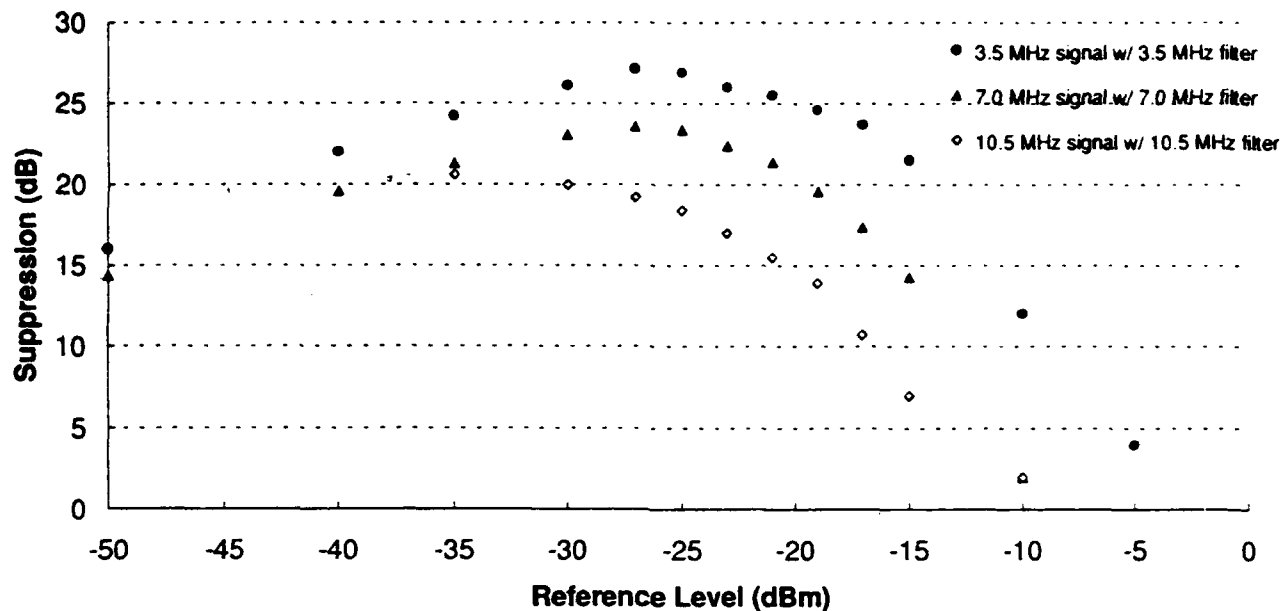
Figure 7.26. Suppression of Broadband Signal Using Low Noise Read Laser
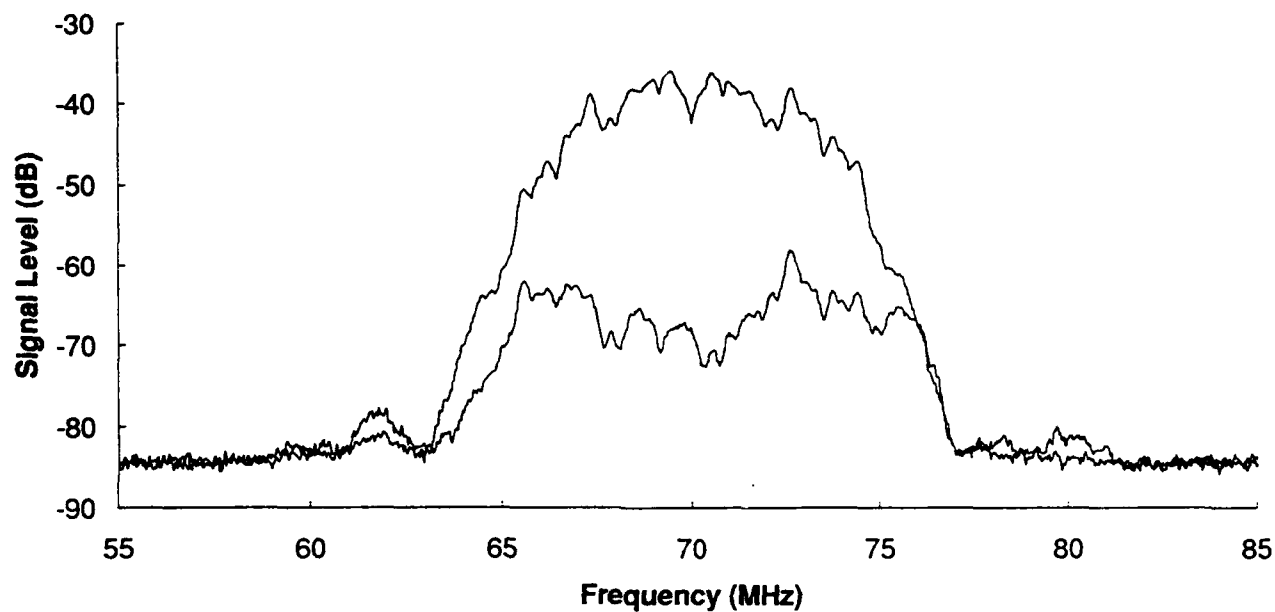
Figure 7.27. Spectrum of 7 MHz Signal With and Without Suppression
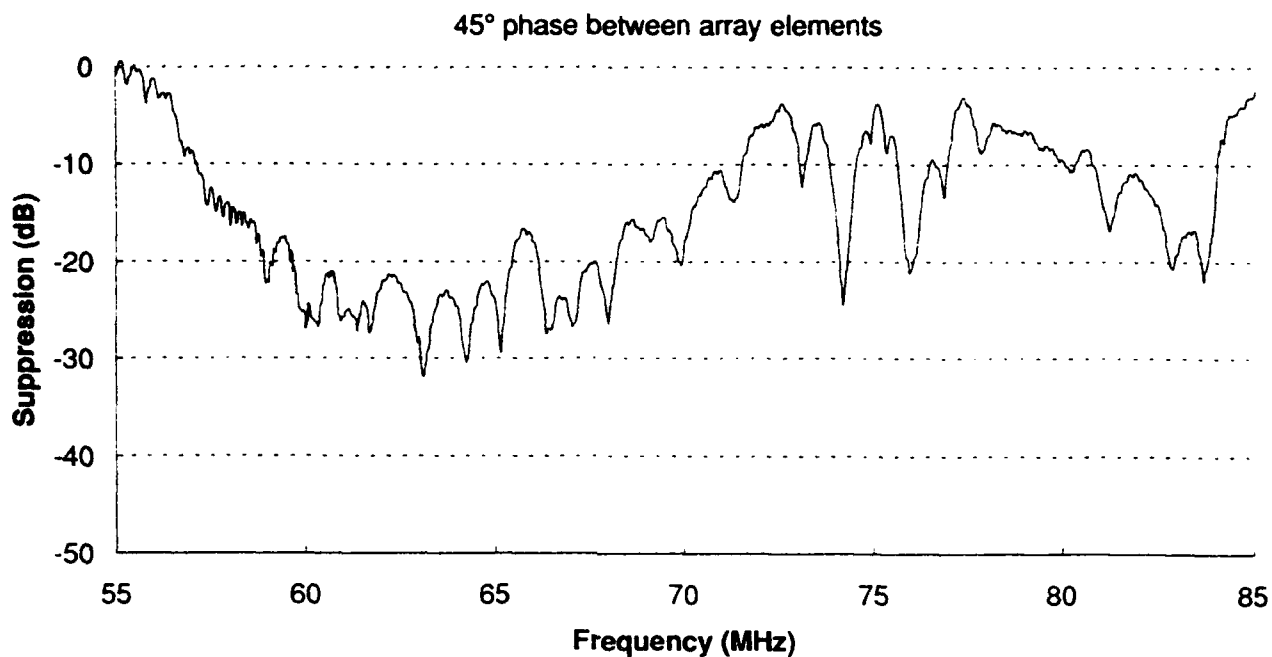
Figure 7.28.   Suppression Measured With 45 Degree Phase/Element

Compare these figures with Figures 7.22–7.25 for the case where both signals are incident at bore-sight. Significant improvement occurs as the phase angle between elements increases.

127° phase between array elements
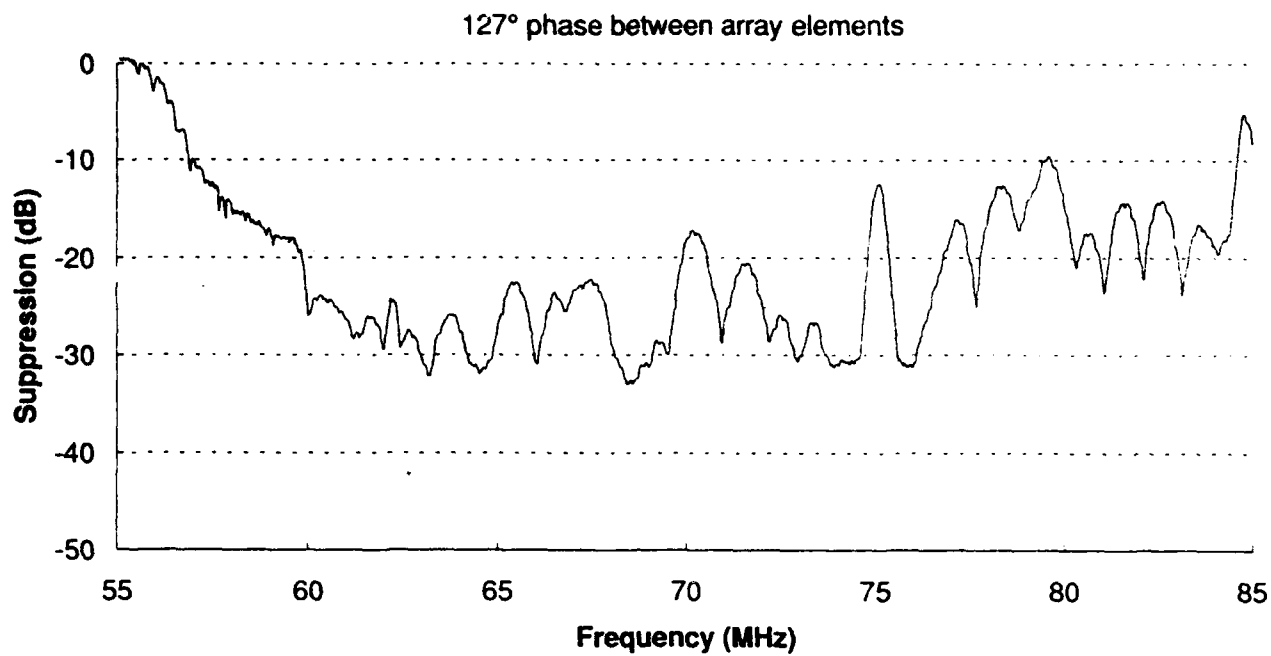
Figure 7.29. *Suppression Measured With 127 Degree Phase/Element*

90° phase between array elements
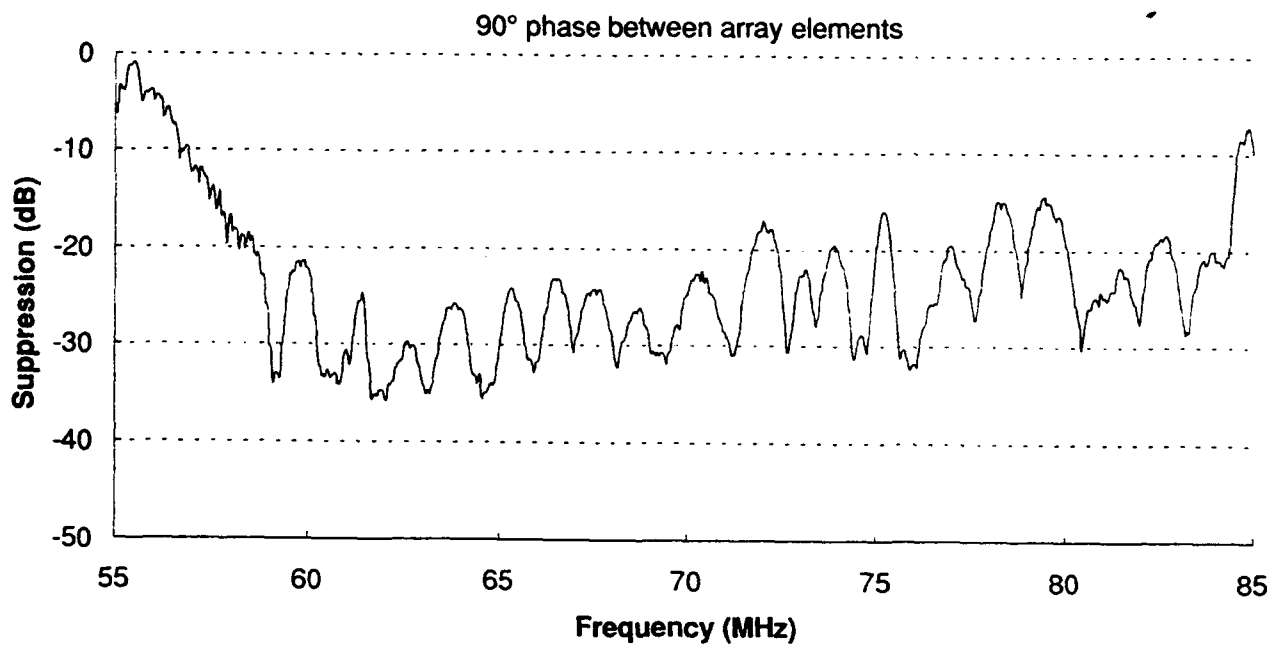
Figure 7.30. *Suppression Measured With 90 Degree Phase/Element*

8.0 CONCLUSION

The photorefractive processor is a simple design which is tolerant of minor imperfections in the optical system. The simplicity and compactness in the design make it a robust system in terms of mechanical stability and alignment. It also allows the system to perform near its theoretical limits without serious degradation due to optical imperfections.

Even though it was performing near its theoretical performance level the system performed only marginally well on broadband signals in terms of required specifications. This poor performance against broadband sources was shown to be inherent in the algorithm itself. This inherent limitation arises from the fact that the system has many degrees of freedom (available independent tap weight values) but it uses only a few of them for a particular broadband interferer. It uses all the tap weights when cancelling a CW interferer. Therefore, it has good suppression performance against CW interference.

We developed a concept of CW loop gain which shows that the CW gain increases linearly with the number of degrees of freedom (taps) if the gain per tap is held constant. Also, we showed that the gain per tap times the number of taps actually utilized by the system is the effective gain for a broadband signal with a uniform spectral distribution. This effective gain is equal to the CW gain divided by the time bandwidth product of the delay line maximum delay and the signal bandwidth. A signal delay line time bandwidth product of 10 reduces the effective loop gain (and, therefore, the suppression) by 20 dB.

In addition to this effective gain reduction, which is inherent in the algorithm, there is an additional degradation (also inherent in the algorithm) for signals which have a nonuniform spectrum. When the spectrum is nonuniform the LMS algorithm suppresses the strong signal components but has little effect on the weak ones. This well-known characteristic arises from the fact that the effective loop gain for each frequency component is proportional to the power of that component (or power spectral density).

Both of the effects described above are effective in creating the poor broadband suppression results achieved by the experimental system.

It is the excellent performance of the system as compared to theory which has allowed us to observe the limitations at work. Many programs for developing optical adaptive filters simply have not achieved adequate performance to see the fundamental limitations stand out from the limitations imposed by the equipment, materials, and design of the specific experiment.

The unprecedented CW performance results achieved by the optical processor on this program are indicative of the basic performance capability. This CW performance, unfortunately, has been shown to be not sufficient to guarantee broadband performance. However, the CW performance is necessary for broadband performance and it is a good benchmark for comparing processors.

9.0 REFERENCES

1. White, Warren D., *Wideband Interference Cancellation in Adaptive Sidelobe Cancellers*, IEEE Trans. A&ES, AES-19, (Nov. 1983), pgs. 915–925.

2. Widrow, B., et al, *Adaptive Antenna Systems*, Proceedings of the IEEE, 55, 2143 (1967).

3. Penn, W.A., *Status Report on the Acousto-Optic Adaptive Processor*, Proceedings of the 1986 Alsilomar Conference on Computing, IEEE pub. 1987, pg. 196.

4. Friedman, Dan, *Design Requirements Development for the AONSP Acousto-Optic Adaptive Processor*, SPIE Proceedings, Vol. 1703, 1992, pgs. 387–404.

5. Montgomery, R.M., *Adaptive Filter With Correlation Weighting Structure*, U.S. Patent #5173790, Dec. 22, 1992.

Uncited relevant publications

6. Montgomery, R.M., Lange, M.R., *Development of a Photorefractive Grating Via Temporally Modulated Photoconductivity and a Correlated ac Bias*, J. Appl. Phys., 66 (5), 1915 (1989).

7. Montgomery, R.M., *Acousto-Optic/Photorefractive Processor for Adaptive Antenna Arrays*, SPIE Proceedings 1217 Conference on Optoelectronic Signal Processing for Phased-Array Antennas II, January 1990.

8. Montgomery, R.M., Beaudet, William R., Lange, M.R., *Photorefractive Adaptive Sidelobe Canceller for Phased Array Antennas*, SPIE Proceedings 1703 Conference on Optoelectronic Signal Processing for Phased-Array Antennas III, April 1992. pgs. 405–410.

10.0

10.1 Time Domain Simulation Program

```
c simulation of sidelobe cancelling tdl filter
c with random sq. wave signal and limiting
 PROGRAM mcpn
 REAL SDL(1:6,0:1024),W(1:6,0:1024),BUFERR(0:1024)
 REAL spc(1:10),Ang(1:10),sigbuf(0:1024)
 REAL fracdel(1:6,1:10)
 REAL T,DT,DE,F1,F2,OMEGA1,OMEGA2,DELAY,BCLEN,TAUPR
 REAL DECR,LGAIN,ALPHA,EST,megsn
 REAL ref,A2,THETA1,DTHETA1,theta2,dtheta2
 REAL srate,chipval,MSE,MSEal,PWRLimit,Alimit,pdn,MSR
 Integer ADEL(1:6,1:10),sigdel(1:10)
 INTEGER LMDA,TML,NTAPS,TAPSDELAY,buflen,NDEL,Nc,Nch
 INTEGER Njam,Nj,NT,MICROSEC,TOLD,Nint,Din
 INTEGER runcount,chiplen
CHARACTER*2 runchar
c increment a file which keeps track of the run number
                open(unit=25,file='mcrun.num')
                read(25,*)runcount
                runcount=runcount+1
                rewind(unit=25)
                write(25,*)runcount
                close(unit=25)
c Read parameters for this run. -
c These parameters can be changed by editing the text file "mcparam.dat"
                open(unit=24,file='mcparam.dat')
                read(24,*)chiplen
                read(24,*)bclen
                read(24,*)delay
                read(24,*)Nch
                read(24,*)Njam
                read(24,*)Lgain
                read(24,*)F1
                read(24,*)Tmax
                read(24,*)taupr
                read(24,*)Tapsdelay
                read(24,*)(ang(j),j=1,Njam)
                read(24,*)(sigdel(j),j=1,Njam)
```

```fortran
            close(unit=24)
            runchar=char(48+mod(runcount/10,10))//
      & char(48+mod(runcount,10))
            TWOPI=6.28318531
            srate=8.0*70.0e6
            f2=67.0e6
            DT=1/srate
c phodet. noise is 79 db below ref in 1 MHz bw)
            megsn=79.0
            pdn=sqrt(10**(-megsn/10)*srate/(2.0*1.0e6))
c pdn=0.0
c set sine wave amplitude
            A2=1.0
            chipval=1.414
c limit level in dB relative to ref power.
            PWRLimit=-22.0
c compute amplitude limiting level from dB level
            alimit=10**((PWRlimit-3)/20.0)*chipval
            OMEGA1=TWOPI*F1
            OMEGA2=TWOPI*F2
            DTHETA1=OMEGA1*DT
            DTHETA2=OMEGA2*DT
c Bclen=length of bragg cell delay lines
c Nch=number of antenna elements (channels)
c element location (spacing) in wavelengths
            do i=1,Nch
            spc(I)=0.5*real(I-1)
            end do
c MAXIMUM DELAY IN SAMPLES
            NTAPS=INT(BCLEN/DT)
            if (Ntaps .GT. 1024) then
            buflen=Ntaps
            else
            buflen=1024
            endif
c ** trap to terminate program when ntaps exceeds array size **
            if (NTAPS.GT.1024) THEN
            WRITE(*,*)"DELAY LENGTH EXCEEDS ARRAY CAPACITY"
            T=TMAX
            endif
```

```
c TAUPR=P HOTOREFRACTIVE TIME CONSTANT
c DECR=INTEGRATOR LOSS DECREMENT PER SAMPLE
          DECR=1.0-DT/TAUPR
c convert loop gain from db to multiplier ALPHA (factor 2 from eq 2.9)
          ALPHA=2.0*EXP(LGAIN/8.68)*(DT/TAUPR)/(Nch*NTAPS)
c NO. OF SAMPLES DELAY IN ERROR CHANNEL
          NDEL=INT(DELAY/DT)
c NUMBER OF TAPS DELAY BEFORE 1ST NON ZERO WT
c TAPSDELAY=1
c ** INITIALIZE delay line and tap wts **
            do Nc=1,Nch
            do NT=0,buflen
            SDL(Nc,NT)=0.0
            W(Nc,NT)=0.0
            BUFERR(NT)=0.0
            END do
            End do
C Open a file to write the suppressed signal amplitude.
            open(unit=20,file='trak.'//runchar)
C
c ** Begin iteration of samples **
            NT=-1
            THETA1=-DTHETA1
            Theta2=-Dtheta2
            T=0.0
            Nint=1024
            MSE=0.0
            MSEal=0.0
            MSR=0.0
            do WHILE (T.LT.TMAX)
            NT=NT+1
            T=DT*NT
            THETA1=AMOD(THETA1+DTHETA1,TWOPI)
            THETA2=AMOD(THETA2+DTHETA2,TWOPI)
            MICROSEC=INT(1.0E6*T)
c **At 1 microsec intervals compute power in delayed error
c signal. Nint points are used for the integration time const
            IF (TOLD.NE.MICROSEC) THEN
            Told=MICROSEC
C ** RECORD MSE **
```

```fortran
              if (MSE.GT.40.0) t=tmax
              WRITE(20,*)1*MICROSEC,10*LOG10(MSE/MSR),
            @ 10*LOG10(MSEal/MSR)
              ENDIF
c Signal angles and frequencies
c DIN is the DELAY INDEX FOR Ntaps ring buffer
              DIN=MOD(NT,buflen)
c chipval is value of (random) data chip, rann is library call to random number
              if (mod(nt+1,chiplen) .eq. 0) chipval=sign(1.414,rann(0,100))
c put random square wave into signal delay buffer
              sigbuf(din)=chipval*sin(theta1)
c initialize reference (sum of element signals)
              ref=0.0
              Do Nc=1,Nch
c sum all jammer components at each element
              SDL(Nc,DIN)=0.0
              do Nj=1,Njam
c Adel is antenna delay truncated to integer sample interval (dt)
c 8 samples/cycle gives possible 45 deg phase error
c so we use interpolation for the antenna element phase
              Adel(Nc,Nj)=int(SRate/f1*spc(Nc)*sin(ang(Nj)))
              fracdel(Nc,Nj)=AMOD((SRate/f1*spc(Nc)*sin(ang(Nj))),1.0)
c Interpolate to get delayed signal at each element
              SDL(Nc,DIN)=SDL(Nc,DIN)+(1.0-fracdel(Nc,Nj))*
            @ A2*sigbuf(mod(NT+buflen-adel(Nc,Nj)-sigdel(Nj),buflen))
            @ +fracdel(Nc,Nj)*
            @ A2*sigbuf(mod(NT+buflen-(adel(Nc,Nj)+1)
            @ -sigdel(Nj),buflen))
              end do
c ref is sum of all element signals with no additional phase
c this points the ref beam broadside
              ref=ref+SDL(Nc,mod(buflen+Din-NTAPS/2,buflen))/real(NCH)
c dividing by NCH normalizes the ref to the signal when
c the signal arrives broadside. There is a loss in ref level
c and ref/N when the arrival angle is different.
              End do
              EST=0.0
C
c ** COMPUTE SIGNAL ESTIMATE AS A WEIGHTED SUM OF DELAYED SIGNAL+-
NOISE **
```

```fortran
c NOT USING 1ST TAPSDELAY TAPS TML STANDS FOR T MINUS LAMBDA
          do LMDA=TAPSDELAY,NTAPS-1
          TML=MOD(NT+buflen-LMDA,buflen)
          do Nc=1,Nch
c ** ADD ERROR*(DELAYED SIGNAL) TO THE APPROPRIATE TAP WT **
          W(Nc,LMDA)=DECR*W(Nc,LMDA)+SDL(Nc,TML)*DE*ALPHA
          EST=EST+W(Nc,LMDA)*SDL(Nc,TML)
          END do
          End do
c ERROR = PRESENT REFERENCE-ESTIMATE+det. noise
          ERROR=(ref-EST+rann(0.0,pdn))
          MSE=MSE+(error**2-MSE)/NINT
          MSR=MSR+(ref**2-MSR)/NINT
c Limit error to value Alimit
          if (abs(ERROR).GT.Alimit) ERROR=sign(Alimit,ERROR)
          MSEal=MSEal+(error**2-MSEal)/NINT
c Store error in delay buffer, buffer length=buflen
          BUFERR(MOD(NT,buflen))=ERROR
c DE=DELAYED ERROR filtered in a 2 sample aperture filter
          DE=(BUFERR(MOD((NT+buflen-NDEL),buflen))+
       &  BUFERR(MOD((NT+buflen-NDEL-1),buflen)))/2.0
          end do
          open(unit=21,file='ersig.'//runchar)
          open(unit=23,file='tapwts.'//runchar)
          do in=1,buflen
          write(21,*)in,sdl(1,in),buferr(in),w(1,in)
          end do
          do in=1,Ntaps
          write(23,10)in,(w(i,in),i=1,6)
          end do
   10 Format(1I3,1p,6(1x,E9.2))
          close(unit=21)
          close(unit=20)
          close(unit=23)
          open(unit=24,file='mcparam.'//runchar)
          write(24,*)runcount,' run number for this run'
          write(24,*)chiplen,' chip length in samples'
          write(24,*)bclen,' bclen=length of bragg cells (2e-6 max)'
          write(24,*)delay,' loop delay'
          write(24,*)Nch,' No of channels (antenna elements)'
```

```
write(24,*)Njam,' Number of interferers'
write(24,*)lgain,' loop gain (db)'
write(24,*)F1,' center frequency'
write(24,*)tmax,' length of run'
write(24,*)taupr,' pr time constant'
write(24,*)tapsdelay,' samples delay before 1st tap'
write(24,*)(ang(j),j=1,Njam),' angles'
write(24,*)(sigdel(j),j=1,Njam),' delays'
write(24,*)PWRLimit,' Power limiting level in dB ref'
write(24,*)megsn,' Ref to noise ratio in 1 MHz bw'
close(unit=23)
STOP
END
```

10.2 Setup and Alignment Procedure

The optical system of the Photorefractive Adaptive Array Processor (PAAAP) processor consists of few optical components, reducing the alignment and optimization of the system to a few simple procedures. This appendix details this alignment procedure step by step enabling an operator to rebuild the system from ground zero.

10.2.1 Electrical Connections

The optical system requires two current limiting power supplies to drive the read and write laser diodes. The read diode maximum current recommended is 330 mA, and the write laser maximum current is 170 mA. The power supply connections are labeled on the detector boxes as (-) and (RTN). The leads labeled (-) should be connected to the negative terminal of the power supply and the RTN lead to the positive terminal.

The photorefractive crystal requires two 1.8 kV supplies. The negative marked lead from the photorefractive cell is connected to a negative voltage while the other lead is connected to a positive voltage, creating a total 3.6 kV differential between leads. The twisted pair leads drive the thermoelectric cooler situated on the mount. This requires a 2 A supply, with the red lead attached to the positive terminal.

The detector power supply is a 5 V supply. The connection for this is labeled "5 V" on the side of the detector housing. Also in the detector housing are two amplifiers requiring +15 V. This connection is on the side of the housing labeled "15 V."

The loop amplifier requires a 15 V power supply. The same supply that is used for the detector amplifiers can be used provided it can supply 1 A of current.

The six Bragg cell drive ports are connected to the signal generating chassis outputs marked "sig."

The signal supplied to the system should be capable of +10 dBm of power. A network analyzer has proven useful as a signal source. Care should be taken however to limit the power into the Bragg cells to 0.5 W per channel. Operating power should not exceed 200 mW per channel at the Bragg cell. The signal is connected to a splitter with one leg leading to the RF3 input to the signal generating chassis, and the other leg leading to the input of the loop amplifier via a variable attenuator.

The loop amplifier output is connected to the write laser modulation port. Attenuators should be placed in this path to set the amplifier saturated output at +23 dBm.

10.2.2 Optical Alignment

The first step in aligning the optical system is to set both laser diodes such that the beams are collinear. The adjustments for doing this are: Read transverse translation stage, Write transverse translation stage, two beam combiner tilt screws, and manual beam combiner placement (done by hand). With both beams on, use a IR viewer card to monitor the laser beams. No optics should be in the system beyond the beam combiner cube. The beams should overlap at the beam combiner and at the far end of the optics rail. Beam overlaps can be seen by partially closing one laser shutter to reveal a partially obscured laser beam which can easily be aligned with the other full beam. Beam offset adjustments can be made with the laser translation stages and manual adjustment of the beam combiner cube. Angular adjustments are made using the tilt screws on the combiner cube mount.

After making the adjustments with the raw laser beams as outlined, fine adjustments can be made by placing a 100 mm focal length lens in the beam. Small angular misalignments are more evident in the focal plane by offsets in the focused spots of the lasers. A hand held IR viewer scope will provide more accuracy than a phosphorescent card. Tuning the drive current of the lasers to dim the spots seems to help with this step. Once the focused beams are aligned, check the raw beam overlap once again to verify the colinearity of the beams.

10.2.3 Bragg Cell Placement

The laser beams are larger than the optical aperture of the Bragg cell to allow for uniform illumination of the cell. When the cell is placed in the system use the vertical adjustment inherent in the post mount and the transverse translation stage to center the aperture of the cell on the laser beams. Adjustment of the Bragg interaction is accomplished as follows: 1) Set the RF signal source to sweep from 50 to 90 MHz with a sweep rate of approximately 2–5 sweeps per second. 2) With an Allen wrench loosen the set screw located on the front of the rotation stage. This allows the rotation stage to be adjusted. 3) Use the adjustment screw on the rotation stage to rotate the cell until the diffracted light can be seen. The diffracted light is seen as a spot of light the approximate size of the undiffracted light moving sideways as the frequency of the signal is swept across the band. 4) Once the diffracted light is observed slightly adjust the rotation until the diffracted intensity is uniform across the entire sweep. Then lock the rotation stage at this point by tightening the set screw on the front of the stage. 5) The deflection angle of the 1.2 m laser and the 1.3 m laser is slightly different. To optimize the performance of the system we advise that this difference be "split." With the 100 mm lens placed after the Bragg cell and the signal source set at a

CW frequency, adjust the beam combiner rotation to offset the undiffracted beam spots. The 1.2 m diffracted beam has a smaller deflection angle; therefore, the 1.2 m undiffracted spot should be offset towards the direction of the diffracted spots. The two spots produced by the 1.2 m laser should be between the two spots produced by the 1.3 m laser. The diffracted spots should be offset from each other the same amount as the undiffracted spots. This should produce the optimum condition for diffraction by both the Bragg cell and the photorefractive crystal.

10.2.4 Photorefractive Crystal and Filter Placement

The photorefractive crystal and filter need no special adjustments. They can be simply set into the post mounts and adjusted so that the apertures line up with the laser beams.

10.2.5 Collection Lens

With the signal source sweeping across the frequency band, place the lens into the post mount and adjust the height of the lens relative to the beams. The lens can be placed such that the diffracted beams are completely separate from the undiffracted beam and blocked by the lens mount and yet all of the diffracted light will pass through the lens at any frequency. This is only used as a setup convenience, not an operational requirement. The lens could be placed directly behind the filter if desired. The transform properties of the lens will separate the diffracted and undiffracted light at the focal plane. To adjust the position of the lens a IR viewer scope is handy. Looking at the lens mount any diffracted light that is being blocked by the lens mount can be seen. Move the lens sideways by loosening the Allen head screws at the base of the post mount and slide the post sideways until no diffracted beam is blocked by the lens mount.

10.2.6 Detector

Detector alignment is done with the processor in the open loop configuration. Both lasers are at nominal current and the photorefractive crystal is at operating voltage. The output of the detector is monitored by attaching the detector output to the network analyzer or spectrum analyzer that tracks the signal source frequency. When the detector comes into position the detected signal will increase in power. A properly aligned system will saturate with a detected signal between +5 and +10 dBm. If the response is not flat across the band (varies by more than 3–5 dB) the light beam may be sweeping off the detector surface. The detector can be moved transversely with the translation stage it is mounted on. Vertical alignment is accomplished by adjusting the post mount, which is equipped with a vertical adjustment. Focus adjustments must be made by loosening the rail platform and translating.

10.2.7 Final Adjustments

After aligning the detector at the lens focal plane readjust the Bragg match by loosening the set screw on the front of the rotation stage of the Bragg cell. Adjust the rotation until the detected response is optimized. Adjust the laser drive currents until the detected response is maximized.

Check the signal level detected when one or the other of the two laser beams are shut off. If the write beam is shut off and the read beam is left on the signal detected should drop by about 40 dB. Conversely with only the write beam on and the read beam off, the signal will drop about 25 dB.

10.2.8 Close the Loop

After optical alignment is completed remove the signal input from the loop amplifier and place it in the sum port of the detector housing. Connect the detector output to the loop amplifier input with a short cable. Place a low pass filter (100 MHz) at the amplifier input also. Use the sum port of the amplifier to monitor the signal suppression by connecting it to the network analyzer or a spectrum analyzer.

Optimize the suppression by adjusting the laser drive currents until maximum suppression is achieved. If the suppression band is not centered about 70 MHz, a different length cable can be used between the detector and the loop amplifier. A longer cable will shift the suppression region towards lower frequencies and a shorter cable will increase the frequency of suppression. If desired, one last adjustment of the Bragg angle may gain a few dB of suppression.

10.2.9 Notes

The loop amplifier housed in the aluminum housing exhibits an intermittent loss of performance after it heats up. If the system appears to loose 3-5 dB suppression after 10-15 minutes of operation try lifting one end of the amplifier up about 1 inch and dropping it. This tends to fix the problem. Several attempts were made to track down the culprit but were unsuccessful in locating the problem.

When operating the loop amplifier provide a heat sink for it to sit on to avoid overheating.

Monitor the current drawn by the photorefractive crystal. If the current reaches 200 μA turn off the voltage and allow the thermoelectric cooler to cool the crystal down. The crystal could find itself in a thermal runaway situation with possible damage to the crystal.

MISSION

OF

ROME LABORATORY

Rome Laboratory plans and executes an interdisciplinary program in research, development, test, and technology transition in support of Air Force Command, Control, Communications and Intelligence (C3I) activities for all Air Force platforms. It also executes selected acquisition programs in several areas of expertise. Technical and engineering support within areas of competence is provided to ESC Program Offices (POs) and other ESC elements to perform effective acquisition of C3I systems. In addition, Rome Laboratory's technology supports other AFMC Product Divisions, the Air Force user community, and other DOD and non-DOD agencies. Rome Laboratory maintains technical competence and research programs in areas including, but not limited to, communications, command and control, battle management, intelligence information processing, computational sciences and software producibility, wide area surveillance/sensors, signal processing, solid state sciences, photonics, electromagnetic technology, superconductivity, and electronic reliability/maintainability and testability.